UNIVERSITY OF BIRMINGHAM

Microstrip Antenna Design with Improved Fabrication Tolerance for Remote Vital Signs Monitoring and WLAN/WPAN Applications at Mm-wave and THz Frequencies

by

Muhammad Saqib Rabbani

Supervisor: Dr. Hooshang Ghafouri-Shiraz

A thesis submitted to the University of Birmingham for the degree of DOCTOR OF PHILOSOPHY

Department of Electronic Electrical and System Engineering

College of Physical Sciences

University of Birmingham

June 2017

Abstract

A novel approach is introduced to design microstrip patch antennas (MPAs) with improved fabrication tolerance for highly demanded Millimetre-wave (mm-wave) (30-300GHz) and Terahertz (THz) (0.3-3THz) frequency applications. The presented MPA designing method overcomes the challenges which exist with the fabrication and implementation of the conventional MPA designs at mm-wave and THz frequencies. The following research contributions have been added to the state-of-the-art work: (i) designing of improved size MPAs at 60GHz, 100GHz, 635GHz and 835GHz to prove the designing concept, (ii) detail measurements and analysis of Remote Vital Signs Monitoring (RVSM) with various sizes of the proposed MPA arrays at 60GHz for high detection accuracy and sensitivity, (iii) designing and testing of MPAs for 60GHz wireless local and personal area networks (WLAN/WPAN) in point-to-pint, point-to-multipoint and dual-band applications, (iv) implementation and testing of particular Partially Reflective Surface, Dielectric Lens and Defected Ground Structures on the proposed MPA designs with novel configurations at 60GHz for bandwidth and gain enhancement, and (v) a comprehensive experimental study on the performance of large array designs with the proposed MPA elements for mm-wave applications. The mentioned research work is explained in the coming chapters in details. Moreover, all mentioned work has already been published.

I dedicate my PhD to my wonderful family especially my Uncle **Al-Shaikh Pir Muhammad Abdullah Ateeq** for his support during my education, my grandfathers **Hazrat Mufti Fazal Ellahi** (paternal) and **Sobdaar Muhammad Malik** (maternal) for setting the tradition of love for knowledge, father **Molana Abdul Rashid** and mother **Zeenat Kausar** for their affection, and my wife **Reahana Ateeq** who supported me throughout the journey and my wonderful children **Muhammad Mustafa Rabbani** and **Umme-Ayman Rabbani**.

Acknowledgement

First and foremost I would like to thank my supervisor Dr. Hooshang Ghafouri-Shiraz for his extraordinary supervision and guidance to build up my research understanding and skills through the course of my PhD work. Without his exceptional support this project would not have been so successful.

I am grateful to Dr. Peter Gardner (Head of Electronic, Electrical and System Engineering, Chair in Microwave Engineering) for his academic assistance.

I am thankful to other staff members Professor Dr. Michael John Lancaster, Dr. Costas Constantinou and Dr. Xiaobang Shang for their assistance in prototype testing and measurements at Millimetre-wave and Terahertz frequencies, Senior Technician Alan Yates for fabrication of my antennas' prototypes, and Mary Winkles for her administration.

Contents

List of Figures

List of Tables

List of Publications

Published Journals:

1. **M. S. Rabbani** and H. Ghafouri-Shiraz, "Size improvement of rectangular microstrip patch antenna at MM-wave and terahertz frequencies," Microwave and Optical Technology Letters 57, no. 11. 2585-2589. DOI: 10.1002/mop.29400. 2015.

2. **M. S. Rabbani** and H. Ghafouri-Shiraz, “Improvement of Microstrip Patch Antenna Gain and Bandwidth at 60GHz and X Bands for Wireless Application," IET Microwaves, Antennas & Propagation, DOI: 10.1049/iet-map.2015.0672, 2016.

3. **M. S. Rabbani** and H. Ghafouri-Shiraz, "Microstrip antennas for X-band and MM-wave frequencies based on diamond shape defected ground structure and size extension method," Microwave and Optical Technology Letters 58, no. 12. 2836-2841. DOI: 10.1002/mop.30159. 2016.

4. **M. S. Rabbani** and H. Ghafouri-Shiraz, “Fabrication tolerance and gain improvements of microstrip patch antenna at terahertz frequencies,” Microw. Opt. Technol. Lett., 58: 1819–1824. DOI: 10.1002/mop.29920. 2016.

5. **M. S. Rabbani** and H. Ghafouri-Shiraz, “High Gain Microstrip Antenna Array for 60GHz Band Point to Point WLAN/WPAN Communications,” Microw. Opt. Technol. Lett. 2016.

6. **M. S. Rabbani** and H. Ghafouri-Shiraz, “Ultra-wide Patch Antenna Array Design at 60GHz Band for Remote Vital Sign Monitoring with Doppler Radar Principle," Journal of Infrared, Millimetre and Terahertz Wave. 2016

7. **M. S. Rabbani** and H. Ghafouri-Shiraz, “Frequency Selective Surface Antenna for Remote Vital Sign Monitoring with Ultra-wide Band Doppler Radar,” Microwave and Optical Technology Letters. 2016

8. **M. S. Rabbani** and H. Ghafouri-Shiraz, “Liquid Crystalline Polymer Substrate Based THz Microstrip Antenna Arrays for Medical Applications," IEEE Antennas and Wireless Propagation Letters.

9. **M. S. Rabbani** and H. Ghafouri-Shiraz, "Resonant Cavity Based Dielectric Lens Antenna for 60GHz-band Wireless Applications," *Electronics Letters, IET*. 2017. DOI: 10.1049/el.2017.0559

10. **M. S. Rabbani** and H. Ghafouri-Shiraz, "10GHz Patch Antenna Array Design for Accurate Remote Vital Sign Monitoring with Ultra-wide Band Doppler Radar," International Journal of Electronics and Communications. 2017

Submitted Journals:

11. **M. S. Rabbani** and H. Ghafouri-Shiraz, "Dual Layer Partially Reflective Surface Antennas based on Extended Size Unit Cells for 60GHz Band WLAN/WPAN," IET Microwaves," Antennas & Propagation. 2017

12. **M. S. Rabbani** and H. Ghafouri-Shiraz, "Double Frequency Selective Surface High Gain Antenna with Deep Resonant Cavity and E-Field Reflectors," Microwave and Optical Technology Letters. (2017).

13. **M. S. Rabbani** and H. Ghafouri-Shiraz, "A Single Patch Dual Band Antenna for 60GHz-band Duplexer Applications," Microwave and Optical Technology Letters. (2017).

14. **M. S. Rabbani** and H. Ghafouri-Shiraz, "Practical Evaluation of Gain Enhancement in Microstrip Antenna Arrays for Mm-wave Applications," International Journal of Electronics and Communications. 2017.

Conference Publications and Presentations:

15. **M. S. Rabbani** and H. Ghafouri-Shiraz, "Simple methods for enhancing bandwidth of a rectangular microstrip patch antenna." IET Conference Proceedings. The Institution of Engineering & Technology, 2014.

16. **M. S. Rabbani** and H. Ghafouri-Shiraz, "Improvement of microstrip antenna's gain, bandwidth and fabrication tolerance at terahertz frequency bands," Wideband and Multi-Band Antennas and Arrays for Civil, Security & Military Applications. IET proceedings, London, UK. 2015.

17. **M. S. Rabbani** and H. Ghafouri-Shiraz, "Liquid Crystalline Polymer Substrate Based THz Microstrip Antenna Arrays for Medical Applications," EMN Meeting on Terahertz Technologies, San Sebastian, Spain, 2016. (Invited Speaker for oral presentation)

18. **M. S. Rabbani** and H. Ghafouri-Shiraz, "UWB Doppler Radar Antenna for Remote Vital Sign Monitoring," Inter-universities Radar Conference, Oxfordshire, UK, 2016. (Postal presentation)

19. **M. S. Rabbani** and H. Ghafouri-Shiraz, "60 GHz Microstrip Antenna for Remote Vital Sign Monitoring in Automobile Applications," Antennas, Propagation & RF Technology for Transport and Autonomous Platforms. IET proceedings, Birmingham, UK, 2017.

20. **M. S. Rabbani** and H. Ghafouri-Shiraz, “Evaluation of Gain Enhancement in Large Microstrip Antenna Arrays for Mm-wave Applications,” IET Colloquium on Millimetre-wave and Terahertz Engineering & Technology. IET Proceedings. Glasgow. UK. 2017.

21. **M. S. Rabbani** and H. Ghafouri-Shiraz, "60GHz Doppler Radar Antenna for Remote Vital Sign Monitoring," Inter-universities Radar Conference, Birmingham NEC, UK, 2017. (Postal presentation)

Chapter-1

Introduction

1.1 Motivation

In this PhD thesis, a research study has been conducted on designing of microstrip patch antenna (MPA) with improved fabrication tolerance and performance for remote vital signs monitoring (RVSM) and wireless local area network (WLAN) or wireless personal area network (WPAN) applications at millimetre-wave (mm-wave) (30-300GHz) and terahertz (THz) (0.3-3THz) frequencies. Furthermore, various conventional techniques have been applied on the proposed MPA structure so that their impact may be examined and evaluated in order to enrich the antenna's overall performance at the mentioned high frequencies. The motives behind this research are explained in detail in the following sub-sections.

1.1.1 Millimetre-wave and Terahertz Frequencies for Wireless Applications

The mm-wave and THz frequency bands are anticipated to be vital spectral inhabitations of many existing and emerging wireless applications due to several attractive features. Some of these features include the availability of huge continuous spectral bandwidth, small wavelength and high resolution [1]. The wireless applications at mm-wave and THz frequency bands encompass high speed short distance wireless communications like WLAN/WPAN at 60GHz band (57.24-65.88GHz) [1-9] and 300GHz band (275-300GHz) [10, 12] , T-bits/sec radio links at 237.5GHz, 350GHz and 840GHz [13-15], medical diagnosis at 420GHz, 500GHz, 800GHz [15-17], explosive and arm detection at 410GHz [16,19], and space communications [20]. Therefore, the development of wireless systems for

various existing and emerging applications at mm-wave and THz bands is of interest to both academia and industry.

1.1.2 Remote Vital Signs Monitoring with Doppler Radar at Millimetre-wave at Terahertz Frequencies

Non-contact detection of respiration and heart beat rates with a Doppler radar is a more convenient way to check the vitality signs of a person as compared to conventional vital sign monitoring devices such as Electrocardiogram (ECG), Pulse Oximetry, Capnography, etc. The conventional devices need direct sensor plantation on the subject body and cause a lot of discomfort for the patient as well as they consume comparatively much longer implementation time to start the measurements [21]-[25]. RVSM finds its applications in regular and special health care, emergency services, security and defence sectors [21-31]. In the recent years, mm-wave and THz frequencies have drawn a remarkable research interest for RVSM implications [32-41]. The main motives of RVSM at mm-wave and THz frequencies include (i) improvement in detection accuracy by employing a shorter wavelength of the signal (ii) smaller form factor for device compactness and (iii) the possibility of more subject focused signal transmission and reception, to avoid interference of unwanted side reflections [39]-[42]. Amongst mm-wave bands, 60GHz band has appeared more attractive for RVSM [35-38] because this band is free of licence and is quite mature due to its extensive use for several other wireless services [32].

1.1.3 Wireless Local Area Network and Wireless Personal Area Network at Millimetre-wave Frequencies

Since the last decade, the demand of wireless data throughput has dramatically increased and a radio link of multi-gigabits/sec data rate is projected to be essential for various existing and

emerging wireless applications like the replacement of high data handling cable networks, High Definition video steaming, uncompressed data file transfer, and mobile data off-loading [5-7]. The data rates of WLAN/WPAN technologies operating at lower microwave frequencies band i.e. 2.4GHz and 5.8GHz bands have reached closer to the Shannon Capacity limit with the help of complex signal coding and multi-input and multi out-put (MIMO) transmission techniques [8]. Alternatively, in order to satisfy the demand of very high data rates, it is proposed to operate the wireless link at even higher frequencies like mm-wave and THz bands which contain much wider spectral band. In this regard, since the last decade, 60GHz band has been heavily investigated for multi-gigabits/sec WLAN/WPAN applications [2-9]. The 60GHz band offers (i) 8.64GHz license-free continuous spectral bandwidth, (ii) higher user density due to frequency re-use opportunity because of extended atmospheric attenuation and (iii) compact component size due to the small form factor because of the short wavelength [9]. In these paradigms, two standards, namely IEEE 802.11ad [2] and IEEE 802.15.3c [3], have been introduced for 60GHz band WLAN and WPAN applications, respectively, which determine channel characterization and the system requirements for radio link configurations. However, based on these standards, various channel constraints are still to be overcome appropriately to realize a robust 60GHz band WLAN/WPAN system for commercial applications. Therefore, 60GHz band WLAN/WPAN still demands a remarkable amount of research and study towards its comprehensive industrial implementations.

1.1.4 Microstrip Antenna Design for Millimetre-wave and Terahertz Applications

Microstrip antennas exhibit attractive features for the aforementioned wireless applications including compact size, low profile, low cost, and compatibility with on-chip and in package devices [43, 44]. However, the conventional microstrip antennas inherently suffer, as having insufficient gain (8-9dB), narrow return loss bandwidth (<4%), and incredibly small

dimensions when designed for mm-wave and THz frequencies [1,44]. Fortunately, for RVSM application with Doppler radar at mm-wave/THz frequencies the mentioned antenna bandwidth is enough for acceptable resolution and the results' accuracy. Also, the antenna's required gain and radiation characteristics are achievable when the antenna is designed appropriately [45]. On the other hand, for 60GHz band WLAN/WPAN applications, higher antenna gain is required in order to sustain a reliable wireless link across the extensive path losses, and a wider antenna bandwidth is essential for the required exceptionally fast data throughput [9]. Ultimately, MPA design with adequate performance for RVSM and WLAN/WPAN at mm-wave and THz is an active subject of the current research.

1.2 Objectives and Contributions

The general purpose of this work is to design and test MPA and arrays for wireless applications at mm-wave and THz Frequencies. The applications have been chosen from the highly demanding areas of the current research e.g. RVSM at 60GHz and 100GHz bands, 60GHz band WLAN/WPAN and cancer detection at 0.835THz frequency. The objectives of this work are further segregated as follows:

1.2.1 Size Improvement of MPA at Mm-wave and THz Frequencies for Higher Fabrication Tolerance

A MPA is usually a small fraction of the operating wavelength, and since the wavelength is very short (0.03mm-10mm) at mm-wave THz frequencies, the manufacturing of microstrip antennas at mm-wave and THz frequencies with acceptable tolerance is challenging when the cost-effect fabrication process like printed circuit board (PCB) etching is employed [my IEEE letter]. Therefore, one of the objectives of this research is to study and develop new methods to improve the dimensions of the MPAs, arrays and their related feeding transmission line

(TL) networks at mm-wave and THz frequencies to convince the fabrication limitations imposed by the conventional cost-effective laboratory based PCB etching technique. Subsequently, the applicability of the proposed improved size designing methods are verified by designing, fabricating and testing of MPA and Arrays at 60GHz and 100GHz bands and then the fabrication tolerance levels are studied.

1.2.2 MPA Design and RVSM Measurements at 60GHz and 100GHz Bands

The second aim is to design MPA arrays for Doppler radar RVSM measurements at 60GHz and 100GHz bands and to study the accuracy of respiration and heart beat rates by taking detailed measurements from various distances and different time durations, both with single antenna and double antenna methods. In this regard, a comprehensive study of the feasibility of RVSM at 60GHz channel is carried out under Doppler radar theory. Furthermore, a complete Matlab code is written for the Doppler radar signal processing to purify and extract the breathing and heart beat signals from the received noisy signal. Moreover, a comparison is drawn on the accuracy improvement of RVSM results obtained at 60GHz and 100GHz band to the RVSM results measured at 10GHz band by designing MPAs and taking RVSM measurements at 10GHz band at various distances.

1.2.3 MPA Design for 60GHz-band WLAN/WPAN Applications

Another major purpose of the current research is to design MPAs and arrays based on the proposed cost-effective size improvement methods for multi-gigabits/sec 60GHz-band WLAN/WPAN point-to-point and point-to-multipoint applications and to study the service coverage areas in an indoor dynamic environment. For these regards, the antennas appropriate bandwidth and far-field radiation characteristics including gain and beamwidth are analysed in detail to meet the applications requirements. On the other hand, novel methods are

investigated for the feeding and power distributing transmission line networks in high gain large MPA arrays for point-to-point 60GHz WLAN/WPAN applications to mitigate the fabrication concerns and ohmic losses. Furthermore, an improved size dual band MPA is designed for 60GHz band duplexer applications operating on the orthogonal TM modes. All of the antennas' performances designed for 60GHz-band WLAN/WPAN are approved by fabricating and testing them at 60GHz frequency band.

1.2.4 Implementations of other Techniques on the Proposed MPAs for Performance Improvement at mm-wave and THz Frequencies

The final task of this work is to study and implement various conventional techniques, with some sort of modifications for performance improvement, on the proposed improved size MPAs at mm-wave and THz frequencies. For this cause, the following techniques are investigated:

- Various sizes and number of layers of partially reflective surface (PRS) are analysed, implemented and tested on the proposed improved size MPA for gain enhancement at 60GHz band. A comparison of the results accuracy is made by designing and testing the similar antenna structures at 10GHz frequency.
- A dielectric dome is employed and analysed on the designed improved size MPA at 60GHz frequencies for gain improvement.
- A diamond shape defected ground structure (DGS) is deployed on the improved size MPA at 60GHz frequencies for bandwidth improvement. The accuracy of the measured results of the 60GHz DGS based MPA is compared with that of the results obtained at 10GHz frequency.

- Larger antenna arrays are designed with the proposed MPA structure on the various substrate thicknesses to evaluate the gain improvement limitations due to the losses raised in the larger feeding and impedance matching transmission line networks. For this purpose, a number of the proposed MPA arrays are designed and tested at 10GHz frequency band and their performances are analysed and compared.

1.3 Challenges and Limitations

1.3.1 Sensitivities between MPA Computation, Simulation and Measurements

The MPA is developed by passing through various steps i.e. dimensions computation with the employed formulas based on the required specifications, computer modelling and simulation with CST Microwave Studio, fabrication with the PCB etching method and assembling. Then, the prototype is tested using the lab apparatus i.e. Vector Network Analyser (VNA), anechoic chamber, cables, connectors and adopters. All of these MPA designing steps inherit some sort of approximations and tolerance levels which are much significant when the MPA is designed at mm-wave and THz frequencies and cause a considerable deviation between the expected and measured results. Consequently, development of MPA at mm-wave and THz frequencies within a close agreement of the measured and expected results is a challenging task for which sometimes it has to go through a lot of work repetitions during the course of the designing stages which ultimately consumes a huge amount of effort, time and unrecoverable facilities. Mitigation of this challenge is a matter of understating the tolerance levels involved between the MPA designing stages through experience and patience.

1.3.2 Fabrication and Assembly of MPA at Mm-wave and THz Frequencies

The low cost laboratory based PCB etching method limits the minimum PCB line width/gap to >0.3mm for an acceptable tolerance level of 5% [37]. However, some commercial PCB etching shops do accept the PCB line width/gap down to 0.152mm but with 20% tolerance level [43, 46]. On the other hand, since the PCB substrate thickness (h) deployed to design MPA has to be a small fraction of the operating wavelength (λ) (i.e. $h<\lambda/10$ [47,48]) for the best antenna performance in terms of ohmic, dialectic and surface wave losses, a thin PCB substrate is required for MPA design at mm-wave and THz frequencies. However, commercially available thin PCB materials have some limited thicknesses i.e. RT/Duroid5880 with the minimum h=127μm and low loss tan(δ)=0.0009 at 10GHz [49], Ultralam3850 with minimum h=25μm and comparatively higher loss tan(δ)=0.0025 at 10GHz [50], etc. and are applicable only up to a certain high THz frequency MPA applications. Furthermore, accurate assembling of connectors and fixtures and fine soldering of the incredibly small antenna structure need extra caution to minimize their side effects on the overall antenna performance [51]. Consequently, the mentioned fabrication limits, availability of the PCB material and assembling/soldering concerns altogether set challenges and restrictions on MPA designs at mm-wave and THz frequencies. Therefore, for the present work, the MPA geometries are designed appropriately to comply with these constraints and cautiously fabricated with the low cost production process for an optimized performance.

1.3.3 Test and Measurement Techniques and Resources for MPA at Mm-wave and THz Frequencies

Since, the research on practical wireless system design and measurement at THz frequencies through the route of RF and microwave technologies is not mature enough yet, the testing

facilities of the THz wireless systems including VNA, connectors, adaptors, cables, VNAs, anechoic chamber, etc. are too expensive and sometimes inaccessible too. For the current work, this problem has limited the verification of some THz antenna designs and their applications through testing and practical measurements to go above 100GHz frequency. For instance, the lower THz (<0.5THz) VNA frequency extension module test port interferences are rectangular metallic waveguide components which need Waveguide Infinity Probe (WIP) transition adaptor to connect it to planar/microstrip circuit. The cost of the WIP adaptors is in thousands of pounds, and they are very vulnerable to be damaged during the measurement process of antenna's radiation patters which could lead to further heavy repair cost. Therefore, the proposed designing principles are proved by scaling the THz MPAs down and testing them at mm-wave frequencies.

1.4 Thesis Organisation

Chapter 2 presents the literature review on the features of mm-wave and THz electromagnetic spectrums and their use in wireless communications and sensors, designing techniques of MPAs at mm-wave and THz frequencies for wireless communications and RVSM with Doppler radar. Moreover, it describes the recent advancements in this area and identifies the research gaps which need to be filled.

Chapter 3 covers the fundamental considerations made to improve the size of MPA at mm-wave and THz frequencies, its fabrication tolerance and performance. It also demonstrates the measured results of MPAs designed based on the size improvement method at 60GHz and 100GHz bands to practically verify the proposed designing approach.

Chapter 4 illustrates detailed work on MPA designs for RVSM with Doppler radar at 60GHz and 100GHz bands and their comparison to the RVSM results accuracy obtained at 10GHz frequency.

Chapter 5 deals with the MPA designs for 60GHz band wireless communications including multi-gigabits/sec WLAN/WPAN indoor point-to-point, point-to-multipoint and dual band communications. It also describes the antenna implementation method for maximum signal coverage of 60GHz band WLAN/WPAN radio link within the environment.

Chapter 6 discusses the design and employment of PRSs on the improved size MPAs for gain enhancement at mm-wave and THz frequencies. It also analyses the gain improvement capability of the various size PRSs when the proposed MPA is used as a feeding element. The measured results of PRS based MPAs at 60GHz and 10GHz frequencies are shown in this chapter.

Chapter 7 describes the study of dielectric dome and DGS implementation on the proposed MPA for the antenna performance improvement. It carries out the parametric analysis of dielectric dome and DGS for their effect on the antenna performance. The measured results of 60GHz dielectric dome antenna, and 10GHz and 60GHz DGS based antennas are presented in this chapter.

Chapter 8 evaluates the gain enhancement potential when large arrays are constructed with the proposed MPA geometry to achieve high gain. Moreover, it presents the comparison of gain improvement when the arrays of the same number of patch elements are designed on different substrate thicknesses. This analytical work is based on the measured MPA arrays' results at 10GHz frequencies and the finally optimized MPA array design is fabricated and tested at 60GHz band.

Finally, chapter 9 concludes the research work and discusses the future of this study.

1.5 References

1. M. S. Rabbani and H. Ghafouri-Shiraz, "Size improvement of rectangular microstrip patch antenna at MM-wave and terahertz frequencies," Microwave and Optical Technology Letters 57, no. 11, pp. 2585-2589. 2015.

2. N. Moraitis and P. Constantinou, "Indoor channel measurements and characterization at 60 GHz for wireless local area network applications," Antennas and Propagation, IEEE Transactions on, 52(12), 3180-3189. 2004.

3. Kärnfelt, C., Hallbjörner, P., Zirath, H., & Alping, A. (). High gain active microstrip antenna for 60-GHz WLAN/WPAN applications. Microwave Theory and Techniques, IEEE Transactions on, 54(6), 2593-2603. 2006.

4. Biglarbegian, B., Fakharzadeh, M., Busuioc, D., Nezhad-Ahmadi, M. R., & Safavi-Naeini, S. (2011). Optimized microstrip antenna arrays for emerging millimeter-wave wireless applications. Antennas and Propagation, IEEE Transactions on, 59(5), 1742-1747.

5. Qasim, A. M., & Rahman, T. A. (2010, November). A compact & high gain series array planar antenna for 60-GHz WPAN applications. In Applied Electromagnetics (APACE), 2010 IEEE Asia-Pacific Conference on (pp. 1-5). IEEE.

6. Vettikalladi, H., Lafond, O., & Himdi, M. (2009). High-efficient and high-gain superstrate antenna for 60-GHz indoor communication. Antennas and Wireless Propagation Letters, IEEE, 8, 1422-1425.

7. Artemenko, A., Maltsev, A., Mozharovskiy, A., Sevastyanov, A., Ssorin, V., & Maslennikov, R. (2013). Millimeter-wave electronically steerable integrated lens antennas for WLAN/WPAN applications. Antennas and Propagation, IEEE Transactions on, 61(4), 1665-1671.

8. Verma, L., Fakharzadeh, M., & Choi, S. (2013). Wifi on steroids: 802.11 ac and 802.11 ad. Wireless Communications, IEEE, 20(6), 30-35.

9. Rabbani, M.S. and Ghafouri-Shiraz, H.: ' Improvement of microstrip patch antenna gain and bandwidth at 60 GHz and X bands for wireless applications' IET Microwaves, Antennas & Propagation. 2016.

10. Nagatsuma, Tadao, Kazutoshi Kato, and Jeffrey Hesler. "Enabling technologies for real-time 50-Gbit/s wireless transmission at 300 GHz." In *Proceedings of the Second Annual International Conference on Nanoscale Computing and Communication*, p. 10. ACM, 2015.

11. Kim, Sooyeon, Jongwon Yun, Daekeun Yoon, Moonil Kim, Jae-Sung Rieh, Miguel Urteaga, and Sanggeun Jeon. "300 GHz integrated heterodyne receiver and transmitter with on-chip fundamental local oscillator and mixers." *IEEE Transactions on Terahertz Science and Technology* 5, no. 1 (2015): 92-101.

12. Song, Ho-Jin, and Tadao Nagatsuma. "Present and future of terahertz communications." *IEEE Transactions on Terahertz Science and Technology* 1, no. 1 (2011): 256-263.

13. S. Koenig, D. Lopez-Diaz, J. Antes, F. Boes, R. Henneberger, A. Leuther, A. Tessmann et al. "Wireless sub-THz communication system with high data rate." Nature Photonics 7, no. 12 (2013): 977-981.

14. K. Huang, and Z. Wang. "Terahertz terabit wireless communication." Microwave Magazine, IEEE 12, no. 4 (2011): 108-116.

15. F. I. Akyildiz, J. M. Jornet, and C. Han. "Terahertz band: Next frontier for wireless communications." Physical Communication 12 (2014): 16-32.

16. D. L. Woolard, E. R. Brown, M. Pepper, and M. Kemp. "Terahertz frequency sensing and imaging: A time of reckoning future applications?." Proceedings of the IEEE 93, no. 10 (2005): 1722-1743.

17. J. Nishizawa, T. Sasaki, K. Suto, T.Yamada, T. Tanabe, T. Tanno, T. Sawai, and Y. Miura. "THz imaging of nucleobases and cancerous tissue using a GaP THz-wave generator." Optics communications 244, no. 1 (2005): 469-474.

18. J. Son, "Terahertz electromagnetic interactions with biological matter and their applications." Journal of Applied Physics 105, no. 10 (2009): 102033.

19. E. Seok, C. Cao, D. Shim, D. J. Arenas, D. B. Tanner, and C. Hung. "A 410GHz CMOS push-push oscillator with an on-chip patch antenna." In Solid-State Circuits Conference, 2008. ISSCC 2008. Digest of Technical Papers. IEEE International, pp. 472-629. IEEE, 2008.

20. S. U. Hwu, K. B. deSilva, and C. T. Jih. "Terahertz (THz) wireless systems for space applications." In Sensors Applications Symposium (SAS), 2013 IEEE, pp. 171-175. IEEE, 2013.

21. Sun, L., Li, Y., Hong, H., Xi, F., Cai, W. and Zhu, X.: 'Super-resolution spectral estimation in short-time non-contact vital sign measurement', Review of Scientific Instruments,86(4), p.044708. 2015.

22. Droitcour, A.D., Seto, T.B., Park, B.K., Yamada, S., Vergara, A., El Hourani, C., Shing, T., Yuen, A., Lubecke, V.M. and Boric-Lubecke, O.: 'September. Non-contact respiratory rate measurement validation for hospitalized patients', In 2009 Annual International Conference of the IEEE Engineering in Medicine and Biology Society (pp. 4812-4815). IEEE. 2009.

23. Villarroel, M., Guazzi, A., Jorge, J., Davis, S., Watkinson, P., Green, G., Shenvi, A., McCormick, K. and Tarassenko, L.: 'Continuous non-contact vital sign monitoring in neonatal intensive care unit. Healthcare technology letters, 1(3), p.87. 2014.

24. Suzuki, S., Matsui, T., Kagawa, M., Asao, T. and Kotani, K.: 'An approach to a non-contact vital sign monitoring using dual-frequency microwave radars for elderly care', Journal of Biomedical Science and Engineering, 6(07), p.704. 2013.

25. Li, C., Cummings, J., Lam, J., Graves, E. and Wu, W.: 'Radar remote monitoring of vital signs', IEEE Microwave Magazine, 10(1), pp.47-56. 2009.

26. Uenoyama, M., Matsui, T., Yamada, K., Suzuki, S., Takase, B., Suzuki, S., Ishihara, M. and Kawakami, M.: 'Non-contact respiratory monitoring system using a ceiling-attached microwave antenna', Medical and Biological Engineering and Computing, 44(9), pp.835-840. 2006.

27. Ren, L., Koo, Y.S., Wang, H., Wang, Y., Liu, Q. and Fathy, A.E.: 'Noncontact Multiple Heartbeats Detection and Subject Localization Using UWB Impulse Doppler

Radar', IEEE Microwave and Wireless Components Letters, 25(10), pp.690-692. 2015.

28. Adib, F., Mao, H., Kabelac, Z., Katabi, D. and Miller, R.C.: 'April. Smart homes that monitor breathing and heart rate', In Proceedings of the 33rd Annual ACM Conference on Human Factors in Computing Systems (pp. 837-846). ACM. 2015.

29. Suzuki, S., Matsui, T., Kawahara, H., Ichiki, H., Shimizu, J., Kondo, Y., Gotoh, S., Yura, H., Takase, B. and Ishihara, M.: 'A non-contact vital sign monitoring system for ambulances using dual-frequency microwave radars', Medical & biological engineering & computing, 47(1), pp.101-105. 2009.

30. Brüser, C., Antink, C.H., Wartzek, T., Walter, M. and Leonhardt, S.: 'Ambient and Unobtrusive Cardiorespiratory Monitoring Techniques', IEEE reviews in biomedical engineering, 8, pp.30-43. 2015.

31. Tariq, A. and Ghafouri-Shiraz, H.: 'Noncontact heart rate monitoring using Doppler radar and continuous wavelet transform', Microwave and Optical Technology Letters, 53(8), pp.1793-1797.2011.

32. H-R. Chuang, H-C. Kuo, F-L. Lin, T-H. Huang, C-S. Kuo and Y-W. Ou, 60-GHz millimeter-wave life detection system (MLDS) for noncontact human vital-signal monitoring, IEEE Sensors Journal 12, no. 3 (2012): 602-609.

33. H-C. Kuo, H-H. Wang, P-C. Wang, H-R. Chuang, and F-L. Lin, 60-GHz millimeter-wave life detection system with clutter canceller for remote human vital-signal sensing, In Microwave Workshop Series on Millimeter Wave Integration Technologies (IMWS), 2011 IEEE MTT-S International, pp. 93-96. IEEE, (2011)

34. H-C. Kuo and H-R. Chuang, Investigation of carrier frequency effect on detection performance of Doppler sensor systems for noncontact human vital-signs sensing, In 2014 8th International Symposium on Medical Information and Communication Technology (ISMICT), pp. 1-4. IEEE, (2014)

35. T-Y. J. Kao, Y. Yan, T-M. Shen, A. Y-K. Chen and J. Lin, Design and analysis of a 60-GHz CMOS Doppler micro-radar system-in-package for vital-sign and vibration detection, IEEE Transactions on Microwave Theory and Techniques 61, no. 4 (2013): 1649-1659

36. T-Y. J. Kao, A. Y-K. Chen, Y. Yan, T-M. Shen and J. Lin, A flip-chip-packaged and fully integrated 60 GHz CMOS micro-radar sensor for heartbeat and mechanical vibration detections, In 2012 IEEE Radio Frequency Integrated Circuits Symposium, pp. 443-446. IEEE, (2012)

37. T-M. Shen, T-Y. J. Kao, T-Y. Huang, J. Tu, J. Lin and R-B. Wu, Antenna design of 60-GHz micro-radar system-in-package for noncontact vital sign detection, IEEE Antennas and Wireless Propagation Letters 11 (2012): 1702-1705

38. J. Gao, K. Li, T. Sato, J. Wang, H. Harada S. and Kato, January. Implementation considerations of patch antenna array for 60GHz beam steering system applications. In 2009 IEEE Radio and Wireless Symposium(pp. 35-38). IEEE, 2009

39. Bakhtiari, Sasan, Thomas W. Elmer, Nicholas M. Cox, Nachappa Gopalsami, Appostolos C. Raptis, Shaolin Liao, Ilya Mikhelson, and Alan V. Sahakian. "Compact millimeter-wave sensor for remote monitoring of vital signs." IEEE Transactions on Instrumentation and Measurement 61, no. 3 (2012): 830-841.

40. S. Bakhtiari, S. Liao, T. Elmer and A. C. Raptis, A real-time heart rate analysis for a remote millimeter wave IQ sensor, IEEE Transactions on Biomedical Engineering 58, no. 6 (2011): 1839-1845

41. D. T. Petkie, C. Benton and E. Bryan, Millimeter wave radar for remote measurement of vital signs, (2009): 1.

42. C. Li, V. M. Lubecke, O. Boric-Lubecke and J. Lin, A review on recent advances in Doppler radar sensors for noncontact healthcare monitoring, IEEE Transactions on microwave theory and techniques 61, no. 5 (2013): 2046-2060

43. Bancroft, R.: 'Microstrip and printed antenna design', The Institution of Engineering and Technology, (2009).

44. Balanis, Constantine A., ed.: 'Modern antenna handbook', John Wiley & Sons, 2011.

45. M. S. Rabbani and H. Ghafouri-Shiraz, " Ultra-wide Patch Antenna Array Design at 60GHz Band for Remote Vital Sign Monitoring with Doppler Radar Principle," Journal of Infrared, Millimeter, and Terahertz Waves. 2016.

46. Online: [http://www.4pcb.com/pcb-design-specifications/], accessed on 24th Nov. 2016

47. K.R. Jha, G. Singh, "Improved Performance Analysis of Square Patch Microstrip Antenna at Terahertz Frequency," Advances in Recent Technologies in Communication and Computing, 2009. ARTCom '09. International Conference on, vol., no., pp.676, 679, 27-28 Oct. 2009

48. Kara, Mehmet. "An efficient technique for the computation of the input resistance of rectangular microstrip antenna elements with thick substrates." *Microwave and Optical Technology Letters* 13, no. 6 (1996): 363-369.

49. Online: (http://www.rogerscorp.com/acs/products/32/RT-duroid-5880-Laminates.aspx), accessed on 24th Nov. 2016

50. Online: (http://www.rogerscorp.com/acs/producttypes/35/ULTRALAM-3000-Flexible-Copper-Clad-Laminate-and-Bondply.aspx), accessed on 24th Nov. 2016

51. Rabbani, M. S. and Ghafouri-Shiraz, H. (2016), Fabrication tolerance and gain improvements of microstrip patch antenna at terahertz frequencies. Microw. Opt. Technol. Lett., 58: 1819–1824. doi:10.1002/mop.29920

52. Form Factor, online: (https://www.cascademicrotech.com/products/probes/rf-microwave/infinity-probe/waveguide-infinity-probe-), accessed on 06th Nov. 2014

Chapter-2

Literature Review

Abstract: Since the last decade, a considerable amount of research has been initiated on MPA design for various mm-wave and THz applications by different groups across the globe. In this chapter, the research outcomes of the reported work on MPA design for mm-wave and THz frequencies, Remote Vital Signs Monitoring (RVSM) and WLAN/WPAN at 60GHz frequency are presented. Furthermore, the recent work on implementation of various types of lenses and defected ground structures (DGS) on MPA for the performance improvement at mm-wave and THz frequencies is reviewed. The shortcomings and gap areas of the recent research are revealed and the scope of this study is described to fill up the research gaps.

2.1 Designing of Microstrip Patch Antenna at Millimetre-wave and Terahertz Frequencies

Microstrip antennas have been extensively studied for their performance improvement and applications in wireless communications since their earlier development in 1960s [1-20]. In the most recent decades, MPAs have also been exploited for mm-wave and THz frequency band for numerous applications [12-23]. Among other candidate antennas for mm-wave and THz applications, like slot antenna [24-26], substrate integrated antenna [27, 28], lens antenna [29-32], etc., potentially MPA inherits more robustness to satisfy the requirements of (i) high gain by constructing antenna arrays with large number of patch elements [33], (ii) low cost and better fabrication tolerance [34], low profile and light weight due to the small form factor because of the short wavelength at the mentioned high frequencies [35]. Despite these facts, MPA can also be incorporated with the mentioned antenna technologies to enhance its performance at mm-wave and THz frequencies [36]. Nevertheless, to exploit the MPA's

valuable features stated above, they sought to be appropriately designed and carefully manufactured to alleviate their fabrication tolerance and performance at mm-wave and THz frequencies.

In recent years, MPA has been investigated considerably for various mm-wave and THz applications [37-44]. In [37], a high gain MPA is designed at 600GHz frequency on a thick substrate of low dielectric constant ε_r=2.08. However, the feeding line width of this antenna is 50μm which is far below the conventional laboratory based PCB fabrication limit of 152μm. Also, the antenna neither shows a single resonance phenomenon at the required frequency nor does it radiate in the plane normal to the patch. In [38], photonic band gap (PBG) material is used to artificially reduce the dielectric constant of the substrate material implemented for MPA design at 600GHz. Although, the designed antenna shows reasonable improvement in simulation results, but the antenna's structure complexity is increased and the feeding line size remains much smaller than the fabrication limit stated above. Moreover, the nano scale PBG structure requires a more advanced fabrication method which raises the production cost [39]. In [40], a dual band MPA is designed at 600GHz and 800GHz frequencies based on multi-layer technology with low and medium dielectric constants (ε_{r1}=3.2, ε_{r2}=6). However, most of the designed antenna dimensions, i.e. coupling gap between the feeding line and the patch (6μm), feeding line width (40μm), substrate height (25μm), etc., are too small to be fabricated by using the conventional PCB etching technique. In [41], an on-chip patch antenna is designed with the conventional method for a 410GHz CMOS push-push oscillator where the antenna contains very fine PCB details which cannot be fabricated with the etching method.

In [45], an MPA array of 16 patch elements is presented at 35.7GHz with 19dBi simulated gain and 67% efficiency. The array contained fine PCB details down to 183μm and was fabricated with Optical Photolithography method. In [26], a dual polarised 2x2 elements MPA array is designed at 92GHz through corporate microstrip lines and rectangular waveguide feeding methods. Only simulation results are presented and the dimensions related information is not provided. On the other hand, a remarkable research study has been published on MPA designs at 60GHz band for wireless applications which will be discussed in the upcoming sections. Consequently, MPA with improved fabrication tolerance and performance at mm-wave and THz frequencies is highly demanded and hence in the present study the research is conducted to meet this requirement.

2.2 Microstrip Patch Antenna Designs for Remote Vital Signs Monitoring at Millimetre-wave and Terahertz Frequencies

In the recent decade, a significant amount of research has been conducted to improve the accuracy of RVSM by employing various techniques including distance and frequency optimization [45-51], robust signal processing methods [52-54], breath holding for heartbeat detection and so on [55,56]. However, most of the reported practical work is based on Doppler radars working at lower microwave (MW) frequency bands around 2.4GHz, 5.8GHz and 10GHz where the wavelength resolution of the electromagnetic wave is low and therefore the accuracy of the vital signs detection, especially the heartbeat rate, remained challenging [57]. Secondly, the radar antenna systems at the mentioned low MW frequencies are quite bulky which may abstain the antenna to be integrated with modern real life compact devices like smart phones and tablets [57]. The Ka-band (26-40GHz) frequencies have also been investigated for RVSM to enhance the sensors sensitivity due to their comparatively shorter wavelength [58-60].

In recent years, mm-wave and THz frequencies have drawn a remarkable research interest for RVSM implications [61-69]. The main motives of RVSM at mm-wave and THz frequencies are (i) improvement in detection accuracy by employing shorter wavelength of the signal (ii) smaller form factor for the device compactness and (iii) possibility of more subject focused signal transmission and reception to avoid interference from unwanted side reflections [65-69]. From mm-wave band, 60GHz band (57GHz-66GHz) has drawn more attraction because this band is free of license and is quite mature due to its extensive use for several other wireless services [61].

Antenna designing for Doppler radar plays a crucial role in the precision of RVSM [61-66]. The antenna should be designed in such a way that it only focuses the radiation beam on the subject [61] and should have an adequate gain to maintain a required signal to noise ratio [66]. Microstrip patch antennas are thought to be the better option for compact mm-wave sensors due to their embedment with on–chip devices, low profile, low cost and ability to make array to attain high antenna gain [64]-[66]. In [65], conventionally designed microstrip patch antennas are integrated with on-chip micro-radar system for RVSM at 60GHz band. However, the narrow microstrip transmission line designed for impedance matching and feeding purpose is fabricated with flip-chip method. In [66], two circularly polarized patch antenna arrays have been presented for vital signs detection at 55GHz. The antenna arrays and the associated narrow feed lines were fabricated by using special technique based on multi-layer low-temperature co-fire ceramic (LTCC) substrate. The antennas gain remained as low as 4.86dBi in case of 2-elements and 9.7dBi in 4-elements arrays. Furthermore, for RVSM with these arrays the subject has to hold breathing for a while for accurate detection of the heartbeat rate. Therefore, regarding RVSM measurements at 60GHz there are still gaps in the literature i.e. cost-effective microstrip antenna array design for accurate and simultaneous

detection of respiration and heartbeat rates and the study of RVSM with single antenna for very short distance and with double antennas for long distance applications.

2.3 Microstrip Patch Antenna Design for 60GHz-band WLAN/WPAN Applications

60GHz-band is expected to be an indispensable spectral host for multi-gigabits/sec WLAN/WPAN applications [70-75]. This frequency band can offer (i) an 8.64GHz wide license-free continuous spectral bandwidth (57.24-65.88GHz), (ii) higher user density due to frequency re-use opportunity because of extended atmospheric attenuation and (iii) compact components size due to short wavelength (~5mm) [48]. Subsequently, it has been projected that 60GHz-band wireless technologies are most likely to open new horizons towards replacement of high data handling cable networks, HD video steaming, uncompressed data file transfer, and mobile data off-loading [74-76]. In these paradigms, two standards namely IEEE 802.11ad and IEEE802.15.3c have already been published for 60GHz WLAN and WPAN applications, respectively, which determine the channel characterization and the system requirements for radio link configurations [70, 72]. According to these standards, 60GHz-band is further segregated into four 2.16GHz wide sub-channels centred at 58.32GHz, 60.48GHz, 62.64GHz and 64.80GHz with the transmission being confined at least in one of these channels [73]. Based on the mentioned IEEE standards recommendations, a high gain, wide band, and highly efficient microstrip antenna is tremendously desirable in order to realise a trustworthy and cost-effective radio link for 60GHz WLAN/WPAN applications [74, 77, 78].

Traditionally, the gain of a microstrip antenna is improved by constituting an array of multiple patch elements [79-82]. In doing so, theoretically the number of identical patch elements should be doubled to enhance the antenna gain by about 3dB. However, at the mentioned high frequencies this approach is limited by the declined antenna efficiency and

gain due to substantial power losses commenced by the extended microstrip feeding network which is vital to deliver matched electrical signal to each radiating element [71-74, 79]. For instance, in [49] a ten-elements microstrip antenna array is designed for 60GHz WLAN/WPAN applications and only about 13dBi gain is achieved with as low antenna efficiency as 63%. In [73], an array of four patch elements is designed for 60GHz wireless applications and a maximum optimized gain of 13dBi is accomplished. Additionally, in both [72] and [73] the fine patterns of the feeding transmission lines degrade the fabrication tolerance when the conventional PCB etching technique is applied.

An alternative method to simultaneously boost the microstrip antenna gain and bandwidth is to employ aperture coupling feeding scheme together with multi-layer technology [70, 83]. However, this approach needs more sophisticated fabrication technologies which ultimately increases fabrication complexities and cost, especially at mm-wave frequencies. Besides this method, several other procedures have been adopted solely to widen the impedance bandwidth of microstrip antenna i.e. etching various slots in the patch [84, 85], employing multi-layer technology [86], implementing thick dielectric material [87] and wide-band feeding network [88, 89]. However, these approaches are incompetent for mm-wave frequency microstrip antenna design due to the fabrication concerns and device efficiency degradation as stated earlier. Moreover, these techniques have been unable to address the peculiarity arisen in the gain fluctuation across the operating frequency band.

Numerous others microstrip antennas have also been reported for WLAN/WPAN at 60GHz-band based on Low Temperature Co-fired Ceramic (LTCC) and their performance is summarised in [90]. In most of the cases described in [90], the gain of LTCC based microstrip antennas were improved between 13 to 17dBi by constituting arrays of 16 patch elements. In [90], the best trade-off between the number of patch elements and gain was found in case of

[91] where a gain of 13.6 dBi is achieved with 8-elements microstrip array. However, for the rest of LTCC based antenna arrays with smaller number of elements the measured gain remained far below 10dBi [90].

MPAs have also been exploited on Liquid Crystal Polymer (LCP) substrate [92]. It has been shown in [92, 93] that a patch antenna fabricated on Polytetrafluoroethylene (PTFE) substrate exhibits better electrical performance as compared to the one fabricated on LCP or LTCC substrate due to low dielectric constant, low loss tangent and low cost of PTFE materials. Therefore, in the present work a compact and cost-effective MPA with improved bandwidth, gain and radiation performance has been proposed for 60GHz-band indoor WLAN/WPAN applications. The implementation of the proposed antenna has also been demonstrated for the full service coverage within an ordinary size room of $10\times10m^2$ area.

2.4 Implementation of Partially Reflective Surface and Dielectric Lens on Microstrip Patch Antenna at mm-wave and THz Frequencies

As described in section 2.1, high gain antennas are vital to compensate the atmospheric path losses for a reliable wireless link at mm-wave and THz frequencies. Apart from constructing arrays with large number of patch elements to get high antenna gain, an adequate choice may be to implement a lens in front of a feeding antenna to enhance its gain by many folds at mm-wave and THz frequencies [94-111]. In the recent years, two types of lens structures have been dominantly reported in the literature for mm-wave and THz applications; (i) partially reflective surface (PRS) lens [95-97, 107-111] and (ii) dielectric lens [103, 104]. PRS based antennas are practically less explored at mm-wave and THz frequencies partially because a very large PRS is required for a considerable improvement in the antenna gain which may not be applicable in the modern compact devices [94-100]. However, a substantial amount of the fundamental research on PRS structures and their implementation at microwave frequencies is

available in the literature [103, 104]. In [95], a 60GHz-band antenna based on thick metallic PRS with periodic holes has been studied in detail and a measured gain of 11dBi is achieved with 64 PRS unit cells. However, the reported PRS contains some incredibly small dimensions which need sophisticated fabrication techniques for production with acceptable fabrication tolerance. In [96] and [97], square loop PRS is employed to enhance the antenna gain at 60GHz-band and maximum simulated gain of 14.26dBi and 17.2dBi are obtained with 16 and 25 PRS unit cells, respectively. However, there are no measured results presented in [96, 97]. On the other hand, the dielectric lenses have been widely exploited in high gain antennas at mm-wave and THz frequencies [103, 105, 112-116]. Usually, a dielectric lens antenna inherits relatively higher weight as compared to a PRS antenna but still it may be feasible for several mm-wave and THz applications due to the small form factor as mentioned in section 1.2 [103].

Lens antennas are normally fed by electromagnetic coupling through dipole, patch, waveguide and slot elements and the gain of the feeding element is enhanced by many folds [103, 112-117]. At mm-wave and THz frequencies, waveguide slot is commonly used for the feeding purpose due to its better loss performance but essentially it is fabricated with Micromachining processes [80, 82]. On the other hand, the patch element is less commonly employed for feeding at the mentioned high frequencies due to its poor loss performance [98, 117].

In the present work, PRS and dielectric lenses are designed at 60GHz-band and the proposed improved size patch antenna is employed to feed the lens for gain enhancement. Both of the mentioned lens structures are numerically analysed and optimised for the desired gain performance. The designed antennas have been tested at 60GHz-band frequencies and the expected results have been achieved successfully. One of the best PRS based 60GHz antenna

is reproduced and tested at 10GHz frequency to assure the validity of the designing concept under more accurate automated testing environments.

2.5 Implementation of Defected Ground Structure on MPA at mm-wave and THz Frequencies

In the past, DGSs have been widely employed on the conventional MPA and filter designs to miniaturize their size as well as to improve their integration, efficiency and frequency response at microwave frequencies [118-129]. However, the reported fine antenna and DGS details employed at the mentioned low MW frequencies make it difficult to design and fabricate them at mm-wave and THz frequencies should the cost-effective etching process mentioned earlier be employed. To the best of the author's knowledge, no DGS based antenna work is reported in the literature at mm-wave and THz frequencies suitable for fabrication with conventional PCB etching process.

In the present work, a diamond shape DGS is analysed and implemented on the improved size MPA at 60GHz frequency band to widen the antenna bandwidth. The antenna is tested at 60GHz-band and a fair agreement between the measured and simulation results is achieved. It may worth mentioning that various DGS shapes (i.e. rectangular, circular and diamond) have been investigated with various sizes and positions to analyse their performances and found that the proposed diamond shape DGS yields the best antenna performance. Finally, the 60GHz DGS based antenna has been scaled down and tested at 10GHz frequency to further clarify the designing approach because the accuracy in measurements at 10GHz is better than 60GHz, as mentioned in the last section.

2.6 References

1. Wood, C., 1980, August. Improved bandwidth of microstrip antennas using parasitic elements. In *IEE Proceedings H (Microwaves, Optics and Antennas)* (Vol. 127, No. 4, pp. 231-234). IET Digital Library.
2. Carver, K.R. and Coffey, E.L., 1979. *Theoretical Investigation of the Microstrip Antenna* (No. PT-00929). NEW MEXICO STATE UNIV LAS CRUCES PHYSICAL SCIENCE LAB.
3. Agrawal, P. and Bailey, M., 1977. An analysis technique for microstrip antennas. *IEEE Transactions on antennas and propagation*, *25*(6), pp.756-759.
4. Munson, R., 1974. Conformal microstrip antennas and microstrip phased arrays. *IEEE Transactions on Antennas and propagation*, *22*(1), pp.74-78.
5. Howell, J., 1975. Microstrip antennas. *IEEE Transactions on Antennas and Propagation*, *23*(1), pp.90-93.
6. Derneryd, A., 1978. A theoretical investigation of the rectangular microstrip antenna element. *IEEE Transactions on Antennas and Propagation*, *26*(4), pp.532-535.
7. Carver, K. and Mink, J., 1981. Microstrip antenna technology. *IEEE transactions on antennas and propagation*, *29*(1), pp.2-24.
8. Johnson, R.C. and Jasik, H., 1984. Antenna engineering handbook. *New York, McGraw-Hill Book Company, 1984, 1356 p. No individual items are abstracted in this volume.*
9. James, J.R., Hall, P.S. and Wood, C., 1981. *Microstrip antenna: Theory and design* (No. 12). Iet.

10. Sullivan, P.L.A.D.H.S. and Schaubert, D., 1986. Analysis of an aperture coupled microstrip antenna. *IEEE transactions on antennas and propagation*, *34*(8), pp.977-984.

11. Waterhouse, R., 1995. Small microstrip patch antenna. *Electronics letters*, *31*(8), pp.604-605.

12. Sabban, A., 1983, May. A new broadband stacked two-layer microstrip antenna. In *Antennas and Propagation Society International Symposium, 1983* (Vol. 21, pp. 63-66). IEEE.

13. Pozar, D.M. and Kaufman, B., 1987. Increasing the bandwidth of a microstrip antenna by proximity coupling. *Electronics Letters*, *23*(8), pp.368-369.

14. Weiss, M., 1981. Microstrip antennas for millimeter waves. *IEEE Transactions on Antennas and Propagation*, *29*(1), pp.171-174.

15. Pozar, D.M., Targonski, S.D. and Syrigos, H.D., 1997. Design of millimeter wave microstrip reflectarrays. *IEEE transactions on antennas and propagation*, *45*(2), pp.287-296.

16. Pozar, D., 1983. Considerations for millimeter wave printed antennas. *IEEE Transactions on antennas and propagation*, *31*(5), pp.740-747.

17. Pozar, D.M., 1992. Microstrip antennas. *Proceedings of the IEEE*, *80*(1), pp.79-91.

18. Bhartia, P., Tomar, R.S. and Rao, K.V.S., 1991. *Millimeter-wave microstrip and printed circuit antennas*. Artech House.

19. James, J.R., 1989. *Handbook of microstrip antennas*. IET.

20. Gauthier, G.P., Courtay, A. and Rebeiz, G.M., 1997. Microstrip antennas on synthesized low dielectric-constant substrates. *IEEE Transactions on Antennas and Propagation*, *45*(8), pp.1310-1314.

21. Rebeiz, G.M., 1992. Millimeter-wave and terahertz integrated circuit antennas. *Proceedings of the IEEE*, *80*(11), pp.1748-1770.

22. Balanis, C.A., 1992. Antenna theory: A review. *Proceedings of the IEEE*, *80*(1), pp.7-23.

23. Levine, E., Malamud, G., Shtrikman, S. and Treves, D., 1989. A study of microstrip array antennas with the feed network. *IEEE Transactions on Antennas and Propagation*, *37*(4), pp.426-434.

24. Zhang, J., Gao, K., Zhang, Y. and Cao, X., 2014, April. A W-band slot array antenna based on substrate waveguide. In *Antennas and Propagation (EuCAP), 2014 8th European Conference on* (pp. 998-1002). IEEE. doi: 10.1109/EuCAP.2014.6901933

25. Harish, S., Srinivasan, S., Srinikethan, M.S. and GA, S.S., 2015, August. 3-D stack of waveguide structures with hour-glass slot structure for terahertz antenna applications. In *Advances in Computing, Communications and Informatics (ICACCI), 2015 International Conference on* (pp. 689-693). IEEE. doi: 10.1109/ICACCI.2015.7275691

26. Liu, Y., Lu, H., Wu, Y., Cui, M., Li, B., Zhao, P. and Lv, X., 2016. Millimeterwave and Terahertz Waveguide-Fed Circularly Polarized Antipodal Curvedly Tapered Slot Antennas. *IEEE Transactions on Antennas and Propagation*, *64*(5), pp.1607-1614. doi: 10.1109/TAP.2016.2536174

27. Wu, K., Cheng, Y.J., Djerafi, T. and Hong, W., 2012. Substrate-integrated millimeter-wave and terahertz antenna technology. *Proceedings of the IEEE*, *100*(7), pp.2219-2232. doi: 10.1109/JPROC.2012.2190252

28. Shang, Y., Yu, H., Fu, H. and Lim, W.M., 2014. A 239–281 GHz CMOS receiver with on-chip circular-polarized substrate integrated waveguide antenna for sub-

terahertz imaging. *IEEE Transactions on Terahertz Science and Technology*, *4*(6), pp.686-695.doi: 10.1109/TTHZ.2014.2352040

29. Alazemi, A.J., Yang, H.H. and Rebeiz, G.M., 2016. Double bow-tie slot antennas for wideband millimeter-wave and terahertz applications. IEEE Transactions on Terahertz Science and Technology, 6(5), pp.682-689. doi: 10.1109/TTHZ.2016.2590947

30. Hassan, W.M., Zainud-Deen, S.H. and Malhat, H.A., 2016, February. Compact multi-function single/dual-beam graphene lens antenna for terahertz applications. In Radio Science Conference (NRSC), 2016 33rd National (pp. 41-48). IEEE. doi: 10.1109/NRSC.2016.7450822

31. Chan, C.H., Ng, K.B. and Qu, S.W., 2015, March. Gain enhancement for low-cost terahertz fresnel zone plate lens antennas. In Antenna Technology (iWAT), 2015 International Workshop on (pp. 66-69). IEEE. doi: 10.1109/IWAT.2015.7365263

32. Alonso-DelPino, M., Llombart, N., Chattopadhyay, G., Lee, C., Jung-Kubiak, C., Jofre, L. and Mehdi, I., 2013. Design guidelines for a terahertz silicon micro-lens antenna. *IEEE Antennas and Wireless Propagation Letters*, *12*, pp.84-87. doi: 10.1109/LAWP.2013.2240252

33. Rabbani, M.S. and Ghafouri-Shiraz, H., 2015. Microstrip Antenna Array for 60GHz Band Point to Point WLAN/WPAN Communications. Microwave and Optical Technology Letters.

34. Rabbani, M.S. and Ghafouri-Shiraz, H., 2015. Size improvement of rectangular microstrip patch antenna at MM-wave and terahertz frequencies. Microwave and Optical Technology Letters, 57(11), pp.2585-2589.

35. Rabbani, M.S. and Ghafouri-Shiraz, H., 2015, December. Improvement of microstrip antenna's gain, bandwidth and fabrication tolerance at terahertz frequency bands. In

Wideband and Multi-Band Antennas and Arrays for Civil, Security & Military Applications (pp. 1-3). IET. doi: 10.1049/ic.2015.0146

36. Okada, K., Kasagi, K., Oshima, N., Suzuki, S. and Asada, M., 2015. Resonant-Tunneling-Diode Terahertz Oscillator Using Patch Antenna Integrated on Slot Resonator for Power Radiation. *IEEE Transactions on Terahertz Science and Technology*, *5*(4), pp.613-618. doi: 10.1109/TTHZ.2015.2441740

37. K.R. Jha, and G. Singh, Improved Performance Analysis of Square Patch Microstrip Antenna at Terahertz Frequency, Advances in Recent Technologies in Communication and Computing, 2009. ARTCom '09. International Conference on, vol., no., pp.676, 679, 27-28 Oct. 2009

38. Jha, K.R. and Singh, G., 2012. Analysis and design of terahertz microstrip antenna on photonic bandgap material. *Journal of Computational Electronics*, *11*(4), pp.364-373.

39. M. Johri, Y. A. Ahmed, and T. Bezboruah. Photonic band gap materials: Technology, applications and challenges. Abdus Salam International Centre for Theoretical Physics, Trieste (Italy), 2006.

40. Jha, K.R. and Singh, G., 2010. Dual-band rectangular microstrip patch antenna at terahertz frequency for surveillance system. *Journal of Computational Electronics*, *9*(1), pp.31-41.

41. Seok, E., Cao, C., Shim, D., Arenas, D.J., Tanner, D.B., Hung, C.M. and Kenneth, K.O., 2008, February. A 410GHz CMOS push-push oscillator with an on-chip patch antenna. In *Solid-State Circuits Conference, 2008. ISSCC 2008. Digest of Technical Papers. IEEE International* (pp. 472-629). IEEE.

42. Jha, K.R. and Singh, G., 2013. Terahertz planar antennas for future wireless communication: A technical review. *infrared physics & Technology*, *60*, pp.71-80.

43. Younssi, M., Jaoujal, A., Yaccoub, M.D., El Moussaoui, A. and Aknin, N., 2013. Study of a microstrip antenna with and without superstrate for terahertz frequency. *International Journal of Innovation and Applied Studies*, *2*(4), pp.369-371.

44. Singh, G., 2010. Design considerations for rectangular microstrip patch antenna on electromagnetic crystal substrate at terahertz frequency. *Infrared Physics & Technology*, *53*(1), pp.17-22.

45. Mavaddat, A., Armaki, S.H.M. and Erfanian, A.R., 2015. Millimeter-Wave Energy Harvesting Using $4\ times4 $ Microstrip Patch Antenna Array. *IEEE Antennas and wireless propagation letters*, *14*, pp.515-518.

46. Li, C., Xiao, Y. and Lin, J., 2008. A 5GHz Double-Sideband Radar Sensor Chip in 0.18$\ mu $ m CMOS for Non-Contact Vital Sign Detection. *IEEE Microwave and Wireless Components Letters*, *18*(7), pp.494-496.

47. Kazemi, S., Ghorbani, A., Amindavar, H. and Morgan, D.R., 2016. Vital-Sign Extraction Using Bootstrap-Based Generalized Warblet Transform in Heart and Respiration Monitoring Radar System. *IEEE Transactions on Instrumentation and Measurement*, *65*(2), pp.255-263.

48. Droitcour, A.D., Boric-Lubecke, O., Lubecke, V.M., Lin, J.E.N.S.H.A.N. and Kovacs, G.T., 2003, June. Range correlation effect on ISM band I/Q CMOS radar for non-contact vital signs sensing. In *Microwave Symposium Digest, 2003 IEEE MTT-S International* (Vol. 3, pp. 1945-1948). IEEE.

49. Huang, M.C., Liu, J.J., Xu, W., Gu, C., Li, C. and Sarrafzadeh, M., 2016. A self-calibrating radar sensor system for measuring vital signs. *IEEE transactions on biomedical circuits and systems*, *10*(2), pp.352-363.

50. Li, C., Yu, X., Li, D., Ran, L. and Lin, J., 2009, June. Software configurable 5.8 GHz radar sensor receiver chip in 0.13 μm CMOS for non-contact vital sign detection. In *Radio Frequency Integrated Circuits Symposium, 2009. RFIC 2009. IEEE* (pp. 97-100). IEEE.

51. Li, C., Xiao, Y. and Lin, J., 2007, August. Design guidelines for radio frequency non-contact vital sign detection. In *Engineering in Medicine and Biology Society, 2007. EMBS 2007. 29th Annual International Conference of the IEEE* (pp. 1651-1654). IEEE.

52. Li, C. and Lin, J., 2008, June. Complex signal demodulation and random body movement cancellation techniques for non-contact vital sign detection. In *Microwave Symposium Digest, 2008 IEEE MTT-S International* (pp. 567-570). IEEE.

53. Li, C., Ling, J., Li, J. and Lin, J., 2010. Accurate Doppler radar noncontact vital sign detection using the RELAX algorithm. *IEEE Transactions on Instrumentation and Measurement*, *59*(3), pp.687-695.

54. Rahman, A., Yavari, E., Gao, X., Lubecke, V. and Boric-Lubecke, O., 2015, January. Signal processing techniques for vital sign monitoring using mobile short range Doppler radar. In *Biomedical Wireless Technologies, Networks, and Sensing Systems (BioWireleSS), 2015 IEEE Topical Conference on* (pp. 1-3). IEEE.

55. Gu, C., Li, C., Lin, J., Long, J., Huangfu, J. and Ran, L., 2010. Instrument-based noncontact Doppler radar vital sign detection system using heterodyne digital quadrature demodulation architecture. *IEEE Transactions on Instrumentation and Measurement*, *59*(6), pp.1580-1588.

56. Li, C., Lubecke, V.M., Boric-Lubecke, O. and Lin, J., 2013. A review on recent advances in Doppler radar sensors for noncontact healthcare monitoring. *IEEE Transactions on microwave theory and techniques*, *61*(5), pp.2046-2060.

57. Kao, T.Y.J., Chen, A.Y.K., Yan, Y., Shen, T.M. and Lin, J., 2012, June. A flip-chip-packaged and fully integrated 60 GHz CMOS micro-radar sensor for heartbeat and mechanical vibration detections. In *Radio Frequency Integrated Circuits Symposium (RFIC), 2012 IEEE* (pp. 443-446). IEEE.

58. Li, C. and Lin, J., 2007, January. Optimal carrier frequency of non-contact vital sign detectors. In *Radio and Wireless Symposium, 2007 IEEE* (pp. 281-284). IEEE.

59. Li, C. and Lin, J., 2007, June. Non-contact measurement of periodic movements by a 22-40GHz radar sensor using nonlinear phase modulation. In *Microwave Symposium, 2007. IEEE/MTT-S International* (pp. 579-582). IEEE.

60. Birsan, N. and Munteanu, D.P., 2012, August. Non-contact cardiopulmonary monitoring algorithm for a 24 GHz Doppler radar. In *Engineering in Medicine and Biology Society (EMBC), 2012 Annual International Conference of the IEEE* (pp. 3227-3230). IEEE.

61. Chuang, H.R., Kuo, H.C., Lin, F.L., Huang, T.H., Kuo, C.S. and Ou, Y.W., 2012. 60-GHz millimeter-wave life detection system (MLDS) for noncontact human vital-signal monitoring. *IEEE Sensors Journal*, *12*(3), pp.602-609.

62. Kuo, H.C., Wang, H.H., Wang, P.C., Chuang, H.R. and Lin, F.L., 2011, September. 60-GHz millimeter-wave life detection system with clutter canceller for remote human vital-signal sensing. In *Microwave Workshop Series on Millimeter Wave Integration Technologies (IMWS), 2011 IEEE MTT-S International* (pp. 93-96). IEEE.

63. Kuo, H.C. and Chuang, H.R., 2014, April. Investigation of carrier frequency effect on detection performance of Doppler sensor systems for noncontact human vital-signs sensing. In *Medical Information and Communication Technology (ISMICT), 2014 8th International Symposium on* (pp. 1-4). IEEE.

64. Kao, T.Y.J., Yan, Y., Shen, T.M., Chen, A.Y.K. and Lin, J., 2013. Design and analysis of a 60-GHz CMOS Doppler micro-radar system-in-package for vital-sign and vibration detection. *IEEE Transactions on Microwave Theory and Techniques*, *61*(4), pp.1649-1659.

65. Shen, T.M., Kao, T.Y.J., Huang, T.Y., Tu, J., Lin, J. and Wu, R.B., 2012. Antenna design of 60-GHz micro-radar system-in-package for noncontact vital sign detection. *IEEE Antennas and Wireless Propagation Letters*, *11*, pp.1702-1705.

66. Gao, J., Li, K., Sato, T., Wang, J., Harada, H. and Kato, S., 2009, January. Implementation considerations of patch antenna array for 60GHz beam steering system applications. In *Radio and Wireless Symposium, 2009. RWS'09. IEEE* (pp. 35-38). IEEE.

67. Bakhtiari, S., Elmer, T.W., Cox, N.M., Gopalsami, N., Raptis, A.C., Liao, S., Mikhelson, I. and Sahakian, A.V., 2012. Compact millimeter-wave sensor for remote monitoring of vital signs. *IEEE Transactions on Instrumentation and Measurement*, *61*(3), pp.830-841.

68. Bakhtiari, S., Liao, S., Elmer, T. and Raptis, A.C., 2011. A real-time heart rate analysis for a remote millimeter wave IQ sensor. *IEEE Transactions on Biomedical Engineering*, *58*(6), pp.1839-1845.

69. Petkie, D.T., Benton, C. and Bryan, E., 2009, May. Millimeter wave radar for remote measurement of vital signs. In *Radar Conference, 2009 IEEE* (pp. 1-3). IEEE.

70. Moraitis, N. and Constantinou, P., 2004. Indoor channel measurements and characterization at 60 GHz for wireless local area network applications. *IEEE Transactions on Antennas and Propagation*, *52*(12), pp.3180-3189.

71. Murugan, D., Madhan, M.G. and Piramasubramanian, S., 2012, July. Design and performance prediction of 10GHz micro strip array antenna structures. In *Computing Communication & Networking Technologies (ICCCNT), 2012 Third International Conference on* (pp. 1-5). IEEE.

72. Karnfelt, C., Hallbjorner, P., Zirath, H. and Alping, A., 2006. High gain active microstrip antenna for 60-GHz WLAN/WPAN applications. *IEEE Transactions on Microwave Theory and Techniques*, *54*(6), pp.2593-2603.

73. Biglarbegian, B., Fakharzadeh, M., Busuioc, D., Nezhad-Ahmadi, M.R. and Safavi-Naeini, S., 2011. Optimized microstrip antenna arrays for emerging millimeter-wave wireless applications. *IEEE Transactions on antennas and propagation*, *59*(5), pp.1742-1747.

74. Qasim, A.M. and Rahman, T.A., 2010, November. A compact & high gain series array planar antenna for 60-GHz WPAN applications. In *Applied Electromagnetics (APACE), 2010 IEEE Asia-Pacific Conference on* (pp. 1-5). IEEE.

75. Vettikalladi, H., Lafond, O. and Himdi, M., 2009. High-efficient and high-gain superstrate antenna for 60-GHz indoor communication. *IEEE Antennas and Wireless Propagation Letters*, *8*, pp.1422-1425.

76. Artemenko, Alexey, et al. "Millimeter-wave electronically steerable integrated lens antennas for WLAN/WPAN applications." *IEEE Transactions on Antennas and Propagation* 61.4 (2013): 1665-1671.

77. Verma, L., Fakharzadeh, M. and Choi, S., 2013. Wifi on steroids: 802.11 ac and 802.11 ad. *IEEE Wireless Communications*, *20*(6), pp.30-35.

78. Pan, H.K., Horine, B.D., Ruberto, M. and Ravid, S., 2011, July. Mm-wave phased array antenna and system integration on semi-flex packaging. In *Antennas and Propagation (APSURSI), 2011 IEEE International Symposium on* (pp. 2059-2062). IEEE.

79. Bancroft, R., 2009. *Microstrip and printed antenna design*. The Institution of Engineering and Technology.

80. Nakajima, M., Sudo, K., Fujii, H., Kobayashi, E. and Hiratsuka, T., 2012, December. A wideband 60GHz chip antenna. In *Microwave Conference Proceedings (APMC), 2012 Asia-Pacific* (pp. 328-330). IEEE.

81. Lu, B., Luo, J., Zhang, L., Zhang, L., Yue, R. and Wang, Y., 2014, June. A patch antenna array for 60-GHz WPAN based on polypropylene composite substrate. In *Electron Devices and Solid-State Circuits (EDSSC), 2014 IEEE International Conference on* (pp. 1-2). IEEE.

82. Al Henawy, M., Richter, M.D. and Schneider, M., 2010, March. New thermoplastic polymer substrate for microstrip antennas at 60 GHz. In *German Microwave Conference, 2010* (pp. 5-8). IEEE.

83. Wang, L., Guo, Y.X. and Sheng, W.X., 2013. Wideband high-gain 60-GHz LTCC L-probe patch antenna array with a soft surface. *IEEE Transactions on Antennas and Propagation*, *61*(4), pp.1802-1809.

84. Cui, H., Zhang, T., Sun, Y., Li, L., Qian, R. and Sun, X., 2010, May. Implementation of CPW-feed patch/slot antennas for 60GHz system applications. In *Microwave and*

Millimeter Wave Technology (ICMMT), 2010 International Conference on (pp. 1883-1886). IEEE.

85. Liu, H., He, Y. and Wong, H., 2013, August. Printed U-slot patch antenna for 60GHz applications. In *Electromagnetics (iWEM), 2013 IEEE International Workshop on* (pp. 153-155). IEEE.

86. Gao, J., Li, K. and Harada, H., 2011, July. 60 GHz wideband antena with air filled stacked patch structure. In *Antennas and Propagation (APSURSI), 2011 IEEE International Symposium on* (pp. 634-637). IEEE.

87. Rabbani, M.S. and Ghafouri-Shiraz, H., 2014, October. Simple methods for enhancing bandwidth of a rectangular microstrip patch antenna. In *Active and Passive RF Devices Seminar, 2nd IET Annual* (pp. 1-4). IET.

88. Adane, A., Gallée, F. and Person, C., 2010, April. Bandwidth improvements of 60GHz micromachining patch antenna using gap coupled U—Microstrip feeder. In *Antennas and Propagation (EuCAP), 2010 Proceedings of the Fourth European Conference on* (pp. 1-5). IEEE.

89. Luk, K.M. and Li, M., 2013, November. Magneto-electric dipole antennas for millimeter-wave applications. In *Microwave Conference Proceedings (APMC), 2013 Asia-Pacific* (pp. 304-306). IEEE.

90. Ullah, U., Mahyuddin, N., Arifin, Z., Abdullah, M.Z. and Marzuki, A., 2015. Antenna in LTCC technologies: a review and the current state of the art. *IEEE Antennas and Propagation Magazine*, *57*(2), pp.241-260.

91. Sun, M., Guo, Y.X., Karim, M.F. and Ong, L.C., 2010, July. Linearly polarized and circularly polarized arrays in ltcc technology for 60ghz radios. In *Antennas and*

Propagation Society International Symposium (APSURSI), 2010 IEEE (pp. 1-4). IEEE.

92. Madhav, B.T.P., Pisipati, V.G.K.M., Kumar, K.S., Khan, H., Rakesh, D., Ratnam, T.A., Atulya, D. and Sreyash, P., 2011. Comparative study of microstrip rectangular patch array antenna on liquid crystal polimer and RT Duroid substrates. *International Journal of Electronics and Communication Engineering*, *4*(2), pp.161-167.

93. Kingsley, N., 2008. Liquid crystal polymer: enabling next-generation conformal and multilayer electronics. *Microwave Journal*, *51*(5), p.188.

94. Jha, K.R. and Singh, G., 2014. Design of Highly Directive Cavity-Type Terahertz Antenna. In *Terahertz Planar Antennas for Next Generation Communication* (pp. 107-124). Springer International Publishing.

95. Hosseini, A., Capolino, F. and De Flaviis, F., 2015. Gain enhancement of a V-band antenna using a Fabry-Pérot Cavity with a self-sustained all-metal cap with FSS. *IEEE Transactions on Antennas and Propagation*, *63*(3), pp.909-921.

96. Dheyab, E. and Qasem, N., 2016. Design and Optimization of Rectangular Microstrip Patch Array Antenna Using Frequency Selective Surfaces for 60 GHz. *International Journal of Applied Engineering Research*, *11*(7), pp.4679-4687.

97. Coulibaly, Y., Nedil, M., Talbi, L. and Denidni, T.A., 2012. Design of high gain and broadband antennas at 60 GHz for underground communications systems. *International Journal of Antennas and Propagation*, *2012*.

98. Jha, K.R. and Singh, G., 2013. Analysis of the Effect of Ground Plane Size on the Performance of a Probe-fed Cavity Resonator Microstrip Antenna. *Wireless personal communications*, *71*(2), pp.1511-1521.

99. Konstantinidis, K., Feresidis, A.P., Tian, Y., Shang, X. and Lancaster, M.J., 2015. Micromachined terahertz Fabry–Perot cavity highly directive antennas. *IET Microwaves, Antennas & Propagation*, *9*(13), pp.1436-1443.

100. Nguyen, T.K., Rotermund, F. and Ikmo, P., 2014, July. Leaky-wave slit antenna incorporated with a frequency selective surface for terahertz application. In *Radio Science Meeting (Joint with AP-S Symposium), 2014 USNC-URSI* (pp. 317-317). IEEE.

101. Chiu, C.H., Tatung Company, 2008. *Partially reflective surface antenna*. U.S. Patent 7,319,429.

102. Feresidis, A.P. and Vardaxoglou, J.C., 2001. High gain planar antenna using optimised partially reflective surfaces. *IEE Proceedings-Microwaves, Antennas and Propagation*, *148*(6), pp.345-350.

103. Alonso-DelPino, M., Llombart, N., Chattopadhyay, G., Lee, C., Jung-Kubiak, C., Jofre, L. and Mehdi, I., 2013. Design guidelines for a terahertz silicon micro-lens antenna. *IEEE Antennas and Wireless Propagation Letters*, *12*, pp.84-87.

104. Artemenko, A., Maltsev, A., Mozharovskiy, A., Sevastyanov, A., Ssorin, V. and Maslennikov, R., 2013. Millimeter-wave electronically steerable integrated lens antennas for WLAN/WPAN applications. *IEEE Transactions on Antennas and Propagation*, *61*(4), pp.1665-1671.

105. Chan, C.H., Ng, K.B. and Qu, S.W., 2015. March. Gain enhancement for low-cost terahertz fresnel zone plate lens antennas. In *Antenna Technology (iWAT), 2015 International Workshop on* (pp. 66-69). IEEE.

106. Nguyen, T.K., Rotermund, F. and Ikmo, P., 2014, July. Leaky-wave slit antenna incorporated with a frequency selective surface for terahertz application. In *Radio*

Science Meeting (Joint with AP-S Symposium), 2014 USNC-URSI (pp. 317-317). IEEE.

107. Hosseini, A., Capolino, F. and De Flaviis, F., 2015. Gain enhancement of a V-band antenna using a Fabry-Pérot Cavity with a self-sustained all-metal cap with FSS. *IEEE Transactions on Antennas and Propagation*, *63*(3), pp.909-921.

108. Dheyab, E. and Qasem, N., 2016. Design and Optimization of Rectangular Microstrip Patch Array Antenna Using Frequency Selective Surfaces for 60 GHz. *International Journal of Applied Engineering Research*, *11*(7), pp.4679-4687.

109. Coulibaly, Y., Nedil, M., Talbi, L. and Denidni, T.A., 2012. Design of high gain and broadband antennas at 60 GHz for underground communications systems. *International Journal of Antennas and Propagation*, *2012*.

110. Jha, K.R. and Singh, G., 2014. Design of Highly Directive Cavity-Type Terahertz Antenna. In *Terahertz Planar Antennas for Next Generation Communication* (pp. 107-124). Springer International Publishing.

111. Feresidis, A.P. and Vardaxoglou, J.C., 2001. High gain planar antenna using optimised partially reflective surfaces. *IEE Proceedings-Microwaves, Antennas and Propagation*, *148*(6), pp.345-350.

112. Konstantinidis, K., Feresidis, A., Constantinou, C., Gashinova, M., Hoare, E., Lancaster, M. and Gardner, P., 2016, June. A THz dielectric lens antenna. In *Antennas and Propagation (APSURSI), 2016 IEEE International Symposium on* (pp. 1493-1494). IEEE.

113. Pan, W. and Zeng, W., 2016. Far-field characteristics of the square grooved-dielectric lens antenna for the terahertz band. *Applied Optics*, *55*(26), pp.7330-7336.

114. Banik, B.K., Vukusic, J., Merkel, H. and Stake, J., 2008. A novel catadioptric dielectric lens for microwave and terahertz applications. *Microwave and Optical Technology Letters*, *50*(2), pp.416-419.

115. Boriskin, A.V., Sauleau, R. and Nosich, A.I., 2009. Performance of hemielliptic dielectric lens antennas with optimal edge illumination. *IEEE Transactions on Antennas and Propagation*, *57*(7), pp.2193-2198.

116. Llombart, N., Lee, C., Alonso-delPino, M., Chattopadhyay, G., Jung-Kubiak, C., Jofre, L. and Mehdi, I., 2013. Silicon micromachined lens antenna for THz integrated heterodyne arrays. *IEEE Transactions on Terahertz Science and Technology*, *3*(5), pp.515-523.

117. Ma, R., Zheng, P., Luo, M., Wen, Z. and Sun, H., 2014, July. Design of W band dual polarized microstrip patch antenna. In *Antennas and Propagation (APCAP), 2014 3rd Asia-Pacific Conference on* (pp. 543-546). IEEE.

118. Breed, G., 2008. An introduction to defected ground structures in microstrip circuits. *High Frequency Electronics*, *7*, pp.50-54.

119. Wang, C.J. and Lin, C.S., 2008. Compact DGS resonator with improvement of Q-factor. *Electronics Letters*, *44*(15), pp.908-910.

120. Raval, F., Kosta, Y.P., Makwana, J. and Patel, A.V., 2013, April. Design & implementation of reduced size microstrip patch antenna with metamaterial defected ground plane. In *Communications and Signal Processing (ICCSP), 2013 International Conference on* (pp. 186-190). IEEE.

121. Arya, A.K., Kartikeyan, M.V. and Patnaik, A., 2010, September. On the size reduction of microstrip antenna with DGS. In *Infrared Millimeter and Terahertz Waves (IRMMW-THz), 2010 35th International Conference on* (pp. 1-3). IEEE.

122. Chung, Y., Jeon, S.S., Kim, S., Ahn, D., Choi, J.I. and Itoh, T., 2004. Multifunctional microstrip transmission lines integrated with defected ground structure for RF front-end application. *IEEE Transactions on Microwave Theory and Techniques*, *52*(5), pp.1425-1432.

123. Zhu, F., Gao, S., Ho, A.T., Abd-Alhameed, R.A., See, C.H., Brown, T.W., Li, J., Wei, G. and Xu, J., 2013. Multiple band-notched UWB antenna with band-rejected elements integrated in the feed line. *IEEE Transactions on Antennas and Propagation*, *61*(8), pp.3952-3960.

124. Tirado-Mendez, J.A., Jardon-Aguilar, H., Flores-Leal, R., Andrade-Gonzalez, E.A. and Iturbide-Sanchez, F., 2010. Improving frequency response of microstrip filters using defected ground and defected microstrip structures. *Progress In Electromagnetics Research C*, *13*, pp.77-90.

125. Abbaspour-Tamijani, A., Rizk, J. and Rebeiz, G., 2002. Integration of filters and microstrip antennas. In *Antennas and Propagation Society International Symposium, 2002. IEEE* (Vol. 2, pp. 874-877). IEEE.

126. Lin, C.K. and Chung, S.J., 2011. A filtering microstrip antenna array. *IEEE Transactions on Microwave Theory and Techniques*, *59*(11), pp.2856-2863.

127. Chen, X., Zhao, F., Yan, L. and Zhang, W., 2013. A compact filtering antenna with flat gain response within the passband. *IEEE Antennas and Wireless Propagation Letters*, *12*, pp.857-860.

128. Zuo, S., Wu, W.J. and Zhang, Z.Y., 2013. A simple filtering-antenna with compact size for WLAN application. *Progress In Electromagnetics Research Letters*, *39*, pp.17-26.

129. Hizan, H.M., Hunter, I.C. and Abunjaileh, A.I., 2010, September. Integrated SIW filter and microstrip antenna. In Microwave Conference (EuMC), 2010 European (pp. 184-187). IEEE.

Chapter-3

Size Improvement of Microstrip Patch Antenna at Millimetre-wave and Terahertz Frequencies

Abstract: In this chapter, a method has been introduced to increase the size of MPA at mm-wave and THz frequencies for improved fabrication tolerance and performance. The method is experimentally tested at 56GHz frequency. The antenna's overall performance is also improved as compared to the conventional MPA. The proposed method is used to design MPA arrays at THz frequencies of 835GHz, 635GHz and 100GHz. The antenna arrays at 835GHz and 635GHz frequencies may be deployed for medical applications including cancer detection through THz spectroscopy techniques and vital sign detection through Doppler radar or on-body techniques. A prototype antenna array at 100GHz frequency has been fabricated and tested, to verify the proposed designing approach. The measured and simulation results of the tested antennas showed good agreement.

3.1. Introduction

Microstrip antenna is one of the most popular antennas in modern wireless communications due to its attractive features including compact size, low cost, reasonable gain and compatibility with planner technology [1-3]. These patch antennas' properties become more advantageous when they are designed for mm-wave and THz frequency bands [4-16]. However, at mm-wave and THz frequencies the patch antenna and its matching microstrip feeding line dimensions fall below the fabrication limit of 152μm when the conventional PCB etching technique is employed [3,17-20]. This problem is even rigorous when a high gain patch antenna array is designed to compensate the radio link budget across extensively high

free space path losses at the mentioned high frequencies [14-16]. Thus, for a cost-effective production, structural simplicity and size improvement of MPA at mm-wave and THz frequencies are highly desirable [21-23]. In order to meet these demands, a detailed analysis of patch antenna's size improvement for mm-wave and THz frequency bands is presented [21]. The proposed method is applied to design, fabricate and test MPA at 56GHz [21]. The proposed method is then employed to design MPA arrays at 835GHz, 635GHz and 100GHz frequencies recommended for medical applications like cancer detection through THz spectroscopy [24, 25] and remote vital sign detection through Doppler radar and on-body methods [26]. A prototype antenna array designed at 100GHz frequency has been fabricated and tested to approve the proposed methodology. Good agreement between the measured and simulation results has been achieved in all the cases.

3.2. Size Improvement Method for MPA Design

Figure 3.1 shows the geometry and parameters of an ordinary MPA. A conventional rectangular patch antenna with length L resonates and radiates efficiently when $L=\lambda/2$, where λ is the operating wavelength [3]. Fig. 3.2 (a) shows that when $L=\lambda/2$ the electric field (E-field) is in-phase along the patch length. Fig. 3.2 (b) indicates that the E-field is maximum but with opposite polarity under the two edges of the patch where it extends out because of the fringing field effect [27]. The current and voltage distributions along the patch antenna of length $L=\lambda/2$ is shown in Fig. 3.2(c). The current is zero at the patch edges, where the voltage is maximum and opposite. These are the basic electrical properties required for a patch antenna to resonate and radiate at a desired frequency [21].

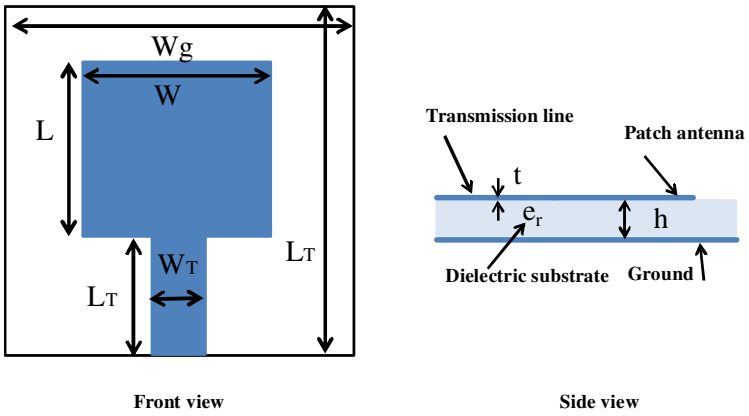

Fig. 3.1. Geometry of a rectangular microstrip patch antenna

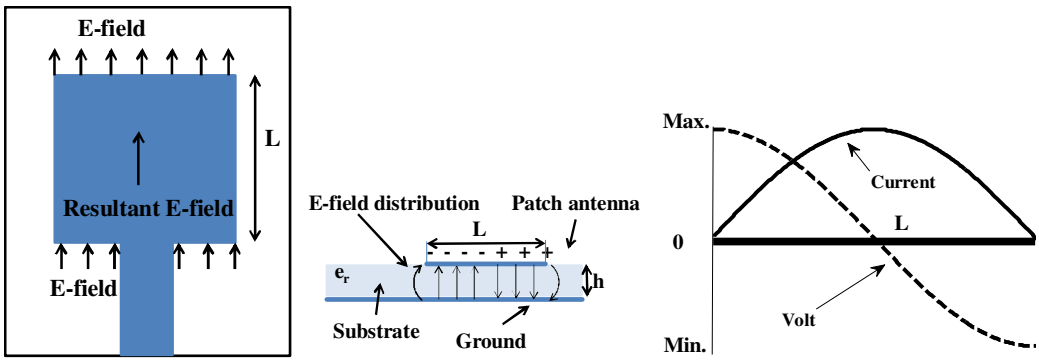

(a) (b) (c)

Fig. 3.2. Electric field distribution in a MPA (a) top view (b) side view and (c) current and voltage wave-forms along the antenna length

Figure. 3.3 represents the voltage and current relation along the patch length where $0 < L \leq 3\lambda$. The arrows in Fig. 3.3 highlight the patch lengths (i.e. $\lambda/2$, $3\lambda/2$ and $5\lambda/2$) at which the voltage and the current relations on the patch edges satisfy the antenna working conditions as shown in Fig. 3.2(c). Hence, ideally the required electric field distribution on a patch antenna can be achieved when patch antenna length $L = (2N+1)\lambda/2$ where N=0, 1, 2… i.e. an odd multiple of the operating half-wavelength [21].

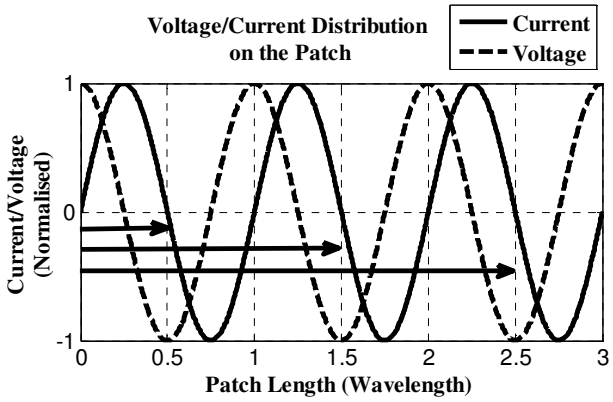

Fig. 3.3. Voltage and current distribution along the patch antenna length $0 < L \leq 3\lambda$.

However, in practice, due to the fringing field effect (see Fig.2b) the extension of patch antenna length 'ΔL' needs to be taken into account [3]. The patch width 'W' is suggested to extend with the same factor as used for the patch length to enhance the antenna gain and to reduce the input impedance which is helpful to widen the transmission line (TL) width in the feeding and matching network [22, 23]. Therefore, a patch antenna can function efficiently when its length and width satisfy the following conditions [21]:

$$W = \frac{(2M+1)}{\sqrt{\frac{\varepsilon_r + 1}{2}}}(\lambda_0/2) \qquad (3.1)$$

$$L = \frac{(2N+1)}{\sqrt{\varepsilon_{eff}}} \times \lambda_0/2 - 2\Delta L \qquad (3.2)$$

where M and N are non-negative integers, ε_{eff} and ε_r are the effective and relative dielectric constants, respectively, and λ_0 is the free space wavelength. In order to minimise the surface wave effect in the dielectric material, the upper limit of the substrate thickness 'h' is set as [29]:

$$h < \lambda_0 / (4\sqrt{\varepsilon_{eff}}) \qquad (3.3)$$

Hence, based on eqs. (3.1) and (3.2) the patch width and length can be increased to resonate and radiate efficiently at a desired frequency. However, the drawback of this method is that if higher values of integers M and N is used in the above equations, the antenna may produce unwanted resonances at frequencies related to the lower multiples of λ/2. This problem can be rectified by proper selection of the smallest values of M and N in eqs. (3.1) and (3.2) so that at the desired frequency the antenna dimensions are above the fabrication limit. Also, by properly matching the antenna input impedance with the standard 50Ω at the desired oscillation frequency the unwanted resonances can be further minimised. The TL width 'W_T' is computed based on the antenna's total input impedance 'Z_a' which is approximated as [3]:

$$Z_a = \frac{59.81\lambda_0}{W} \qquad (3.4)$$

Ultimately, Za is matched with the standard 50Ω impedance through TL impedance transformer with the characteristic impedance $Z_0 = \sqrt{50 \times Z_a}$. This way, W_T is computed as [30]:

$$W_T = \frac{7.475\,h}{e^x} - 1.25t \qquad (3.5)$$

where $x = \left(Z_0\sqrt{\varepsilon_r + 1.41}\right)/87$ and h and t are the substrate thickness and copper cladding, respectively (see Fig. 3.1). Since the TL length 'L_T' provides impedance transformation, it is calculated with the following formula [22]:

$$L_T = (2P+1)\times\frac{\lambda}{4} \qquad (3.6)$$

where P is an integer. Furthermore, improved size MPA arrays can be constructed with the proposed patch elements as illustrated in Fig. 3.4. In that case, eq. (3.4) is modified for the input impedance of 'n' number of symmetrical patch elements fed in series as follows [23]:

$$Z_a = \frac{59.81\lambda_0}{nW} \qquad (3.7)$$

Moreover, since phase matching is vital on the patch elements for a constructive signal phase-front in high gain antenna arrays, the separation between the successive patch elements 'L_{T1}' are calculated as [23]:

$$L_{T1} = (2Q+1)\times\frac{\lambda}{2} + 2\Delta L \qquad (3.8)$$

Where Q is an integer. Consequently, the TL width 'W_{T1}' does not affect the array's total input impedance due to the half-wavelength (or its odd multiples) phase shift in the signal along the patch elements. However, W_{T1} can be adjusted to control the impedance and hence the power weighting on the patch elements if lobes grating is required in the arrays far-field radiation beams [3]. Finally, the MPA dimensions obtained from the above equations may be optimised with the help of CST Microwave Studio for the antenna's best performance.

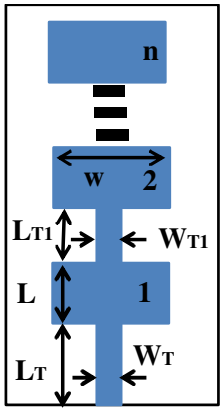

Fig. 3.4. Improved size MPA array

3.3. 56GHz Antenna Results and Discussions

Initially, a MPA is designed at 56GHz using the conventional method given in [3] on RT/Duroid5880 substrate with ε_r=2.2, and t=17µm. The calculated antenna dimensions are listed in Table 3.1. In this design, the size of W_T=60µm which is far below the PCB etching limit of 152µm. Fig. 3.5(a) and (b) show the simulated return loss (S_{11}) response and far-field radiation pattern (FRP), respectively. The antenna S_{11} at 56GHz, -10dB S_{11} bandwidth (BW) and gain are –29.3dB, 1.82GHz and 7.7dBi, respectively. The antenna is then re-designed on the same substrate material using the size improvement method as explained in section 3.2 and N=M=1 are set in eqs. (3.1) and (3.2) and P=1 in (3.6). The new extended size antenna's dimensions are listed in Table 3.1 which clearly indicates that the antenna size has significantly increased and W_T is now well above the fabrication limit.

Table 3.1. Dimensions in mm of the designed 60GHz patch antennas

Dimensions	L	W	L_T	W_T	h
Conventional MPA	1.545	2.12	0.99	0.06	0.17
Improved size MPA	5.587	6.114	5.095	1.443	0.508

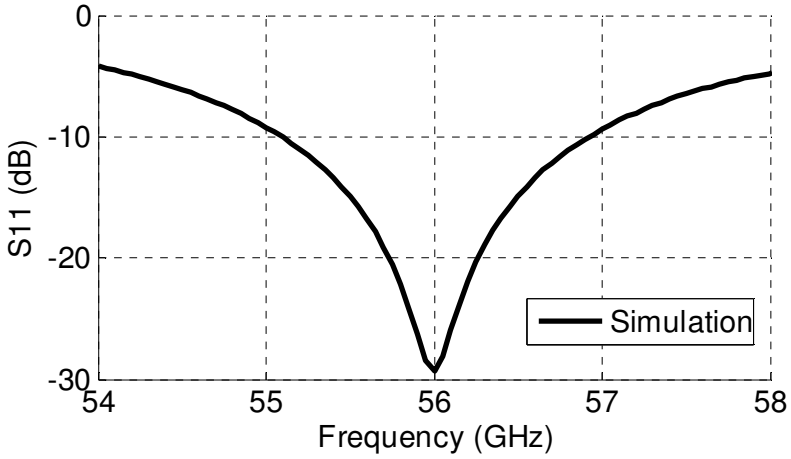

(a)

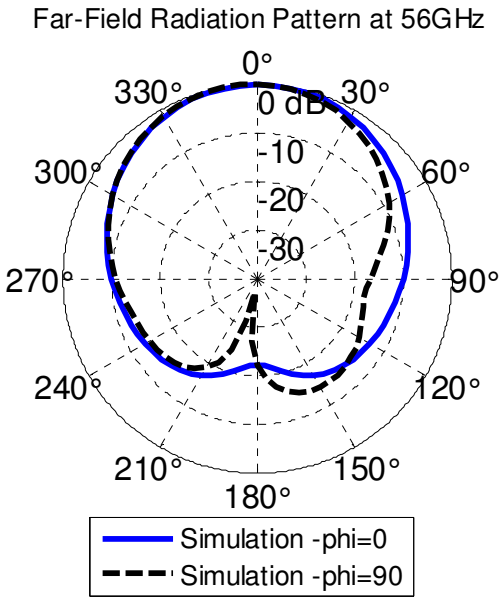

(b)

Fig. 3.5. Conventional MPA simulation results. (a) S_{11} and (b) FRP in H-plane (phi=0^0) and E-plane (phi-90^0) at 56GHz

The antenna is tested with the Rohde & Schwarz 67GHz VNA "ZVA 67" through a V-connector and Glass Bead as shown in Fig. 3.6(a). The central pin of the Glass Bead is connected to the feeding microstrip TL whereas the grounded outer shell of the Glass Bead is soldered with antenna's back side copper cladding. The Glass Bead's is included in the

antenna's CST simulation and a waveguide port is created at the starting end of Glass Bead for feeding purpose which produced 50Ω input impedance, as shown in Fig. 3.6(a). The proposed extended size MPA's simulation model, fabricated prototype, simulated and measured $S_{11,}$ and FRP in both E and H planes are shown in Figs. 3.6(a)-(e), respectively, where it can be seen that in all the cases simulation and measured results are in good agreement.

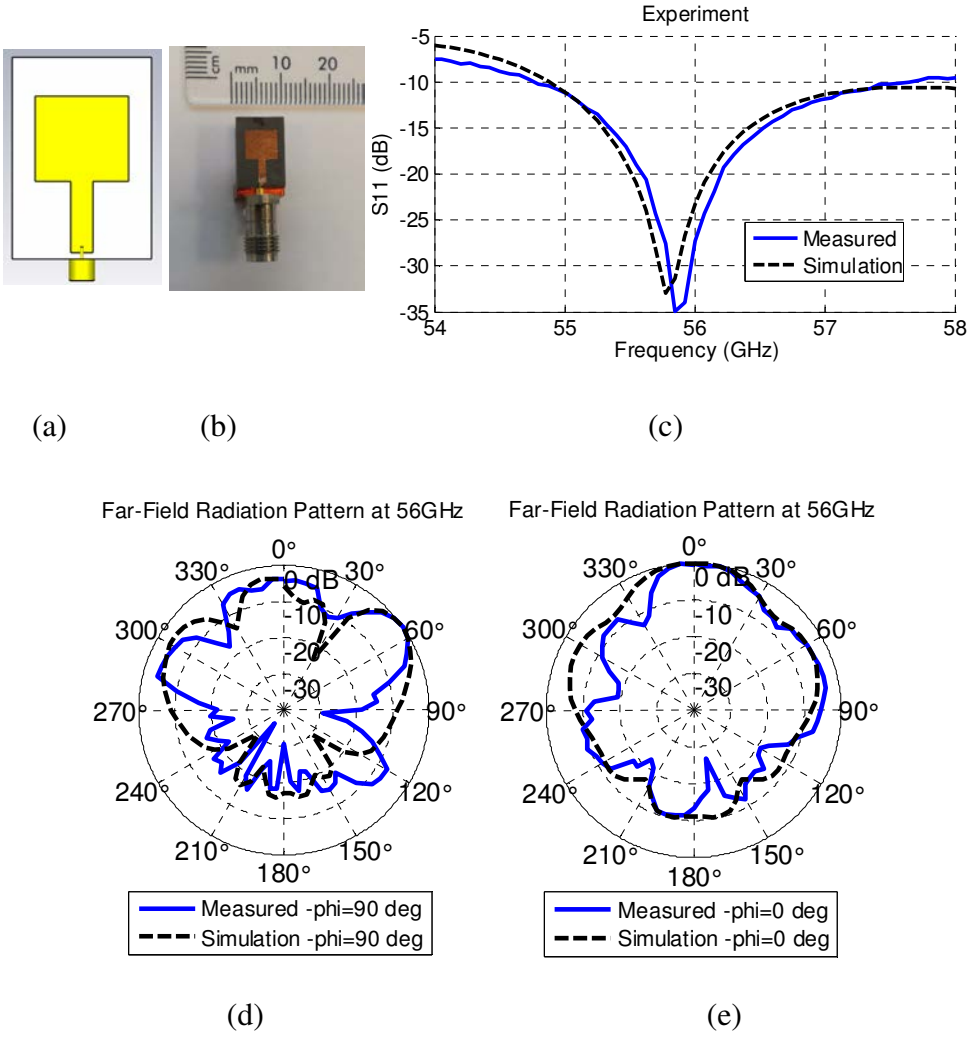

(a) (b) (c)

(d) (e)

Fig. 3.6. (a) Simulated antenna model and (b) fabricated prototype using size extension method, and (c) The S_{11} and FRP in (d) E-plane (phi-90^0) and (e) H-plane (phi=0^0) at 56GHz

The antenna's measured gain and BW are 9dBi and 2.85GHz (i.e. 5.1% of the central frequency of 55.93GHz. It can be noticed from Fig. 3.6(c) that the FRP of the extended size MPA shown in Fig. 3.6(a) has three directional beams at about -60^0, 0^0 and $+60^0$, which may be useful for emerging wireless applications like high speed short distance wireless communications as described in [6, 31].

In order to validate the CST Microwave Studio based simulation results, some analysis has been carried out on the convergence of S11 results of the antenna presented in Fig. 3.6. Fig. 3.7 illustrates the antenna's S11 results for various number of mesh lines per wavelength (MLPW) set in CST simulator where it can be seen that the results start converging when MLPW reaches to about 10. Since some sensitivity is involved between the simulation and measured results due to the fabrication and assembling tolerances, as mentioned in chapter 1, it has been found that MLPW of 10 can yields the antenna results with reasonably good accuracy.

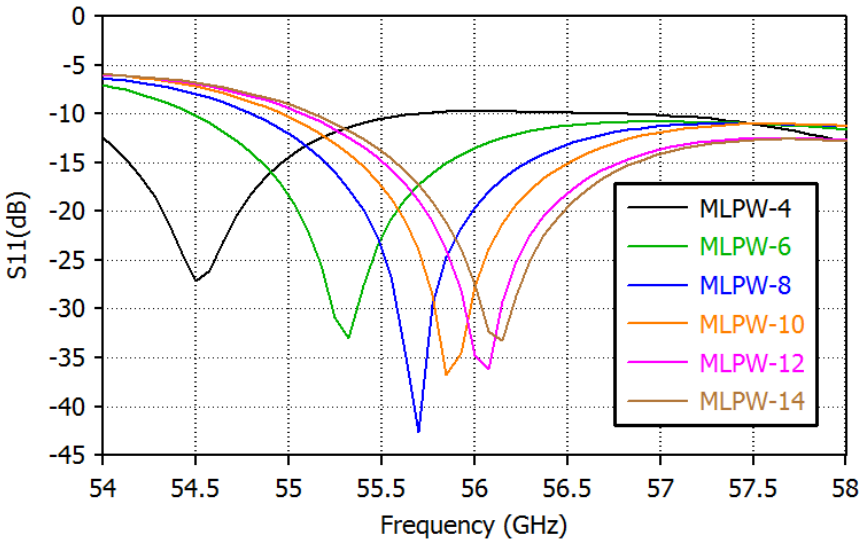

Fig. 3.7. 56GHz antenna's S11 simulation results' accuracy

3.4 MPA Array Design based on the Size Extension Method at THz Frequencies

Since a thin PCB substrate is required for MPA array designs at THz frequencies (see eq. (3.3)), Liquid Crystalline Polymer (LCP) substrate with ε_r=2.91 and loss tangent tan(δ)=0.0025 (measured at 10GHz) is proposed for MPA array designs at THz frequencies. It may worth to mention that the loss tangent values of the LCP material could be significantly different at mm-wave and THz frequency which could contribute towards the results deviation from the expectations. Nevertheless, LCP material exhibits better electrical performance at THz frequencies as compared to RT/Duroid material and also it is commercially available with very small substrate thickness of 25μm which is theoretically applicable for MPA design up to around 1.776THz with negligibly small SW effect [22, 32].

Three MPA arrays are designed at 835GHz, 635GHz and 100GHz frequencies on LCP substrates based on the method explained in section 3.2. The design frequencies of 835GHz and 635GHz are located within the THz transmission windows where the free space path losses are comparatively low [33] and they are recommended for biomedical applications such as liver and skin cancer detection through THz spectroscopy [24, 25]. The optimised dimensions of the arrays are shown in Table 3.2, where it can be seen that in all cases the antennas' dimensions fall within the ordinary PCB etching limit. Figs. 3.8-3.10 present the simulation results of 835GHz, 635GHz and 100GHz antennas, respectively, where (a)-(c) show S_{11}, 3-D and 2-D FRP, respectively [22].

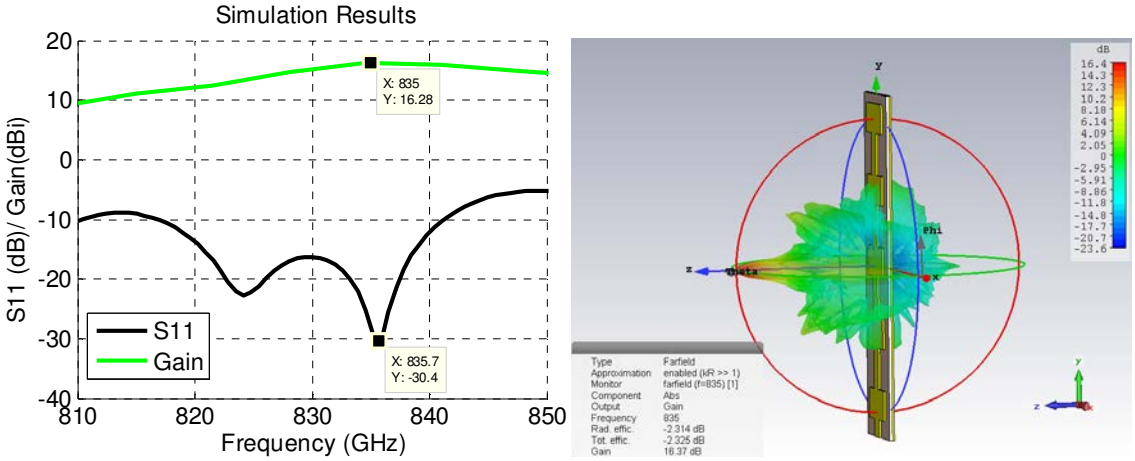

(a) (b)

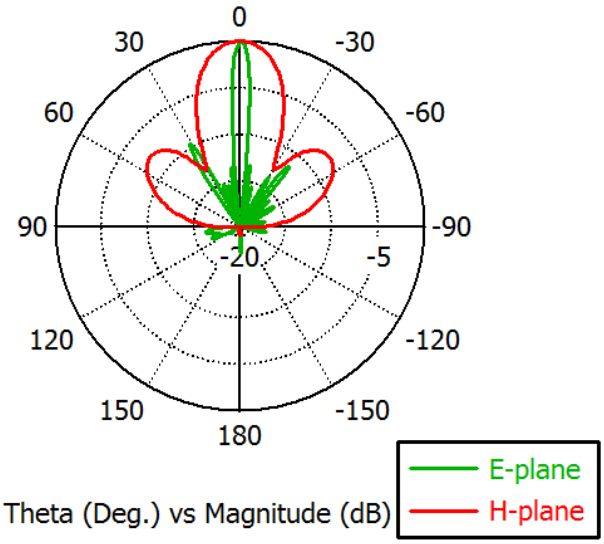

(c)

Fig. 3.8. Simulation results of 835GHz antenna. (a) S_{11}, and FRP at 835GHz (b) in 3-D and (c) in 2-D

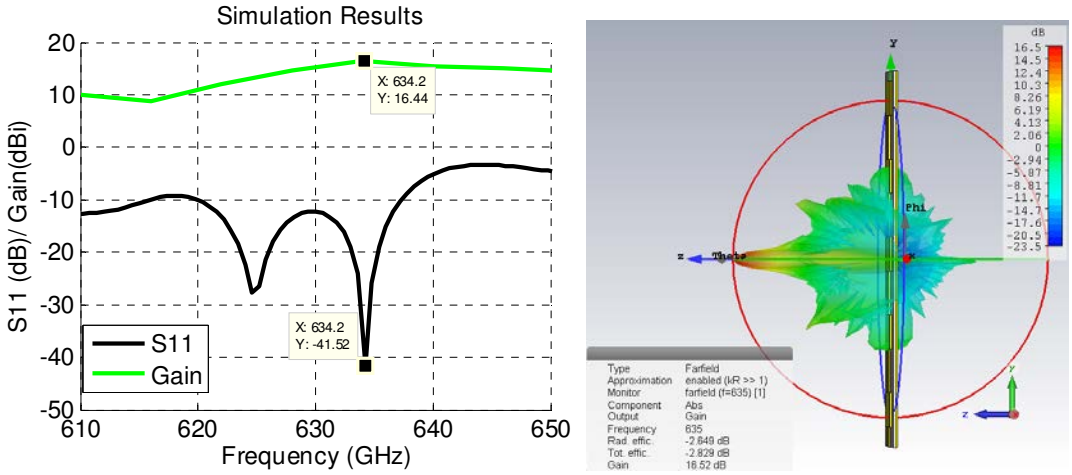

(a) (b)

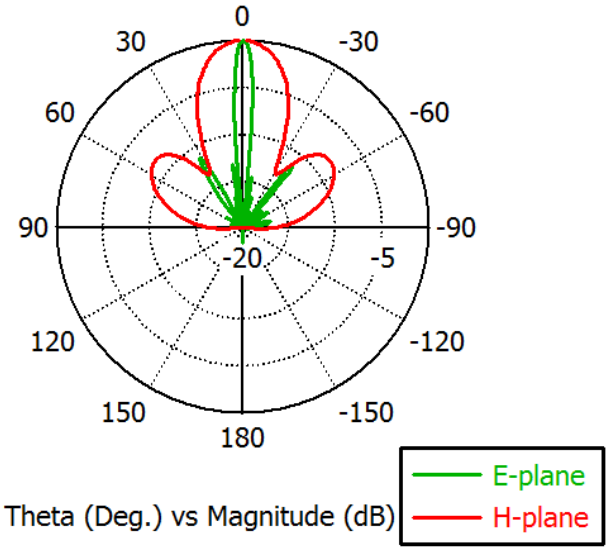

Fig. 3.9. Simulation results of 635GHz antenna. (a) S_{11}, and FRP at 635GHz (b) in 3-D and (c) in 2-D

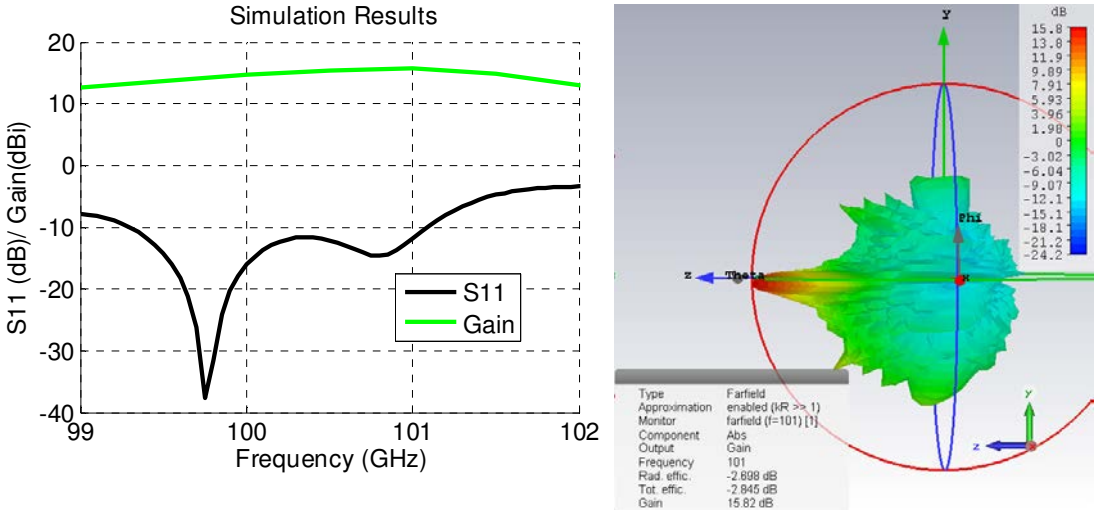

(a) (b)

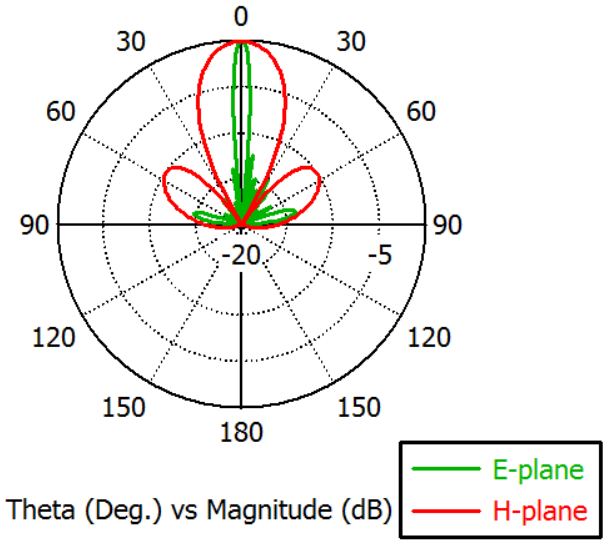

Fig. 3.10. Simulation results of 100GHz antenna. (a) S_{11}, and FRP at 101GHz (b) in 3-D and (c) in 2-D

Table 3.2 Dimensions in μm of the designed THz MPA arrays

Antenna	L	W	L_{T1}	L_{T2}	W_{T1}	h	t
835GHz	260	460	158	337	150	25	18
635GHz	360	590	210	438	182	25	18
100GHz	2489	3078	1293	2685	690	100	9

The simulated performance parameters of the designed MPA arrays are depicted in Table 3.3 where it can be noticed that their fractional bandwidth (FBW) and gain values are in the range of 1.8%-2.93% and 15.82dBi-16.5dBi, respectively, and their efficiency values are within 52%-58% range. However, for the medical applications mentioned earlier, the obtained antenna efficiencies may not be concerned because the antennas have only an instant use for the detection process [24, 25] and they have sufficiently high gain (>15.5dBi) for a short distance (<1m) transmission with a transmitted power of 0dBm and receiver sensitivity of -60dB at 835GHz [3, 22].

Table 3.3 Antenna arrays performance

Antenna	BW(GHz)	FBW (%)	Gain(dBi)	Efficiency (%)
835GHz	24.3	2.93	16.37	58.4
635GHz	17.3	2.75	16.52	52
100GHz	1.8	1.8	15.82	52

In order to practically validate the proposed antenna array designing concept, the MPA array designed at 100GHz has been fabricated and tested. The fabricated antenna and the experimental setup are revealed in Figs. 3.11(a) and (b), respectively. The antenna is connected to the VNA module through 1-mm flange launcher as shown in Fig. 3.11(b). 1-mm flange launcher is an air filled low loss (<0.7dB) coaxial waveguide connector with a gold plated metallic body suitable up to 110GHz frequencies [22].

Fig. 3.12 shows the simulated and measured results of the tested 100GHz antenna array where (a) and (b) are S_{11} and FRP at the central resonant frequency of 100.5GHz, respectively. Figs. 3.12(a) and (b) indicate that the measured S_{11} and FRP results have fair agreement with the

simulation results. A small non-symmetry in E plane FRP may be due to the reflections from the coaxial connector's body. As seen from Fig. 3.12(a), the simulated S_{11} shows two resonances around 100GHz meanwhile in the measured S_{11} response, these resonances are shifted further closer to each other due to the imperfections in the connecting fixture and the soldering. From Fig. 3.11(a) it is clear that the measured minimum S_{11} is -26.04dB at 100.5GHz and -10dB S_{11} BW is 2.24GHz (FBW=2.23%). The measured antenna gain is 15.7dBi at 100.5GHz frequency which is fairly close to the simulated gain of 15.82dBi.

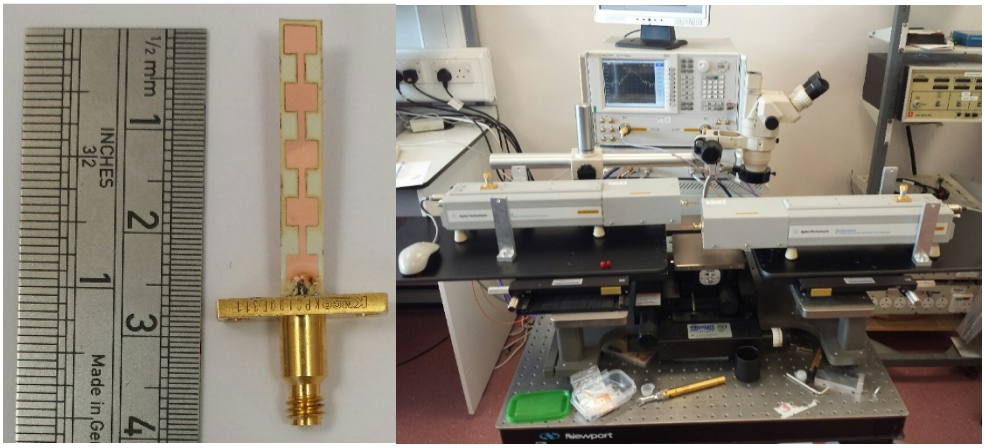

(a) (b)

Fig. 3.11. (a) Fabricated 100GHz antenna array and (b) experiment setup

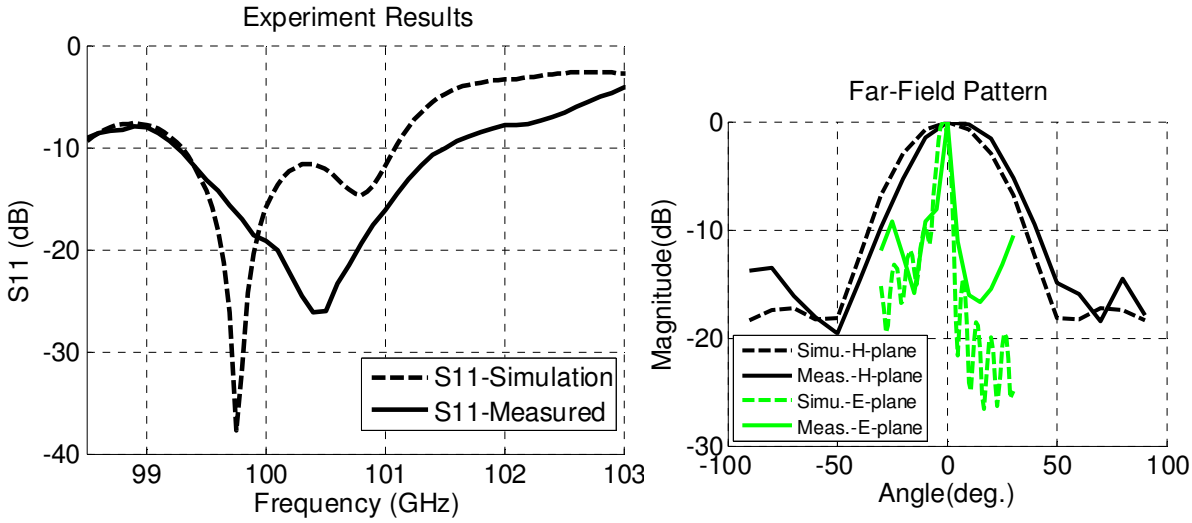

(a) (b)

Fig. 3.12. Simulation and measured results of the 100GHz antenna array. (a) S_{11} and (b) FRP in E and H planes

3.5 Conclusion

A method has been presented to enlarge the dimensions of MPAs for mm-wave and THz frequency applications in order to satisfy the fabrication constraints imposed by the etching technique and also to enhance the antenna performance. To practically verify the method, a MPA is designed and tested at 56GHz frequency. It has been revealed that the designed 56GHz antenna acquired physical dimensions remarkably larger than those obtained by the conventional method and its overall performance is significantly improved. Finally, the MPA size extension method has been used to design patch antenna arrays for medical applications at THz frequencies where the dimension of the conventional MPA are not fabricable with the cost-effective etching method.

3.6 References

1. Balanis, C.A. ed., 2011. *Modern antenna handbook*. John Wiley & Sons.
2. Pozar, D.M., 2009. *Microwave engineering*. John Wiley & Sons.
3. Bancroft, R., 2009. *Microstrip and printed antenna design*. The Institution of Engineering and Technology.
4. Alam, M.S., Islam, M.T., Misran, N. and Mandeep, J.S., 2013. A Wideband Microstrip Patch Antenna for 60 GHz Wireless Applications. *Elektronika ir Elektrotechnika*, *19*(9), pp.65-70.
5. Karnfelt, C., Hallbjorner, P., Zirath, H. and Alping, A., 2006. High gain active microstrip antenna for 60-GHz WLAN/WPAN applications. *IEEE Transactions on Microwave Theory and Techniques*, *54*(6), pp.2593-2603.
6. Huang, K.C. and Wang, Z., 2011. Terahertz terabit wireless communication. *IEEE Microwave Magazine*, *12*(4), pp.108-116.

7. Akyildiz, I.F., Jornet, J.M. and Han, C., 2014. Terahertz band: Next frontier for wireless communications. *Physical Communication*, *12*, pp.16-32.
8. Koenig, S., Lopez-Diaz, D., Antes, J., Boes, F., Henneberger, R., Leuther, A., Tessmann, A., Schmogrow, R., Hillerkuss, D., Palmer, R. and Zwick, T., 2013. Wireless sub-THz communication system with high data rate. *Nature Photonics*, *7*(12), pp.977-981.
9. Woolard, D.L., Brown, R., Pepper, M. and Kemp, M., 2005. Terahertz frequency sensing and imaging: A time of reckoning future applications?. *Proceedings of the IEEE*, *93*(10), pp.1722-1743.
10. Nishizawa, J.I., Sasaki, T., Suto, K., Yamada, T., Tanabe, T., Tanno, T., Sawai, T. and Miura, Y., 2005. THz imaging of nucleobases and cancerous tissue using a GaP THz-wave generator. *Optics communications*, *244*(1), pp.469-474.
11. Son, J.H., 2009. Terahertz electromagnetic interactions with biological matter and their applications. *Journal of Applied Physics*, *105*(10), p.102033.
12. Seok, E., Cao, C., Shim, D., Arenas, D.J., Tanner, D.B., Hung, C.M. and Kenneth, K.O., 2008, February. A 410GHz CMOS push-push oscillator with an on-chip patch antenna. In *Solid-State Circuits Conference, 2008. ISSCC 2008. Digest of Technical Papers. IEEE International* (pp. 472-629). IEEE.
13. Hwu, S.U. and Jih, C.T., 2013, February. Terahertz (THz) wireless systems for space applications. In *Sensors Applications Symposium (SAS), 2013 IEEE* (pp. 171-175). IEEE.
14. Qasim, A.M. and Rahman, T.A., 2010, November. A compact & high gain series array planar antenna for 60-GHz WPAN applications. In *Applied Electromagnetics (APACE), 2010 IEEE Asia-Pacific Conference on* (pp. 1-5). IEEE.
15. Säily, J., Lamminen, A. and Francey, J., 2011, May. Low cost high gain antenna arrays for 60 GHz millimetre wave identification (MMID). In *Sixth ESA Workshop on*

Millimetre-Wave Technology and Applications-Fourth Global Symposium Millimetre Waves, Espoo, Finland.

16. Biglarbegian, B., Fakharzadeh, M., Busuioc, D., Nezhad-Ahmadi, M.R. and Safavi-Naeini, S., 2011. Optimized microstrip antenna arrays for emerging millimeter-wave wireless applications. *IEEE Transactions on antennas and propagation*, *59*(5), pp.1742-1747.
17. Jha, K.R. and Singh, G., 2009, October. Improved performance analysis of square patch microstrip antenna at terahertz frequency. In *Advances in Recent Technologies in Communication and Computing, 2009. ARTCom'09. International Conference on* (pp. 676-679). IEEE.
18. Jha, K.R. and Singh, G., 2012. Analysis and design of terahertz microstrip antenna on photonic bandgap material. *Journal of Computational Electronics*, *11*(4), pp.364-373.
19. Johri, M., Ahmed, Y.A. and Bezboruah, T., 2007. Photonic band gap materials: Technology, applications and challenges. *Current Science*, *92*(10), pp.1361-1365.
20. Jha, K.R. and Singh, G., 2010. Dual-band rectangular microstrip patch antenna at terahertz frequency for surveillance system. *Journal of Computational Electronics*, *9*(1), pp.31-41.
21. Rabbani, M.S. and Ghafouri-Shiraz, H., 2015. Size improvement of rectangular microstrip patch antenna at MM-wave and terahertz frequencies. *Microwave and Optical Technology Letters*, *57*(11), pp.2585-2589.
22. Rabbani, M. and Ghafouri-Shiraz, H., 2017. Liquid Crystalline Polymer Substrate Based THz Microstrip Antenna Arrays for Medical Applications. *IEEE Antennas and Wireless Propagation Letters*.

23. Rabbani, M.S. and Ghafouri-Shiraz, H., 2016. Fabrication tolerance and gain improvements of microstrip patch antenna at terahertz frequencies. *Microwave and Optical Technology Letters*, *58*(8), pp.1819-1824.

24. Nishizawa, J.I., Sasaki, T., Suto, K., Yamada, T., Tanabe, T., Tanno, T., Sawai, T. and Miura, Y., 2005. THz imaging of nucleobases and cancerous tissue using a GaP THz-wave generator. *Optics communications*, *244*(1), pp.469-474.

25. Pickwell, E. and Wallace, V.P., 2006. Biomedical applications of terahertz technology. *Journal of Physics D: Applied Physics*, *39*(17), p.R301.

26. Kurzweil-Segev, Y., Brodsky, M., Polsman, A., Safrai, E., Feldman, Y., Einav, S. and Ishai, P.B., 2014. Remote monitoring of phasic heart rate changes from the palm. *IEEE Transactions on Terahertz Science and Technology*, *4*(5), pp.618-623.

27. Antenna Theory.com. [Online] available from: http://www.antenna-theory.com/antennas/patches/antenna.php, accessed on March the 26th, 2015

28. Hong, J.S.G. and Lancaster, M.J., 2004. *Microstrip filters for RF/microwave applications* (Vol. 167). John Wiley & Sons.

29. James, J.R. and Henderson, A., 1979. High-frequency behaviour of microstrip open-circuit terminations. *IEE Journal on Microwaves, Optics and Acoustics*, *3*(5), pp.205-218.

30. Analog Devices, MT-094: Microstrip and Stripline Design - Analog Devices, [Online] Available at: http://www.analog.com/static/imported-files/tutorials/MT-094.pdf, accesses on June the 26th, 2014

31. Saeedkia, D. ed., 2013. *Handbook of terahertz technology for imaging, sensing and communications*. Elsevier.

32. ULTRALAM® Flexible Copper Clad Laminates, online at: https://www.rogerscorp.com/acs/producttypes/35/ULTRALAM-Flexible-Copper-Clad-Laminates.aspx, (accessed on 27 April, 2016)

33. Yang, Y., Shutler, A. and Grischkowsky, D., 2011. Measurement of the transmission of the atmosphere from 0.2 to 2 THz. *Optics express*, *19*(9), pp.8830-8838.

Chapter-4

MPA Design for Remote Vital Signs Monitoring at Millimetre-wave Frequencies

Abstract: In this chapter, three ultra-wide patch antenna arrays have been presented at 60GHz-band frequencies with improved gain and beam-width capabilities for remote detection of respiration and heartbeat rates of a person using Doppler radar principle. The antennas' measured and simulation results showed close agreement in all the cases. The breathing rate (BR) and heartbeat rate (HR) of a male (aged 31 years) have been accurately detected from various distances ranging from 5cm to 1m with both, a single antenna and double antennas operations. In the case of single antenna operation, the signal is transmitted and received with the same antenna, whereas in the double antenna operation two identical antennas are employed, one for transmission and the other for reception. It has been found that the accuracy of remote vital signs monitoring (RVSM) in double antenna operation is better than the one in single antenna operation. It has also been observed that the visual results are more obvious when the higher gain antennas are employed due to the radar's main beam being confined on the subject's chest. Finally, the sensitivity of 60GHz RVSM is compared to that of 10GHz RVSM. This has been carried out by re-designing one of the antenna arrays at 10GHz and taking the RVSM measurements. It has been discovered that the respiration and heartbeat signals are respectively 2.35 and 12.96 times more rigorous at 60GHz than they are at 10GHz frequency.

4.1. Introduction

Non-contact detection of respiration and heartbeat rate with Doppler radar is a convenient way to check the vitality signs of a person, as compared to conventional vital sign monitoring devices [1, 2]. Consequently, RVSM is demanded in regular and special health care, emergency services, and security and defence sectors [3-6]. However, the accuracy and reliability of RVSM system need to be dealt appropriately for its real life applications [7,8].

In the present work, three microstrip antenna arrays of ultra-wide patch elements have been designed for accurate detection of human BR and HR at 60GHz-band frequencies. The use of array antenna is made to minimise the interference of the reflected signal from side objects because the radiation beamwidths of the proposed antenna arrays are narrower than that of the single element patch antenna [9]. Suitability of 60GHz-band for RVSM has been studied under the Doppler radar theory. Both, the BR and HR have been simultaneously measured of the subject sitting in front of the antennas and having normal breathing. The detection process has been studied in two ways; (i) with a single antenna used for both transmission and reception and (ii) with double antennas, one for transmission and the other for reception. The ultra-wide patch elements provide a good trade-off between the arrays gain and size. The low side lobe level, high gain and narrow beamwidth features of the arrays focused the electromagnetic (EM) wave on the subject chest and ultimately improved the accuracy of RVSM. Moreover, all of the arrays' dimensions were wide enough for conventional cost-effective fabrication with the ordinary PCB etching technology.

4.2. Antenna Designs for RVSM

In order to study the robustness in improvement of RVSM results' accuracy at 60GHz, three microstrip patch antenna arrays have been designed with moderate to high gain at 60GHz-

band based on the MPA size extension method explained in Chapter 3. The antenna arrays are designed with two, six and twelve number of patch elements to obtain the gain values of about 13dBi, 16dBi and 19dBi, respectively. The antenna arrays have been designed on low loss RT/Duroid5880 substrate with thickness 'h'=254μm and dielectric constant 'ε_r'=2.2. The structure diagrams of the proposed arrays are presented in Fig. 4.1 where the arrays in Figs. 4.1(a), (b) and (c) are comprised of 2×1, 3×2 and 6×2 patch elements, respectively.

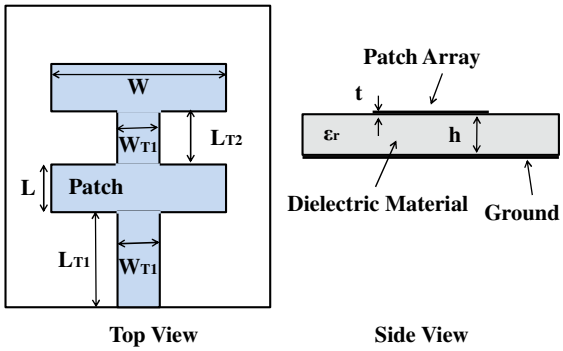

(a)

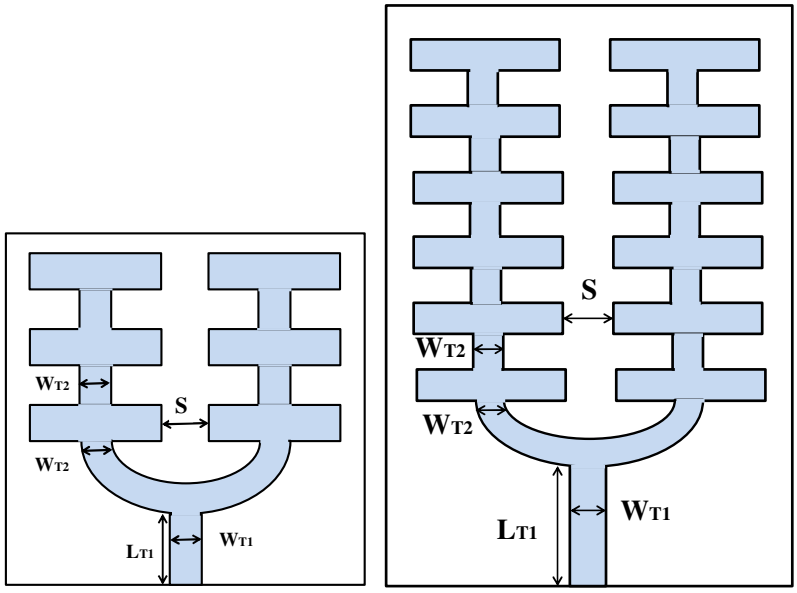

(b) (c)

Fig. 4.1. Structures of the proposed antenna arrays with (a) 2×1, (b) 3×2 and (c) 6×2 patch elements (Figs. are not in scale)

The patch width (W) and length (L) are calculated with the method explained in section 3.2 by putting M=1 and N=0 in eqs. (3.1) and (3.2), respectively. The patch elements are reasonably large for fabrication when N=0 at 60GHz so there is no need to choose a higher value of N. On the other hand, M=1 is adopted to improve the arrays gain by around 3dB as compared to the gain of an array with conventional patch width (i.e. M=0). Secondly, by employing the ultra-wide patches the antenna's input impedance is reduced which subsequently helped to reduce the characteristic impedances of the matching and feeding transmission lines (TLs). Ultimately, the low impedance TLs acquired wider widths and hence it improved the fabrication tolerance should the conventional low cost PCB etching method be employed [2].

The TL length 'L_{T1}' is deployed as impedance transformer which is computed from eq. (3.6) by putting P=1. The inter-separations between the successive series patch elements are obtained from eq. (3.8) by putting Q=0 and S is set to be $\lambda/2$, to match the current phase on the patch elements (see Fig. 4.1).

The total input impedance (Z_a) of the array with n number of symmetrical patch elements is computed by eq. (3.7). Z_a is matched with the standard 50Ω impedance through TL impedance transformer 'L_{T1}' with the characteristic impedance $Z_1 = \sqrt{50 \times Z_a}$. The total input impedance (Z_2) of the series patch elements on one side of the array is given as $Z_2 = 59.81\lambda_0/(\mathrm{mW})$, where m is number of patch elements in series. Subsequently, eq. (3.5) is used to calculate the TL widths W_{T1} and W_{T2} based on their characteristic impedance Z_1 and Z_2, respectively. In this way, we could produce the desired improved gain microstrip antenna arrays with overall PCB details wider enough to be produced with the conventional

low cost etching process. The final dimensions of the arrays given above are optimised with CST Microwave Studio for the best antenna performance.

4.3. Antenna Arrays Results

Figure 4.2 demonstrates the fabricated antenna arrays where (a)-(b), (c)-(d) and (e)-(f) are two copies of the array with $2\times1, 3\times2$ and 6×2 number of patch elements, respectively [14].

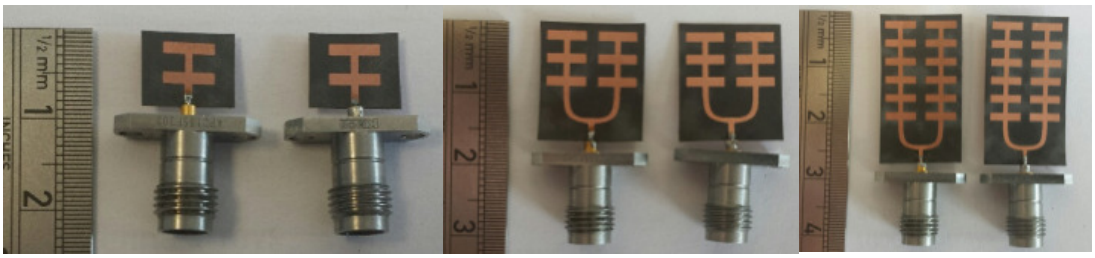

(a) (b) (c) (d) (e) (f)

Fig. 4.2. Fabricated antenna arrays with (a)-(b) 2×1, (c)-(d) 3×2 and (e)-(f) 6×2 patch elements

Table 4.1 shows the dimensions of the fabricated arrays where it can be seen that all of the arrays' dimensions are well above the PCB etching limit of 152μm line width/gap.

Table 4.1. Dimensions in mm of the fabricated 60GHz antenna arrays

Dimension	L	W	L_{T1}	L_{T2}	W_{T1}	W_{T2}	S
Ant. 2(a)	1.34	5.1	1.88	2.42	0.86	0.86	0
Ant. 2(c)	1.45	5.47	1.73	2.37	0.9	0.7	1.58
Ant. 2(e)	1.45	5.47	2.13	2.39	0.93	0.75	2

Figures 4.3(a)-(c) illustrate the simulation and measured return loss (S_{11}) responses of the arrays shown in Figs. 4.2(a)-(b), (c)-(d) and (e)-(f), respectively. It can be seen from Fig. 4.3 that the simulation and measured S_{11} results show a close agreement. The resonances of antennas 4.2(a)-(b) are centred at around 63.4GHz, and that of antennas 4.2(c)-(f) are centred

in the range of 64.5GHz to 65GHz but are better than -15dB at 64.8GHz. Therefore, 63.4GHz and 64.8GHz frequency tones have been respectively selected for the RVSM when antennas 4.2(a)-(b) and 4.2(c)-(f) are employed.

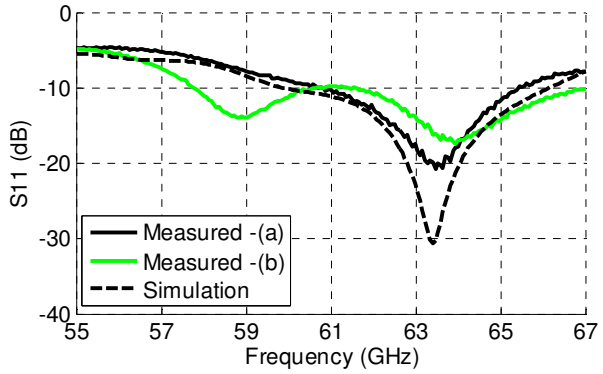

(a)

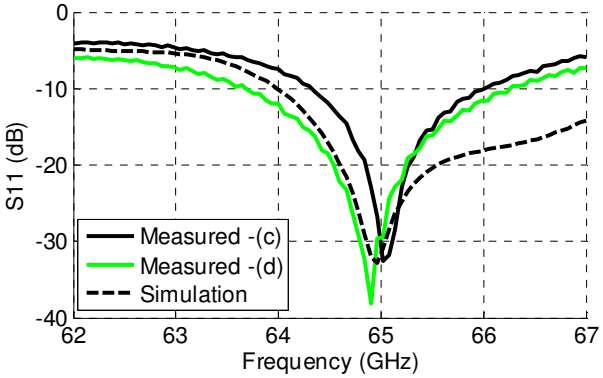

(b)

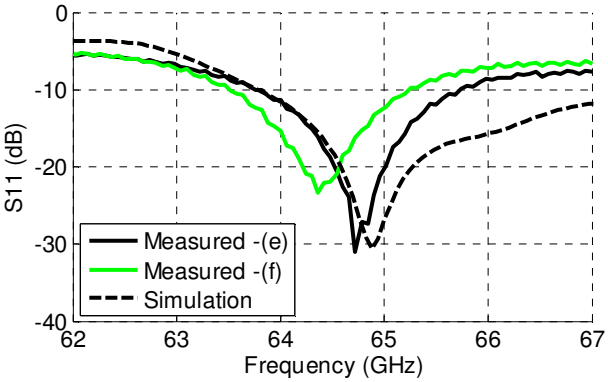

(c)

Fig. 4.3. Measured and simulation S_{11} results of antenna arrays shown (a) in Figs. 4.2(a)-(b), (b) in Figs. 4.2(c)-(d), and (c) in Figs. 4.2(e)-(f)

Figures 4.4(a)-(c) present the simulated far-field radiation patterns (FRP) in 3 dimensions (3-D) of the antennas shown in Figs. 2(a)-(b), (c)-(d) and (e)-(f), whereas Figs. 4.5-4.7 respectively show their simulation and measured FRP results in E and H planes at their selected frequencies as mentioned in the last paragraph. All of the antennas measured S_{11} and FRP results are within the PCB fabrication tolerance of 5% [15-16]. Some distortions in the antennas FRP in Figs. 4.6 and 4.7 can be observed which are due to the reflections from the surroundings and test fixtures [10-11]. It can be noticed from Figs. 4.4-4.7 that the antennas' main radiation lobes are directed almost towards 0^0 in both E and H planes in all the cases. The antennas' measured -10dB S_{11} bandwidths (BW) and gains are summarised in Table 4.2 where it is obvious that gain of the arrays has significantly improved when more patch elements have used but the BW has reduced. However, the BW is not crucial for our current application of RVSM because only a single tone frequency will be used for the detection process.

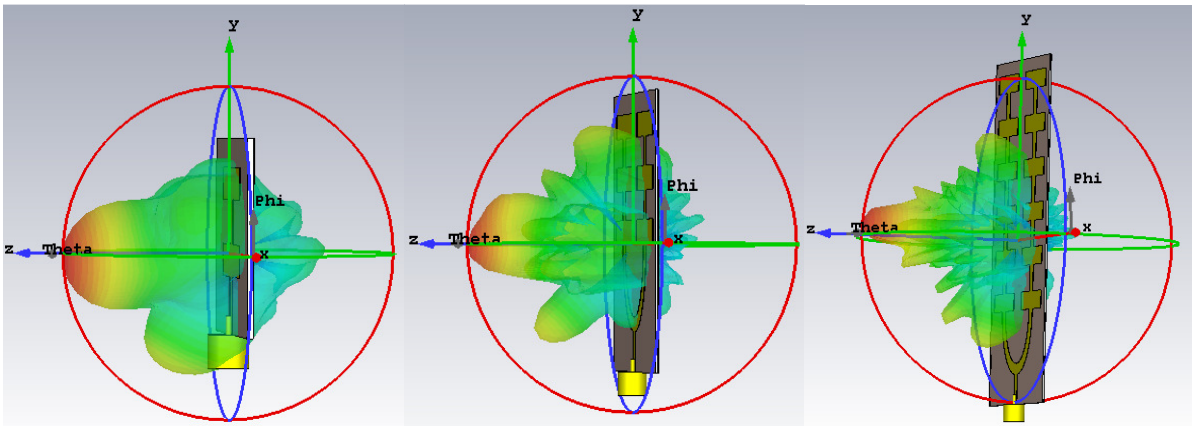

(a) (b) (c)

Fig. 4.4. Simulation 3-D FRP of antenna arrays shown (a) in Figs. 4.2(a)-(b), (b) in Figs. 4.2(c)-(d), and (c) in Figs. 4.2(e)-(f)

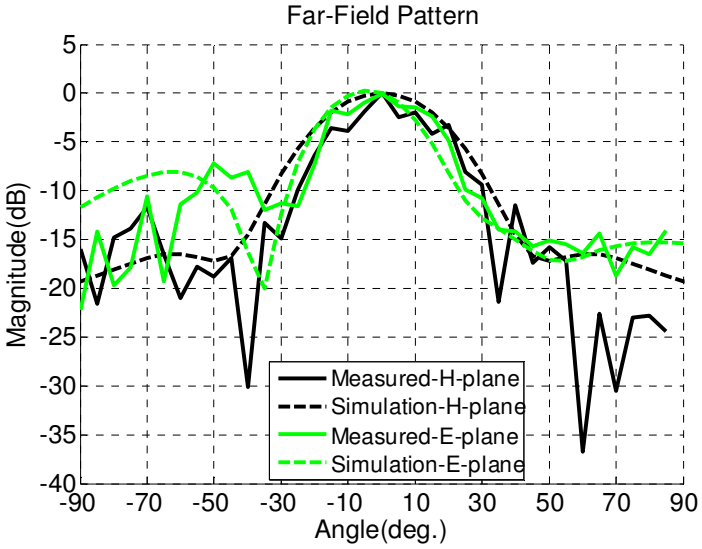

(a)

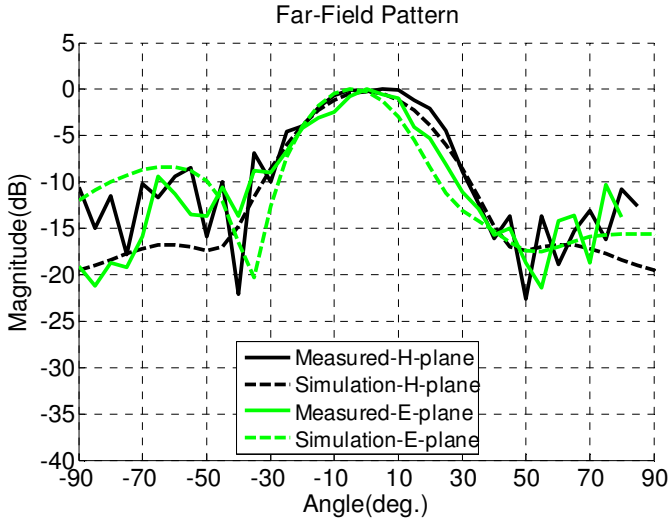

(b)

Fig. 4.5. Measured and simulation FRP of antenna arrays shown (a) in Fig. 4.2(a), and (b) in Fig. 4.2(b)

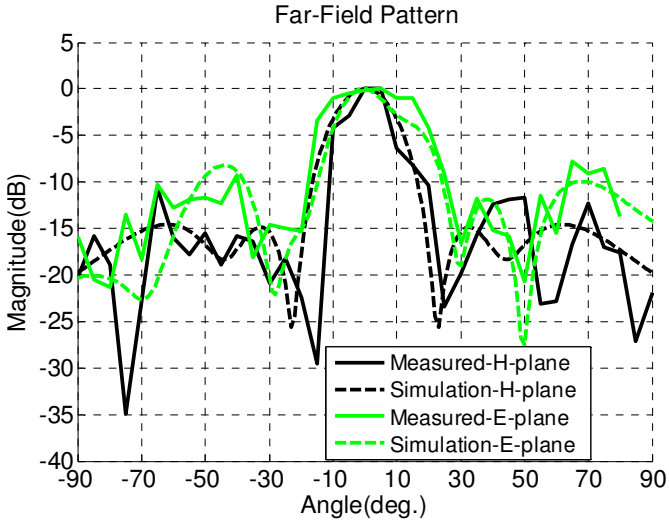

(a)

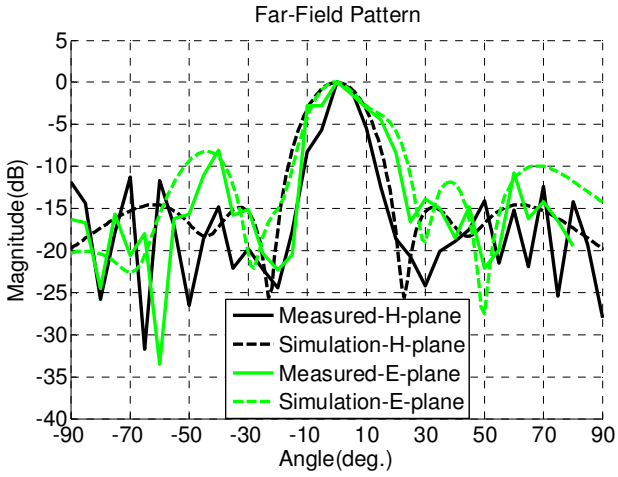

(b)

Fig. 4.6. Measured and simulation FRP of antenna arrays shown (a) in Fig. 4.2(c), and (b) in Fig. 4.2(d)

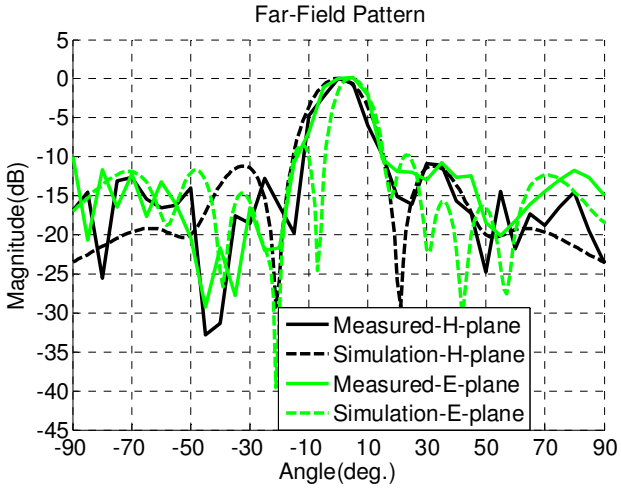

(a)

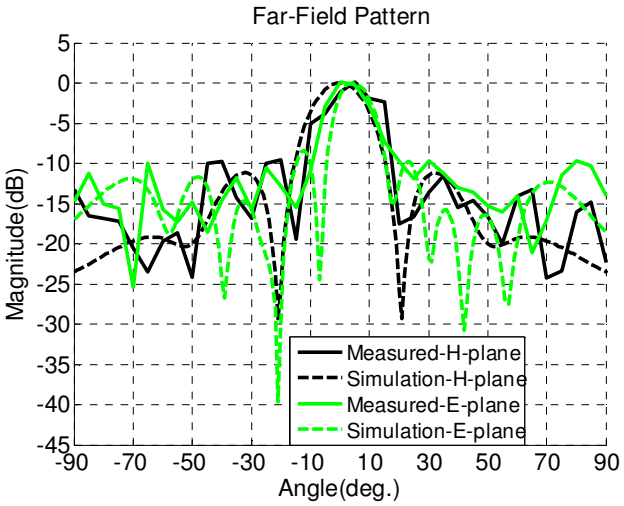

(b)

Fig. 4.7. Measured and simulation FRP of antenna arrays shown (a) in Fig. 4.2(e), and (b) in Fig. 4.2(f)

Table 4.2. Performance of antenna arrays shown in Figs. 2(a)-(f)

Ant.	(a)	(b)	(c)	(d)	(e)	(f)
BW (GHz)	4.62	5.52	1.68	2.57	1.9	1.73
Gain (dBi)	13.4	13.5	16	16.15	18.2	18.55
Beam-widths (E-H planes)	28^0-36^0		18^0-18^0		18^0-13^0	

4.4. Applicability of 60GHz Doppler Radar for RVSM

Figure 4.8 shows the block diagram of various stages of RVSM process when Doppler radar principle is used for the vital signs detection. A single frequency tone of continuous EM wave is transmitted through a transmitter (T_x) antenna. The wave is reflected back from the subject chest located at a certain distance 'd' and is received by a receiver (R_x) antenna. The quasi-periodic vibration of the chest due to respiration and heartbeat is phase modulated on the received signal. This phase modulated signal at R_x is demodulated and correlated with transmitted signal and the outcome data is recorded for a certain period of time. Subsequently, the recorded raw data which is in time domain, is processed through various signal processing techniques i.e. digital filtering, Fourier Transformation, etc. to extract the respiration and heartbeat rate of the subject.

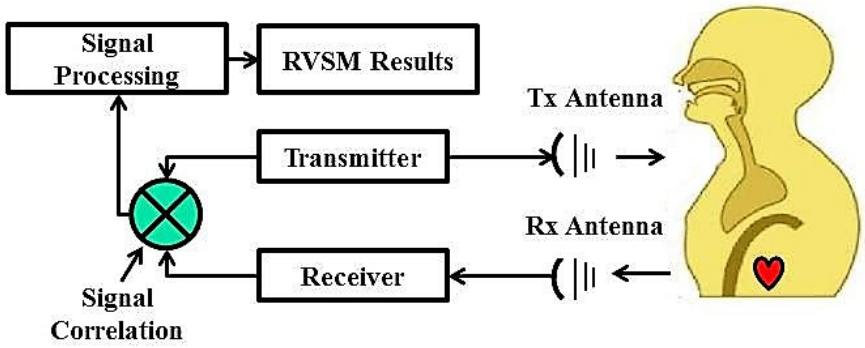

Fig. 4.8. Block diagram of RVSM process

According to the Doppler radar theory, for a transmitted signal $S(t) = \cos(2\pi f t + \varphi(t))$, where f and $\varphi(t)$ are the frequency and phase of the transmitted wave, respectively, the received base band signal R(t) may be approximated as [12]:

$$R(t) = \cos\left[\theta(t) + \frac{4\pi x_b(t)}{\lambda} + \frac{4\pi x_h(t)}{\lambda}\right] \qquad (4.1)$$

where $\theta(t)$ is the total phase shift due to the signal path (d), reflections from the subject and surroundings and residual phase noise. λ, $x_b(t)$ and $x_h(t)$ are the operating wavelength, chest vibration signals due to respiration and heartbeat, respectively. Due to the periodic nature of the $x_b(t)$ and $x_h(t)$ they may be approximated as: $x_b(t) = m_b \sin(2\pi f_b t)$ and $x_h(t) = m_h \sin(2\pi f_h t)$, where m_b and m_h are the displacement amplitudes of the chest motion due to respiration and heartbeat, respectively. f_b and f_h are the frequencies of BR and HR, respectively. This way, the expansion of equation (4.1) in Fourier series leads to [13]:

$$R(t) = \sum_{i=-\infty}^{\infty} \sum_{j=-\infty}^{\infty} J_j\left[\frac{4\pi m_b}{\lambda}\right] J_i\left[\frac{4\pi m_h}{\lambda}\right] \cos(j\,2\pi f_b t + i\,2\pi f_h t + \theta) \qquad (4.2)$$

Where $J_n(X)$ is Bessel function of first kind with argument X. Taking the first positive harmonics of both f_b and f_h into account the above equation can be written as:

$$\begin{aligned} R(t) = {} & J_1\left[\frac{4\pi m_b}{\lambda}\right] J_0\left[\frac{4\pi m_h}{\lambda}\right] \cos(2\pi f_b t + \theta) \\ & + J_0\left[\frac{4\pi m_b}{\lambda}\right] J_1\left[\frac{4\pi m_h}{\lambda}\right] \cos(2\pi f_h t + \theta) \end{aligned} \qquad (4.3)$$

where $J_1\left[\frac{4\pi m_b}{\lambda}\right] J_0\left[\frac{4\pi m_h}{\lambda}\right]$ and $J_0\left[\frac{4\pi m_b}{\lambda}\right] J_1\left[\frac{4\pi m_h}{\lambda}\right]$ are the amplitudes of the phase variations in R(t) due to respiration and heartbeat, respectively. Equation (4.3) contains the essential information related to the applicability of 60GHz-band frequencies for RVSM. Based on eq. (4.3), we are going to analyse and visualise the key factors involved in RVSM at 60GHz band.

Fig. 4.9(a) shows the plots of $J_0(X)$, $J_1(X)$ and their product for the argument X up to 30 where it can be noticed that $J_0(X)$ and $J_1(X)$ are the periodic functions with some phase shift

and the maximum amplitude of their product is much smaller than their individual maximum amplitudes and it passes through null values twice as compared to individual $J_0(X)$ and $J_1(X)$ curves. Furthermore, the amplitude of $J_0(X)\times J_1(X)$ diminishes for higher values of argument X. However, in the present case the amplitude of the received BR and HR signal is comprised of the product of $J_0(X)$ and $J_1(X)$ but at the different values of argument X which are controlled by m_b and m_h (see eq. (4.3)). For our current case of RVSM at 60GHz-band, λ is around 4.65mm, $m_b = (8-12)$mm and $m_h = (0.2-0.5)$mm for a person at rest with normal breathing [14]. Figs. 4.9(b)-(d) show the phase amplitude variations of R(t) signal for various combination of m_b and m_h with BR and HR in combined, only BR and only HR, respectively. From Fig. 9(b) it can be seen that the maximum R(t) amplitude goes to around 40^0 which is high enough for RVSM detection however there is a null detection line at chest amplitude of around 9.9mm. Fig. 4.9(c) indicates a similar null line position for just BR signal. On the other hand, Fig. 4.9(d) shows that in case of the received HR signal, there are two null detection lines at chest displacements of 8.8mm and 11mm and the maximum phase amplitude of heartbeat is about one third of that of respiration. However, the probability of these undesired m_b and m_h combinations and hence the null detection points is very low and a small variation in λ can be made to avoid these points (see eq. (4.3)) [13]. As a conclusion so far, both BR and HR signals have high probability of detection with RVSM at 60GHz-band but the received BR signal may be clearer than HR signal.

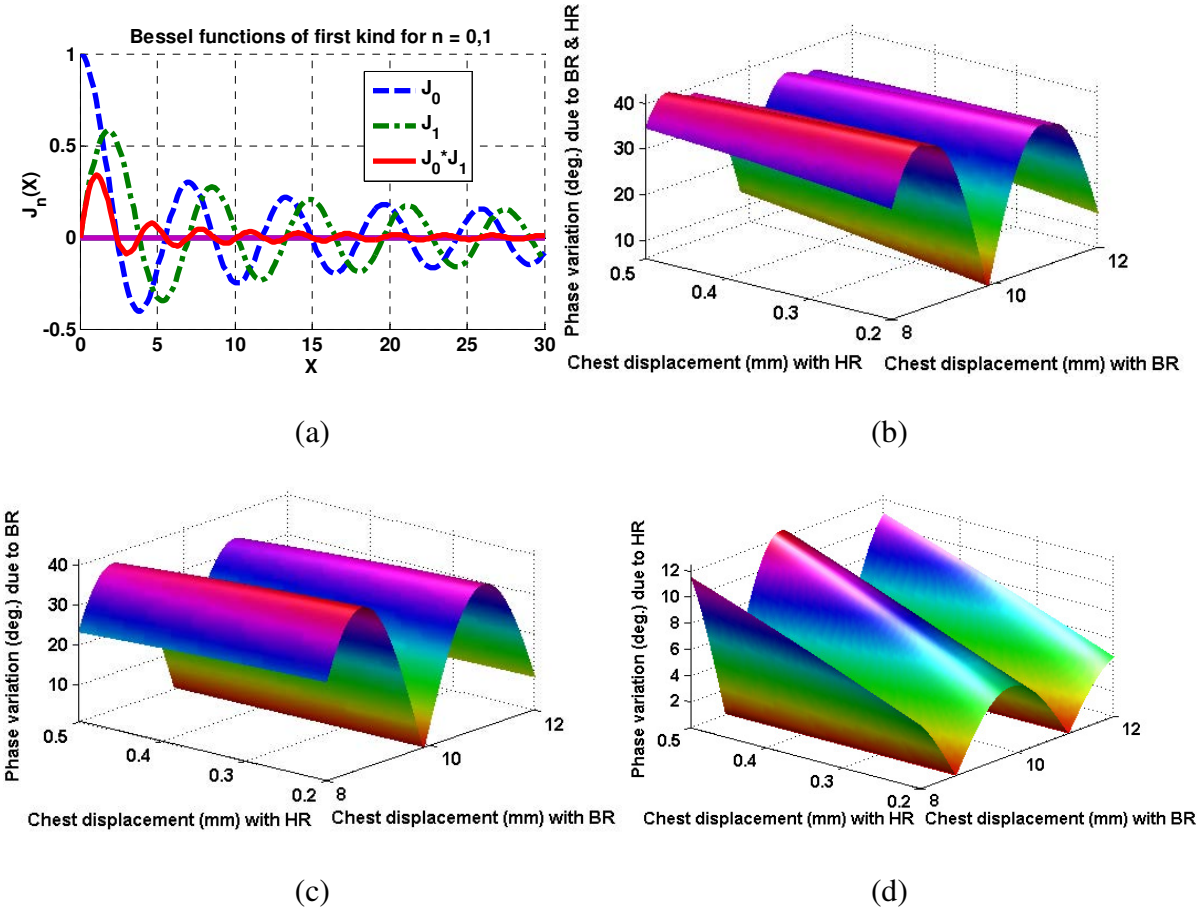

Fig. 4.9. (a) Plots of Bessel functions $J_0(X)$, $J_1(X)$ and their product $J_0(X)\times J_1(X)$ for argument X. Magnitude of the phase amplitude of R(t) in equation (4.3) due to (b) both BR and HR in combined, (c) just BR signal and (d) just HR signal, for various combinations of m_b and m_h.

4.5. RVSM Results and Discussions

Figure 4.10 shows the experiment setup of the RVSM measurements at 60GHz-band. The 67GHz Rohde & Schwarz VNA is used as a transceiver. The three antenna presented in section 4.3 (see Fig. 4.2) have been employed one by one for RVSM. As mentioned in section 4.1, for each of the antenna designs the RVSM data has been acquired in two ways; (i) with a single antenna employed for both transmission and reception and (ii) with double antennas (two similar antennas), one for transmission and the other for reception. A normally breathing

person sits in front of the antennas iteratively at different distances ‘d’ and the RVSM data is recorded for 60 seconds for each iteration. The recorded data is then acquired and processed in Matlab through various digital signal processing techniques and the targeted BR and HR information is extracted. The measured BR and HR results are compared with the results obtained with manual counting by using a stopwatch as well as with Finger Pulse Oximeter (FPO). The major parts of digital signal processing include digital filtering of the recorded raw data in time domain and Discrete Fast Fourier Transformation (DFFT) of the filtered data. The full Matlab program written for RVSM is presented in Appendix A.

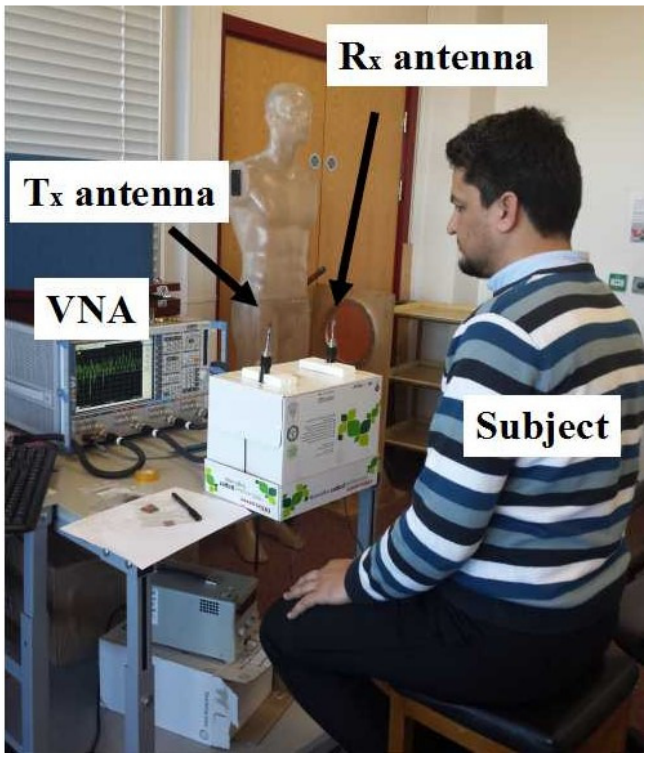

Fig. 4.10. Experiment setup to measure the RVSM at 60GHz-band

4.5.1 RVSM with Single Antenna

As mentioned earlier, in the single antenna operation only one antenna from each of the three designs is employed for both signal transmission and reception. It has been found that with single antenna operation the vital signs can only be accurately detected for very short distance

[1]. The antenna is placed at about 5cm away from the subject chest and the phase of the reflection coefficients (S_{11}), which contain the HR and BR information, has been recorded for 60 seconds. Figs. 4.11-4.13 illustrate the measured RVSM data with the individual antennas shown in Figs. 2(a), (c) and (e), respectively. Figs. 4.11(a), 4.12(a) and 4.13(a) represent the recorded S_{11} phase and Figs. 4.11(b), 4.12(b) and 4.13(b) depict the processed data in frequency (1/min) domain. As seen from Figs. 4.11(b), 4.12(b) and 4.13(b), in each case the first and the second highest peaks represent the expected detected BR and HR, respectively. All of the detected BR and HR are listed in Table 4.3 where it is obvious that both BR and HR are consistent within their respective ranges for the ordinary subject (31 years old man) [15]. The measured BR and HR results also matched with the results obtained with manual counting as well as with FPO. However, it can be noticed that the amplitudes of the detected HR and BR signals are not much higher than the noise ripples which may cause false detection of RVSM in a real-life noisy environment unlike in a lab. Therefore, double antenna operation is investigated and presented in the next section.

Table 4.3. Measured BR and HR with single antenna operation

Antenna	4.2(a)	4.2(c)	4.2(e)
BR (1/min)	19	20	20
HR (1/min)	71	75	74

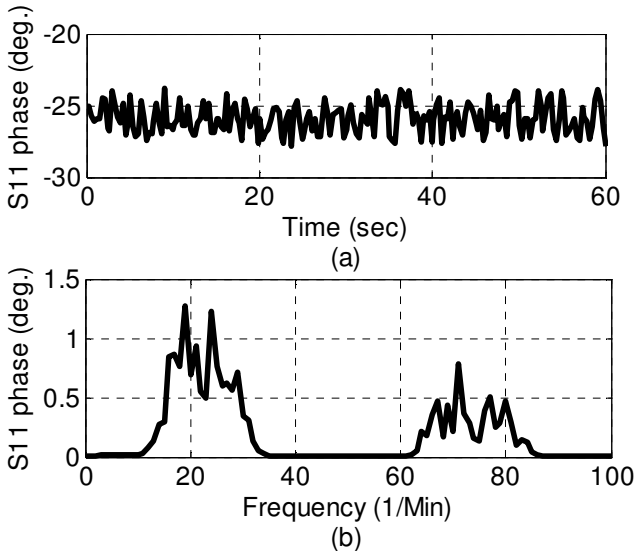

Fig. 4.11. RVSM measurement with antenna shown in Fig. 4.2(a). (a) Recorded raw data in time domain and (b) detected BR and HR peaks

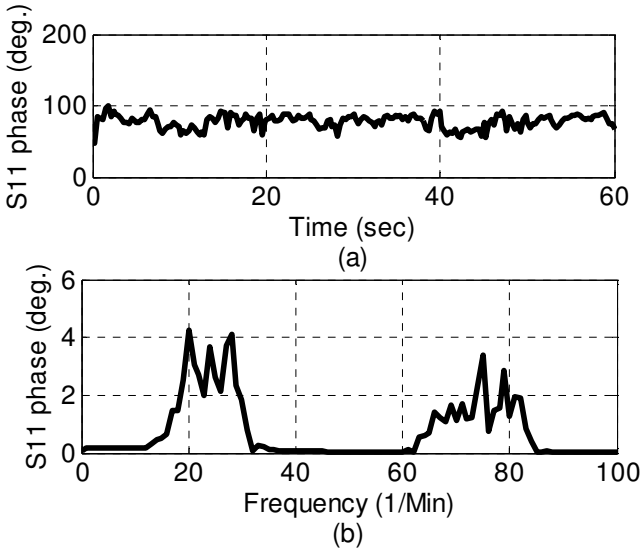

Fig. 4.12. RVSM measurement with antenna shown in Fig. 4.2(c). (a) Recorded raw data in time domain and (b) detected BR and HR peaks

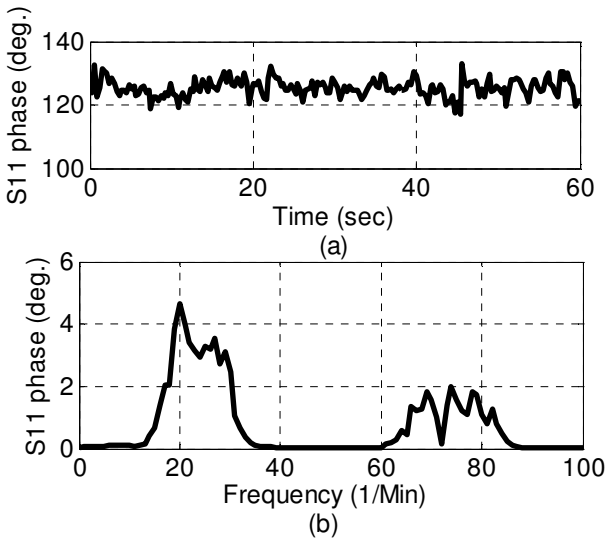

Fig. 4.13. RVSM measurement with antenna shown in Fig. 4.2(e). (a) Recorded raw data in time domain and (b) detected BR and HR peaks

4.5.2 RVSM with Double Antennas

In RVSM with double antennas, two similar antennas are deployed for vital sign detection; one for transmitting the EM wave and the other for receiving the reflected wave. Both the antennas are fixed at an equal distance from the subject's chest with the main beams directed to the chest. The inter-separation between the antennas is set to be about 20cm. The phase of S_{21} is recorded for 60 seconds with each of the antenna designs shown in Figs. 4.2(a)-(f). The accuracy of the RVSM has been studied for 0.25m and 1m distances between the subject and antennas. Figs. 4.14 and Figs. 4.15, demonstrate the RVSM data measured with antenna design shown in Figs. 4.2(a)-(b) from distance d=0.25m and d=1m, respectively. Similarly, Figs. 4.16-4.17 and Figs. 4.18-4.19 demonstrate the RVSM data with antenna designs 4.2(c)-(d) and 4.2(e)-(f), respectively, from distance 0.25m and 1m. The sub-figs. (a) and (b) in Figs. 4.14-4.19 represent the recorded raw data in time domain and the processed data in frequency (1/min) domain, respectively. The first and the second peaks in the processed data in Figs.

4.14-4.19 represent the measured BR and HR, respectively, where it can be seen that both the BR and HR peaks are very obvious across the frequency spectrum. The measured BR and HR results of RVSM with double antennas are shown in Table 4.4. In all the cases both the BR and HR results are consistent within their expected ranges and matched with the results obtained by manual counting and FPO, as mentioned earlier.

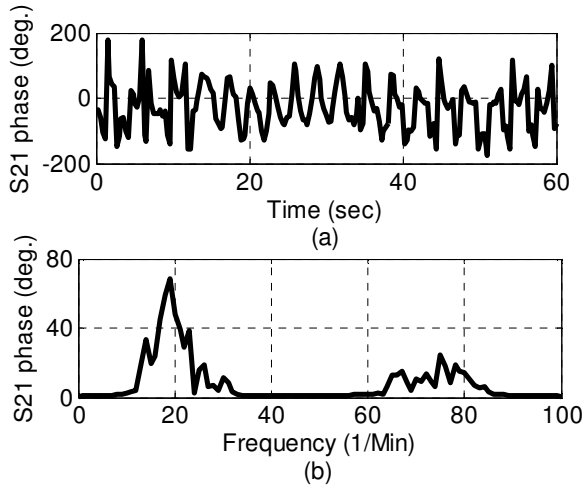

Fig. 4.14. RVSM measurement with antennas shown in Figs. 4.2(a)-(b) from 0.25m.

(a) Recorded raw data in time domain and (b) detected BR and HR peaks

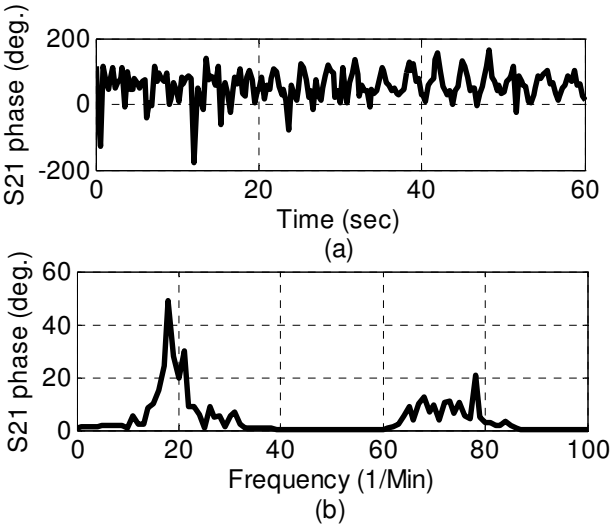

Fig. 4.15. RVSM measurement with antennas shown in Figs. 4.2(a)-(b) from 1m.

(a) Recorded raw data in time domain and (b) detected BR and HR peaks

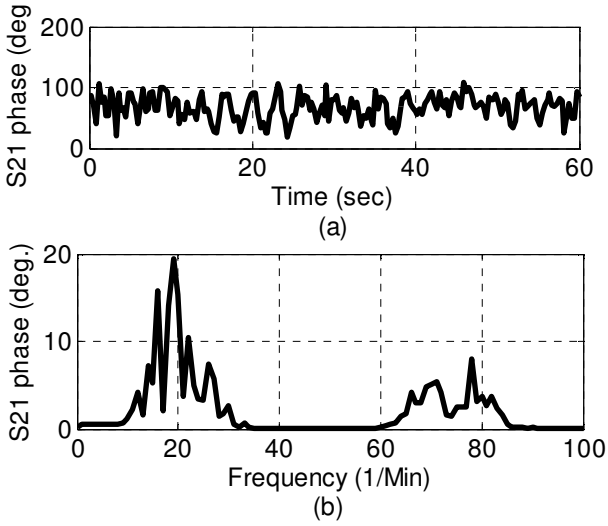

Fig. 4.16. RVSM measurement with antennas shown in Figs. 4.2(c)-(d) from 0.25m.

(a) Recorded raw data in time domain and (b) detected BR and HR peaks

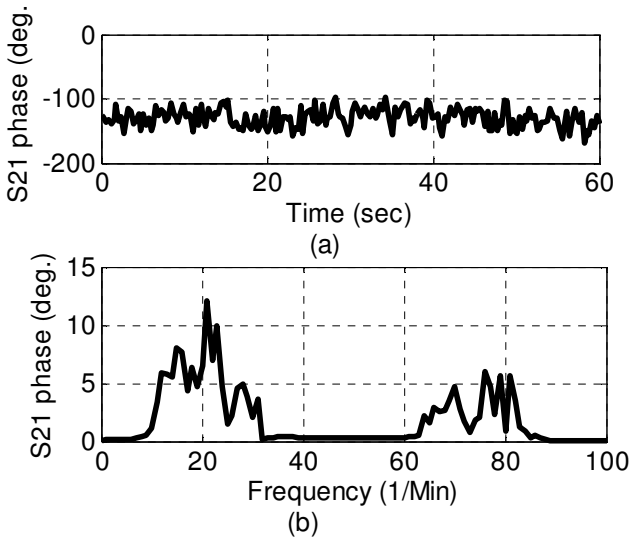

Fig.4.17. RVSM measurement with antennas shown in Figs. 4.2(c)-(d) from 1m. (a)

Recorded raw data in time domain and (b) detected BR and HR peaks

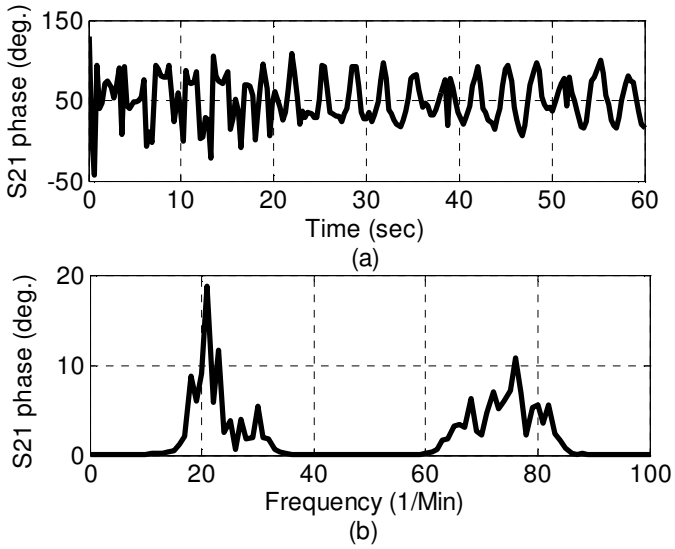

Fig. 4.18. RVSM measurement with antenna shown in Figs. 4.2(e)-(f) from 0.25m.

(a) Recorded raw data in time domain and (b) detected BR and HR peaks

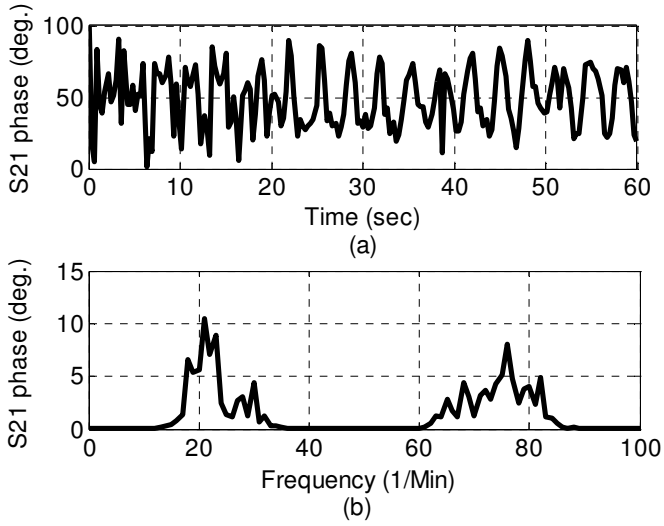

Fig. 4.19. RVSM measurement with antennas shown in Figs. 4.2(e)-(f) from 1m. (a)

Recorded raw data in time domain and (b) detected BR and HR peaks

Table 4.4. Measured BR and HR with double antennas

Antenna	4.2(a)-(b)	4.2(c)-(d)	4.2(e)-(f)
d	BR-HR (1/min)	BR-HR(1/min)	BR-HR(1/min)
0.25m	19-75	19-78	18-76
1m	18-78	21-76	18-72

4.6. RVSM Detection Sensitivity Improvement at 60GHz Compared with RVSM at 10GHz

In order to evaluate the improvement in detection sensitivity of RVSM at 60GHz, as compared to RVSM at conventional microwave wave frequencies, a new experiment is conducted to measure the RVSM results at 60GHz and 10GHz frequencies from a moderate distance of 1m with double antenna operation. In this experiment, the antenna design shown in 4.2(a)-(b) is deployed for 60GHz RVSM, whereas for 10GHz RVSM a similar antenna is designed on the same material but with the substrate thickness h=1.57mm [10]. The rest of the antenna dimensions are as follows: L=9.03mm, W=34.35mm, LT_1=15.39mm, LT_2=9.03mm, WT_1=8.1mm and WT_2=4.05mm. Figs. 4.20(a) and (b) show the two copies of the fabricated 10GHz antenna and (c) shows their simulation and measured S_{11} results. The measured S_{11} BW of antennas shown in Figs. 4.20(a) and (b) is about 1.2GHz which is fairly close to the simulation BW of 1.28GHz. The antennas' measured S_{11} results are below -12dB at 10GHz frequency which is used for RVSM measurements.

Figures 4.21(a) and (b) show the simulation and measured FRP of antennas shown in Figs. 4.20(a) and (b), respectively, and (c) illustrates the 3-D simulation far-field results at 10GHz. As seen from Fig. 4.21, the antennas main lobes are directed to about 0^0 and half power beam-widths are in the range of 32^0-43^0 degrees. The measured gain of antenna 4.20(a) and (b) are 13.9dBi and 13.58dBi, respectively, which are in close agreement with the simulation gain of 13.64dBi.

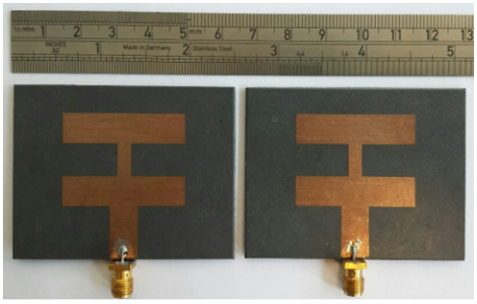

(a) (b)

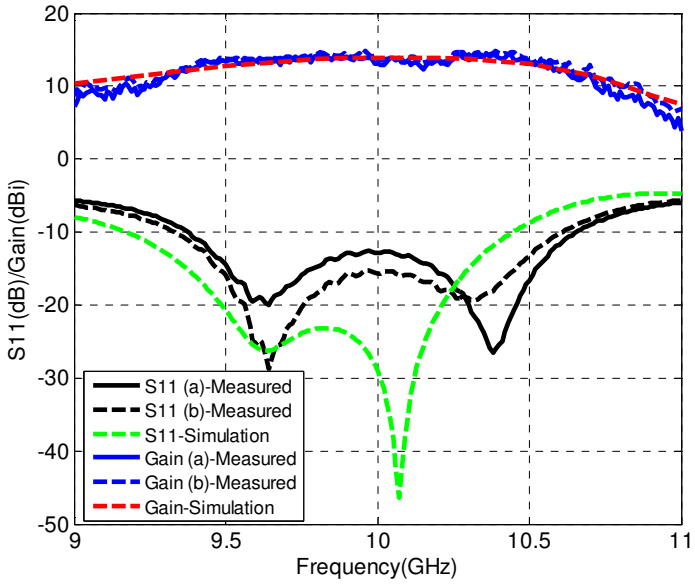

(c)

Fig. 4.20. 10GHz antennas' results. (a) and (b) show the two copies of the fabricated antennas, and (c) shows simulation and measured S_{11} results

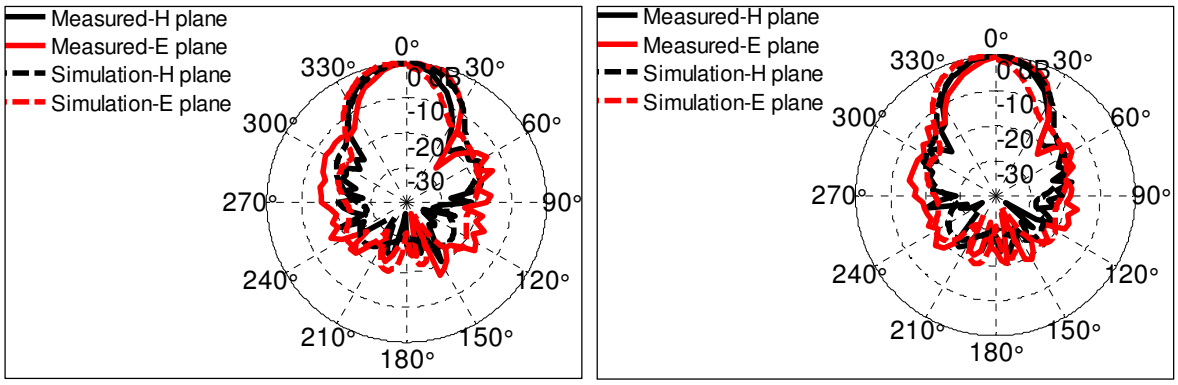

(a) (b)

Fig. 4.21. Simulation and measured FRP at 10GHz of antennas shown in (a) Fig. 4.20(a) and (b) Fig. 4.20(b)

Figure 4.22 shows RVSM results at 60GHz where (a) represents the recorded RVSM raw data in time domain and (b) shows the processed data in frequency domain. It is clear from Fig. 4.22(b) that both the detected BR and HR values are 15/min and 73/min, respectively. Both the measured BR and HR values coincided with their results obtained with the manual counting and FPO.

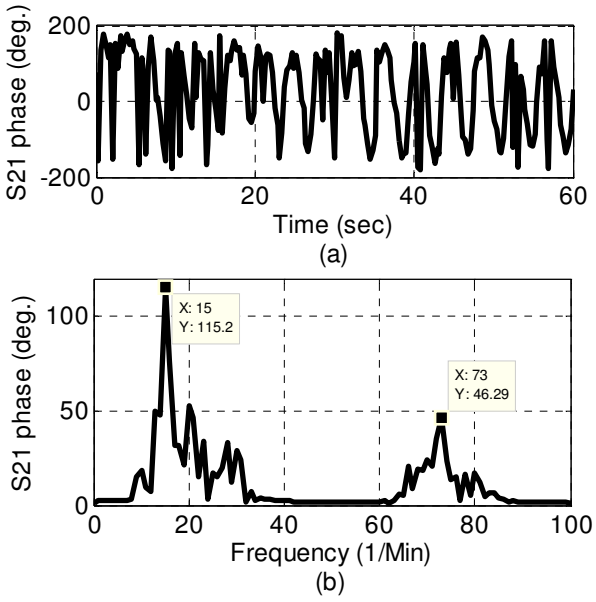

Fig. 4.22. RVSM at 60GHz from 1m distance. (a) measured raw data and (b) detected BR and HR frequency peaks

Figure 4.23 demonstrates the RVSM experiment setup at 10GHz whereas Fig. 4.24 shows the RVSM results at 10GHz where (a) represents the recorded raw data in time domain and (b) shows the processed data in frequency domain. The detected BR=20/min and HR=75/min. It is clear from Fig. 4.24(b) that the amplitudes of the detected BR and HR are 49^0 and 3.55^0, respectively. Comparing Fig. 4.22(b) to Fig. 4.24(b), it is clear that the BR and HR magnitudes detected at 60GHz-band are much higher (i.e. 115^0 and 46^0) than the ones detected at 10GHz (i.e. 49^0 and 3.55^0). Therefore, it can be approximated that the BR and HR detection sensitivities at 60GHz-band are 2.35 and 12.96 times of those at 10GHz. It can also be noticed that the HR sensitivity has improved much more than the BR sensitivity which is due to the inter-modulation between the BR and HR amplitudes as given in eqs. (4.2) and (4.3). This way, the HR signal which is more vulnerable to be faded in noise is evidently detected with 60GHz Doppler radar.

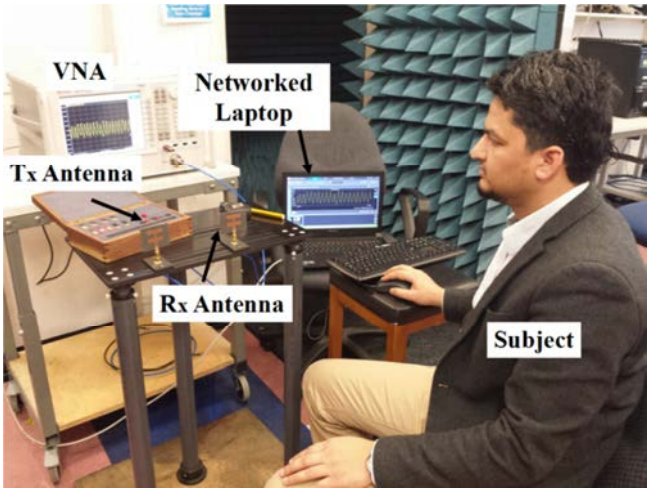

Fig. 4.23. RVSM experiment setup at 10GHz

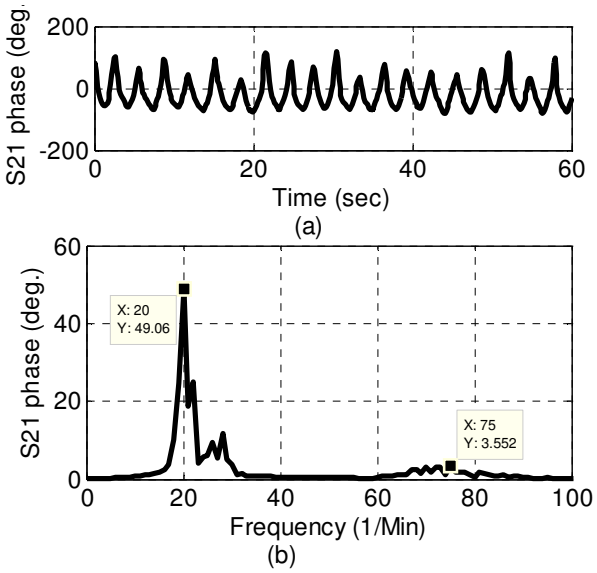

Fig. 4.24. RVSM at 10GHz from 1m distance. (a) Measured raw data and (b) detected BR and HR frequency peaks

Finally, the effect of breath holding on the received phase modulated waveform as well as on the accuracy of HR result is presented. For this purpose, an experiment is conducted at 10GHz with the same antennas as presented in Fig 4.20. The data is acquired with double antenna operation for 60sec time duration where for the first 30sec the subject was breathing as normal but for the rest of 30sec the breathing was on hold. Fig. 4.25(a) and (b) demonstrate

the received phase modulated signal in time domain and the processed data in frequency domain, respectively. From Fig. 4.25(a) it can be clearly seen that the amplitude of the first half of recorded data is dominated by the BR signal which disappears in the second half of the data leaving the HR signal being dominant but with relatively very small amplitude. Fig. 4.25(b) accurately demonstrates the amplitudes of the detected BR (20/min) and HR (75/min) signal peaks. By comparing Fig. 4.25(b) with Fig. 4.24(b), it can be seen that the detected HR signal is more obvious in Fig. 4.25(b) than it is in Fig. 4.24(b). Therefore, breath holding for some time duration in RVSM is employed for enhanced accuracy in HR signal [16].

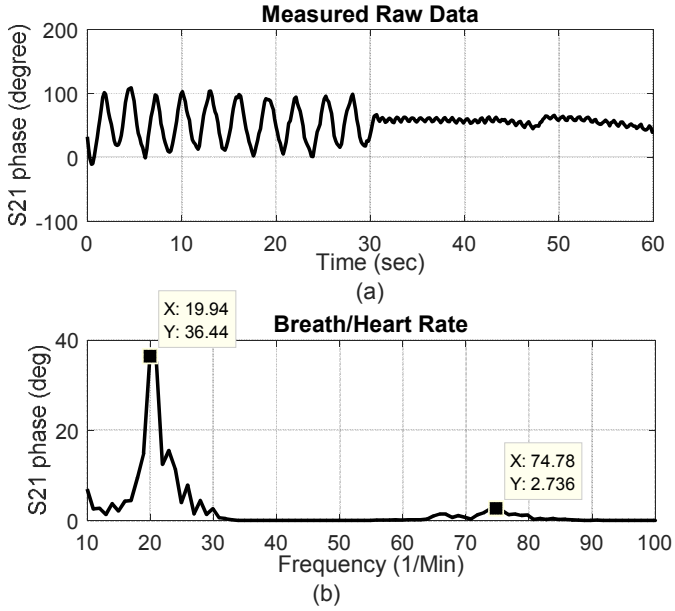

Fig. 4.25. (a) The received phase modulated signal in time domain and (b) the processed BR and HR signals in frequency domain

4.7. Conclusion

Three microstrip antenna arrays have been designed based on ultra-wide patch elements with improved gain and radiation characteristics, for accurate RVSM at 60GHz-band frequencies. The antennas simulation and measured results agreed well in all the cases. The feasibility of

60GHz channel has been studied for RVSM application under the Doppler radar principle. The RVSM measurements have been conducted with each of the designed arrays in (i) single antenna operation; where the same antenna working as T_x and R_x is placed at 5cm from the subject chest, as well as (ii) in double antennas operation where two identical antennas, one for T_x and the other for R_x, have been deployed at various distances from the subject to see the consistency in the results accuracy. Both BR and HR have been detected for the subject with normal breathing throughout the data recording time and breath holding was required for accurate HR detection. In all of the cases, the measured results showed very accurate, clear and robust detection of RVSM with simple digital signal processing techniques. Moreover, the RVSM results at 60GHz have been compared with the ones at 10GHz by conducting an experiment at these frequencies from 1m distance. It has been noticed that the sensitivity in BR and HR detection has improved by respectively 2.35 and 12.96 times at 60GHz as compared to 10GHz. For future work, the proposed antenna arrays could be used for outdoor RVSM detection from an even longer distance. Furthermore, the potential error sources like the signal reflections from the side objects through the antennas' side lobes, and accuracy of the vital signs of the diversity of patients types can be investigated in further detail.

4.8. References

1. Obeid, D., Zaharia, G., Sadek, S. and El Zein, G., 2012. Microwave doppler radar for heartbeat detection vs electrocardiogram. *Microwave and Optical Technology Letters*, *54*(11), pp.2610-2617.
2. Rabbani, M.S. and Ghafouri-Shiraz, H., Ultra-Wide Patch Antenna Array Design at 60 GHz Band for Remote Vital Sign Monitoring with Doppler Radar Principle. *Journal of Infrared, Millimeter, and Terahertz Waves*, pp.1-19.

3. Gu, C., 2016. Short-range noncontact sensors for healthcare and other emerging applications: A review. *Sensors*, *16*(8), p.1169.
4. Droitcour, A.D., Seto, T.B., Park, B.K., Yamada, S., Vergara, A., El Hourani, C., Shing, T., Yuen, A., Lubecke, V.M. and Boric-Lubecke, O., 2009, September. Non-contact respiratory rate measurement validation for hospitalized patients. In *Engineering in Medicine and Biology Society, 2009. EMBC 2009. Annual International Conference of the IEEE* (pp. 4812-4815). IEEE.
5. Villarroel, M., Guazzi, A., Jorge, J., Davis, S., Watkinson, P., Green, G., Shenvi, A., McCormick, K. and Tarassenko, L., 2014. Continuous non-contact vital sign monitoring in neonatal intensive care unit. *Healthcare technology letters*, *1*(3), pp.87-91.
6. Suzuki, S., Matsui, T., Kagawa, M., Asao, T. and Kotani, K., 2013. An approach to a non-contact vital sign monitoring using dual-frequency microwave radars for elderly care. *Journal of Biomedical Science and Engineering*, *6*(7), p.704.
7. Yang, Z., Pathak, P.H., Zeng, Y., Liran, X. and Mohapatra, P., 2016. Monitoring vital signs using millimeter wave. *DOI: http://dx. doi. org/10.1145/2942358.2942381 [Online] Available at:[http://www. phpathak. com/files/mmvital-mobihoc. pdf], accessed on October the 1th*.
8. Kao, T.Y.J. and Lin, J., 2013, April. Vital sign detection using 60-GHz Doppler radar system. In *Wireless Symposium (IWS), 2013 IEEE International* (pp. 1-4). IEEE.
9. Li, V. M. Lubecke, O. Boric-Lubecke and J. Lin, A review on recent advances in Doppler radar sensors for noncontact healthcare monitoring, *IEEE Transactions on microwave theory and techniques* 61, no. 5 (2013): 2046-2060

10. Rabbani, M.S. and Ghafouri-Shiraz, H., 2016. Improvement of microstrip patch antenna gain and bandwidth at 60 GHz and X bands for wireless applications. IET Microwaves, Antennas & Propagation, 10(11), pp.1167-1173.
11. Rabbani, M.S. and Ghafouri-Shiraz, H., 2015. Size improvement of rectangular microstrip patch antenna at MM-wave and terahertz frequencies. *Microwave and Optical Technology Letters*, *57*(11), pp.2585-2589.
12. Gu, C., Li, C., Lin, J., Long, J., Huangfu, J. and Ran, L., 2010. Instrument-based noncontact Doppler radar vital sign detection system using heterodyne digital quadrature demodulation architecture. *IEEE Transactions on Instrumentation and Measurement*, *59*(6), pp.1580-1588.
13. Li, C. and Lin, J., 2007, January. Optimal carrier frequency of non-contact vital sign detectors. In *Radio and Wireless Symposium, 2007 IEEE* (pp. 281-284). IEEE.
14. Obeid, D., Sadek, S., Zaharia, G. and El Zein, G., 2010. Multitunable microwave system for touchless heartbeat detection and heart rate variability extraction. *Microwave and optical technology letters*, *52*(1), pp.192-198.
15. NHS. Online at: http://www.nhs.uk/chq/Pages/2024.aspx, accessed on July the 7th , 2016
16. Gao, J., Li, K., Sato, T., Wang, J., Harada, H. and Kato, S., 2009, January. Implementation considerations of patch antenna array for 60GHz beam steering system applications. In *Radio and Wireless Symposium, 2009. RWS'09. IEEE* (pp. 35-38). IEEE.

Chapter-5

MPA Design for 60GHz-band Wireless Applications

Abstract: In this chapter, the size improvement method has been employed to design MPA arrays for 60GHz-band (57.24-65.88GHz) indoor wireless communications. The designed prototypes have been fabricated with the conventional low cost PCB etching process and tested at 60GHz-band frequencies. The antennas have been designed for three highly demanding applications of 60GHz-band; (i) a medium gain (~13dBi) wide beam antenna is proposed for full indoor point to multi-point wireless coverage in an ordinary size room of $10\times10m^2$, (ii) a high gain (20dBi) narrow beam antenna array is designed for point to point communication up to 20m distance, and finally (iii) a dual band antenna is designed operating at 59GHz and 63.5GHz for duplexer applications. All of the tested antennas convince the requirements of multi-gigabits/s data rate 60GHz-band WLAN and WPAN systems recommended by IEEE 802.11ad and IEEE 802.15.3c standards. The measured and simulation results showed good agreement in all the cases.

5.1. Introduction

Microstrip antennas exhibit attractive features for 60GHz-band WLAN/WPAN applications including compact size, low profile, low cost, and compatibility with on-chip and in-package devices [1]. However, the conventional microstrip antennas inherently suffer as having insufficient gain (~8dB), narrow bandwidth (~3%), and incredibly small dimensions when designed at 60GHz-band frequencies [2-4]. As propagation at 60GHz-band frequencies incur severe free space losses, higher gain antennas are desirable to sustain a reliable wireless link [5, 6]. Furthermore, wider band antennas are essentially required at 60GHz-band to achieve exceptionally fast data throughput [7-10].

60GHz-band offers the required continuous frequency bandwidth for multi-gigabits/s data rate WLAN and WPAN applications as specified by IEEE 802.11ad and IEEE 802.15.3c standards [3, 6]. According to the IEEE standards, an antenna gain of 13.7dBi would be ideal for 10m distance coverage of 60GHz-band WLAN/WPAN when a transmitter power of 0dBm (limited to <10dBm) is used. Moreover, the 60GHz-band is further divided into 4 sub-channels as shown in Fig. 5.1 where each channel contains 2.16GHz bandwidth. For WLAN/WPAN applications, the transmission should be confined in any of these sub-channels [6].

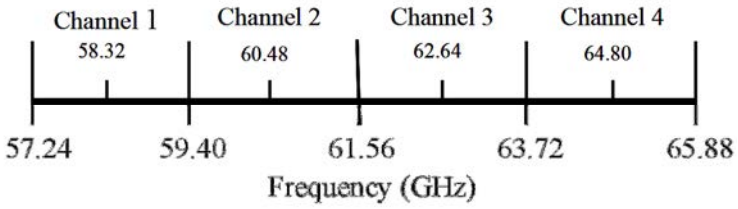

Fig. 5.1. 60GHz-band channels

In this chapter, MPA arrays have been presented for 60GHz-band point to multi-point and point to point wireless communications with substantial improvement in antenna size, gain, beamwidth and bandwidth performance. The antennas have been designed based on size improvement method to mitigate the fabrication constraints imposed by the conventional etching process. The antennas gain is consistently maintained over the operating frequencies. The antennas tested at 60GHz-band frequencies satisfy the performance requirements for multi-gigabits/sec data rate WLAN/WPAN applications as specified by the mentioned IEEE standards.

5.2. MPA Design for Full Indoor 60GHz-band WLAN/WPAN Coverage

5.2.1 Antenna Design and Results

A microstrip antenna array of 2×1 patch elements is designed at 62GHz to cover two frequency channels i.e. channel-2 and channel-3 (see Fig. 5.1) within 60GHz-band. Fig. 5.2 shows the antenna geometry [4]. The antenna dimensions are calculated with the procedure explained in Section 3.2 where the integers M=1, N=0, P=1 and Q=0 are substituted in eqs. (3.1), (3.2), (3.6) and (3.8), respectively. The transmission line (TL) width W_{T2} is set to be equal to $W_{T1}/2$ in order to reduce the side lobe level [1, 4]. The antenna is fabricated on RT/Duroid5880 substrate with substrate thickness 'h'= 0.127mm and t=17µm. The antenna's optimised dimensions are given in Table 5.1 where it can be seen that all of the dimensions are well above the minimum PCB fabrication limit of 152µm imposed by the conventional PCB etching method [1]. The fabricated antenna and experimental setup are shown in Fig. 5.3.

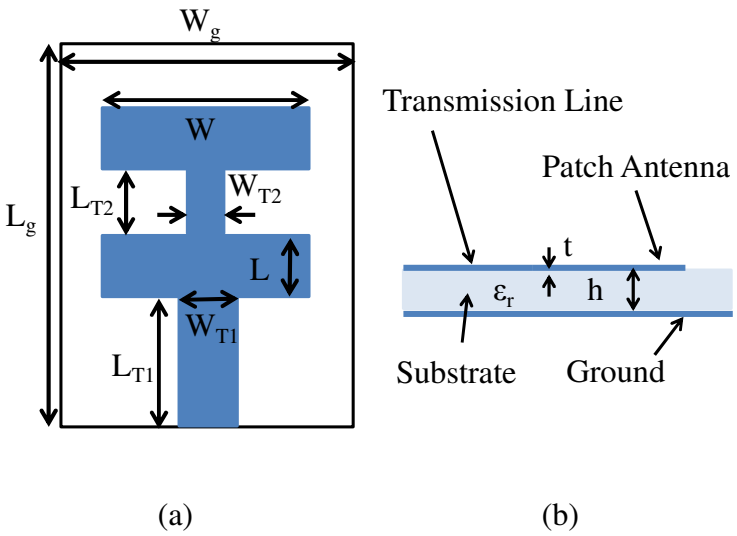

Fig. 5.2. Proposed antenna dimensions. (a) Front view and (b) side view

Table 5.1. Dimensions in mm of 60GHz-band antenna

L	W	L_{T1}	L_{T2}	W_{T1}	W_{T2}	h
1.48	5.54	2.51	1.48	0.595	0.297	0.127

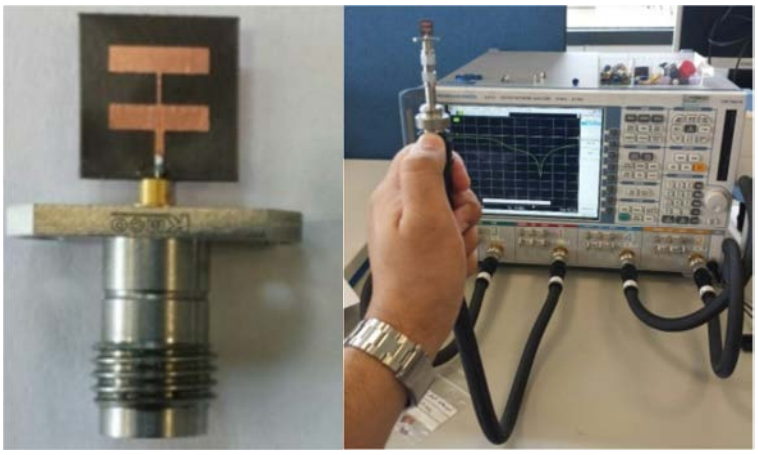

(a) (b)

Fig. 5.3. (a) Fabricated antenna and (b) experiment setup

Figure 5.4(a) shows the measured and simulated S_{11} response of the 60-band antenna, and (b) and (c) represent its FRP results in both E and H planes, respectively, at 62GHz. The measured -10dB bandwidth for this antenna is 4.92GHz which covers channels 2 and 3 for 60GHz WLAN/WPAN as discussed in Section 5.1. Fig. 5.5(a) illustrates the simulation gain frequency response and 5.5(b) presents the 3-dimetional FRP results. The antenna's measured gain is 10.1dBi and its beamwidth values in E and H planes are 32^0, 55^0 respectively. The measured gain is noticed to be about 3dB smaller than the simulation gain (13.2dBi) which may be due to the combined loss contribution of the V-connectors and glass bead (1.6dB) and antenna misalignment (1-2dB) [11]. Some distortions have been observed in the FRP which are due to significant contribution of the multipath reflections and obstruction from the surroundings and V-connector's body. The side lobe level of the proposed antennas can be

further reduced in the absence of V-connectors' transition when integrated with in-package devices for 60GHz wireless applications [4]. Nevertheless, the antenna bandwidth (4.92GHz), gain (~13dBi) and beamwidth characteristics comply with the specifications of aforementioned IEEE standards for 60GHz-band WLAN/WPAN applications [6].

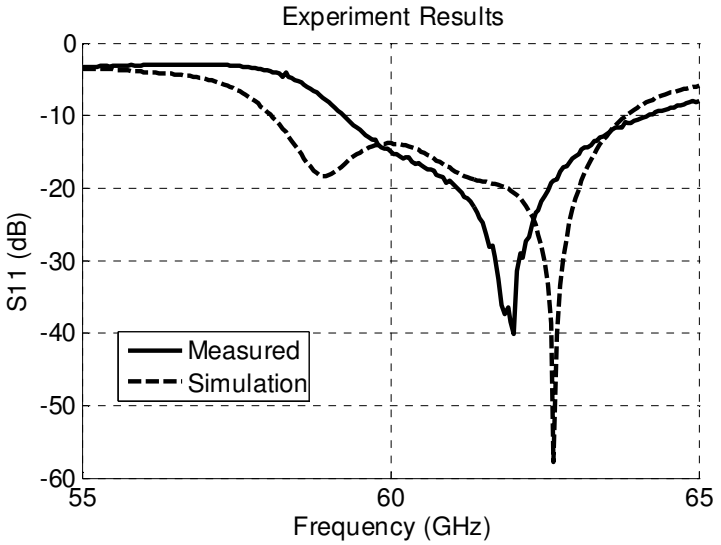

(a)

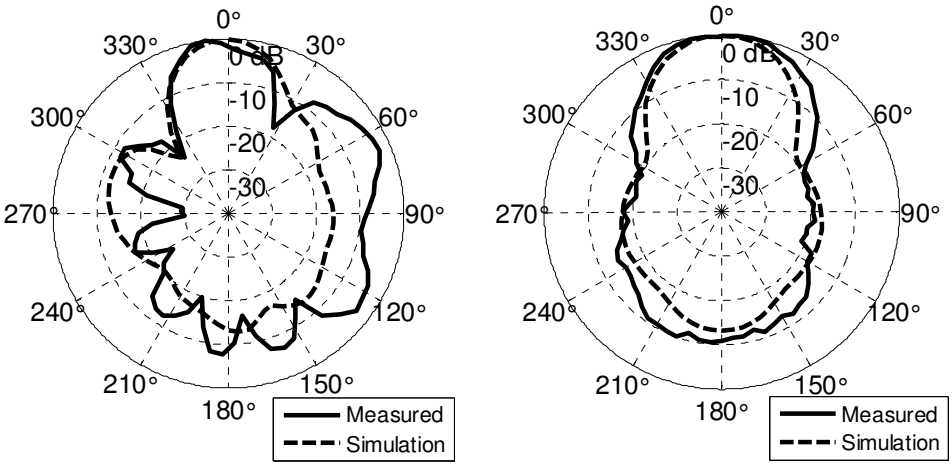

(b) (c)

Fig. 5.4. 60GHz antenna results. The simulated and measured (a) S_{11}, and FRP at 62GHz in (b) E-plane and (c) H-plane

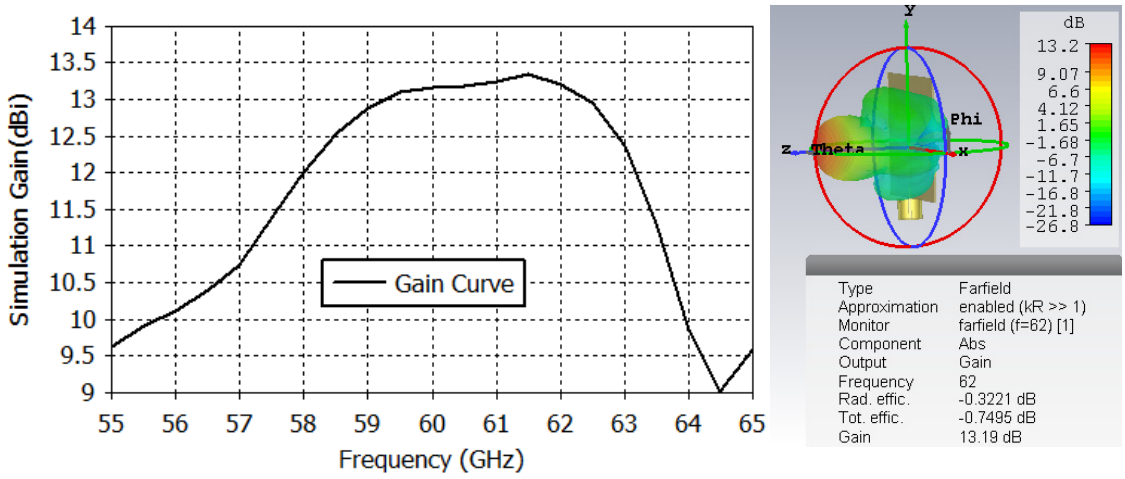

(a) (b)

Fig. 5.5. 60GHz antenna simulation response. (a) Gain vs frequency and (b) 3-dimentional FRP

5.2.2 60GHz-band Antenna Implementation for WLAN/WPAN

Antenna deployment for 60GHz-band WLAN and WPAN applications is a matter of current interest and in the recent years some valuable investigations have been reported on this topic [5-9]. According to the analysis performed in [6], the 60GHz WLAN/WPAN coverage is required in a sector area of a medium sized room (i.e. $\leq$ 10m$\times$10m). In doing so, the 60GHz antenna is ideally desired to have 13.7dBi gain with 0dBm transmitter power and half power beamwidth (HPBW) of 77.5^0 for 100% coverage in 10m$\times$10m room area when it is installed in the centre of the room's ceiling.

Based on the antenna requirement analysis reported in [5, 6], the gain, bandwidth, and radiation patterns of the proposed antenna are suitable for point to point radio link as well as for a reasonable coverage in point to multi-point coverage if installed in the centre of the ceiling. However, in point to multi-point links, the coverage area can be maximized up to 100% by installing two antennas in one of the room's corners with an inter-beam angular

distance of 45^0 as shown in Fig. 5.6 where a square room of 10m diagonal length and 3.5m height is considered for the service coverage. The wireless service is required 1.5m below the ceiling in the xz-plane [6] as shown in Fig. 5.6(b) (i.e. shaded sector). The room is further divided into two sub-sectors across the diagonal line. The two antennas are installed in the access point (AP) located in a corner at 1.5m from the ceiling in such a way that one antenna covers one sub-sector of 45^0 angular width and the other antenna covers the other half sub-sector of the same angular width [4].

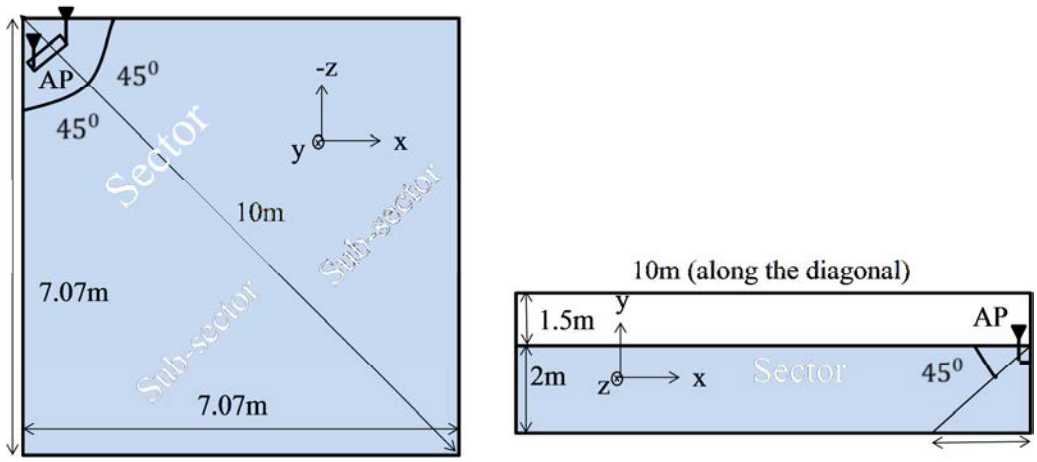

(a) (b)

Fig. 5.6. Proposed antenna implementation for 100% WLAN/WPAN coverage. (a) Top view and (b) side view of the room

5.3. High Gain MPA Array Design for 60GHz-band Point to Point Wireless Communications

According to IEEE802.11ad and IEEE802.15.3c standards' specifications for 60GHz WLAN and WPAN applications mentioned in the last section, an antenna bandwidth of 2.16GHz and gain of 19.7dBi with 0dBm transmitted, are desirable for multi-gigabits/sec data rate transmission over 20m distance through the line of sight wireless link [3,6]. However, designing of high gain (~20dBi) microstrip antenna is challenging for such point to point

wireless applications at 60GHz-band due to the requirement of an exceptionally large size array with so many elements and appropriate feeding and matching TL network with low loss and less fabrication complexity [10]. Therefore, a planar microstrip antenna array is proposed for 60GHz-band point to point WLAN/WPAN applications. The array is designed with 24 ultra-wide patch elements to achieve a gain of about 20dBi. Both series and parallel feeding networks are cooperated together to excite the patch elements in order to attain a good trade-off between the array's size and gain performance. Low impedance matching TLs are employed to enhance the overall array's fabrication tolerance by using low impedance wide TLs with only a single impedance transformation at the bottom end of the feeding network.

5.3.1 High Gain MPA Array Design

Figure 5.7 shows the geometry of the proposed microstrip antenna array [10]. The array is comprised of 6×4 symmetrical ultra-wide patch elements where 4 symmetrical columns of 6 series fed patches are excited through double stage power dividers. The antenna arrays' dimensions are calculated as described in the last Section 5.2 with the method explained in Section 3.2. However, the impedance matching is accomplished for the feeding network design as follows: 'W_{T1}' is calculated based on the total input impedance 'Z_{P1}' of the 6 series fed patch elements at point 'P_1'(see Fig. 5.7). The TL width 'W_{T2}' is calculated based on the input impedance 'Z_{P2}' at point P_2 which is a parallel combination of the two Z_{P1} impedances (i.e. $Z_{P1}\|Z_{P1}= Z_{P1}/2$). Similarly, the total antenna input impedance 'Z_a' at point P_3 is the parallel combination of two 'Z_{P2}' impedances which is eventually matched with the standard 50Ω impedance through TL 'L_{T2}' with the characteristic impedance $Z_0 = \sqrt{50\times Z_a}$. Equation (3.5) is used to calculate all of the TL widths. The array's final dimensions are obtained by using the optimisation tools of CST Microwave Studio.

Based on this procedure, the proposed microstrip patch antenna array is designed on RT/Duroid 5880 substrate with dielectric constant 'ε_r'=2.2, and loss tangent 'tan(δ)'=0.0009, substrate thickness 'h'=0.127mm and copper cladding 't'=17.5µm at 61.56GHz frequency which lies at the centre of 60GHz-band as mentioned earlier. The employed substrate thickness with copper cladding on both sides provides reasonable strength for the antenna to not bend without any additional mechanical support. The calculated input impedances at positions P_1 and P_2 are 8.4Ω and 4.2Ω, respectively, which correspond to the characteristic impedances of TL widths W_{T1} and W_{T2} (shown in Fig. 5.7), respectively, whereas the impedance at P_3 is 2.1Ω which is matched to the standard 50Ω impedance through 10.25Ω impedance transformer of width W_{T3}. Table 5.2 shows the optimised dimensions of the proposed antenna array where it can be seen that all of the dimensions are well above the ordinary PCB etching limit of 152µm line gap/width. The overall antenna size is 27.05x31.62mm^2.

Table 5.2. Dimensions in mm of the designed high gain antenna array

L	W	L_{T1}	L_{T2}	W_{T1}	W_{T2}	W_{T3}	S
1.53	5.12	1.69	2.34	1.15	1.2	0.93	1.56

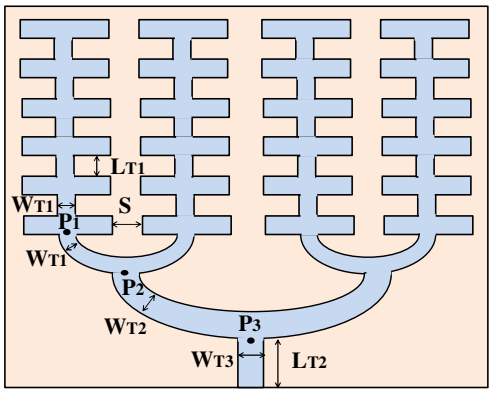

Fig. 5.7. Geometry of the proposed microstrip patch antenna array. (a) Front view (b) side view

5.3.2 Results and Discussions

Figures 5.8(a) and (b) demonstrate the fabricated antenna array and the experiment setup, respectively. Fig. 5.9(a) shows the measured and simulated S_{11} response, Figs. 5.8(b) illustrate the measured and simulated FPR in E and H planes at 61.56GHz, whereas Figs. 5.8(c) shows the simulated 3-dimentional FRP. As seen from Fig. 5.9, the measured -10dB return loss bandwidth is 2.64GHz which is 4.26% of the central frequency and the measured maximum gain is 19.26dBi at 61.75GHz which are in close agreement to the simulation bandwidth and gain of 2.34GHz and 19.94dBi, respectively. From Fig. 5.9(b), it is obvious that the antenna has narrow half power beam-widths of around 11^0 and 8^0 in the E and H planes, respectively, which endorses the antenna's high gain performance. However, it has also been noticed that there is about a 5^0 beam scanning in E-plane across the operating frequency bandwidth due to the series feeding of the patch elements. The measured bandwidth and gain performance of the proposed antenna array satisfies the antenna requirements for 60GHz-band point to point WLAN/WPAN applications specified by IEEE802.11ad and IEEE802.15.3c standards as mentioned earlier.

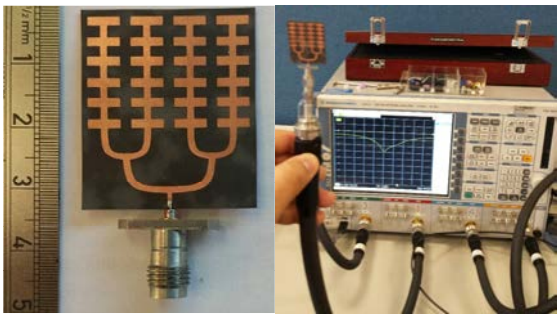

(a) (b)

Fig. 5.8. (a) The fabricated antenna array (b) experiment setup

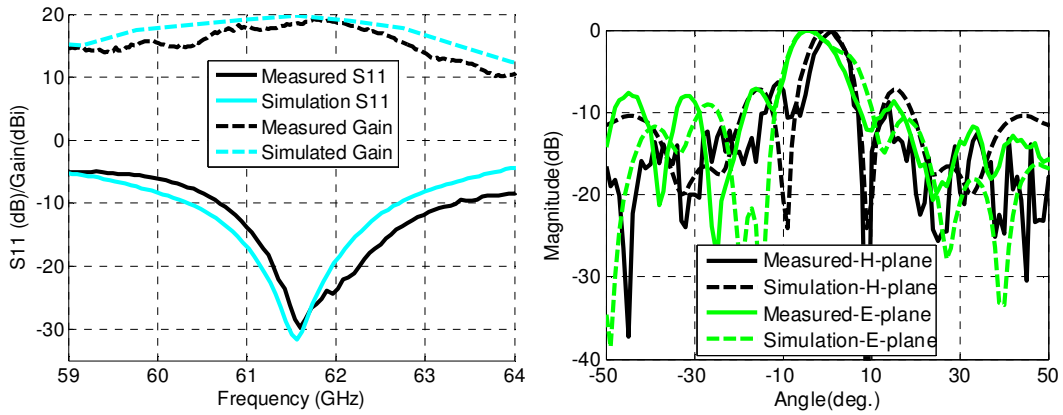

(a) (b)

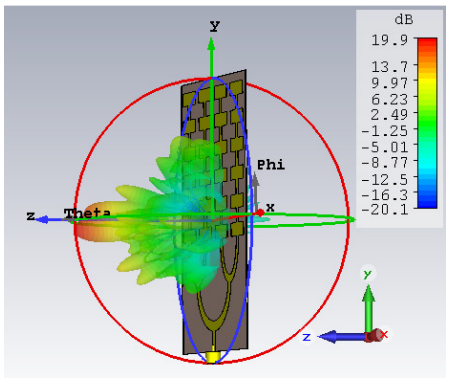

(c)

Fig. 5.9. Simulation and measured results of the proposed antenna array. (a) S_{11} and (b) FRP in E and H planes at 61.56GHz and (c) 3-D simulated FRP

5.4. Dual Band MPA Design for 60GHz-band Duplexer Applications

For 60GHz-band wireless communication systems, duplexer is an essential part of the transceiver's front-end and it has been widely studied in recent years [12-15]. In past, a cross mode conventional single patch dual band antenna is reported in for duplexer applications [16]. However, in the present work a single patch antenna is designed based on the size extension method, as discussed in Chapter-3, for dual band frequencies i.e. f_1=59GHz and f_2=63.5GHz to cover the two significant portions of 60GHz-band for duplexer applications. The antenna is designed on RT/Duroid5880 substrate with substrate thickness 'h'=0.254mm

and copper cladding 't'=17.5µm. Fig. 5.10(a) shows the geometry of the proposed dual band antenna. The patch lengths L_{f1} and L_{f2} define resonant frequencies 59GHz and 63.5GHz, respectively. On the other hand, the patch lengths L_{f1} and L_{f2} act as patch widths for resonant frequencies 63.5GHz and 59GHz, respectively, which are necessarily to be computed first for the rest of the MPA dimensions calculations. Therefore, initially two MPAs are designed separately at the mentioned frequencies and then the length of one patch is set to be the width for the other. Subsequently, both of the TL widths are slightly adjusted to improve the impedance matching at the corresponding frequencies. The optimized antenna dimensions are depicted in Table 5.3 where it can be seen that all of the antenna dimensions are well above the PCB fabrication limit of 152µm.

Table 5.3. Dimensions in mm of the dual band antenna

$L_{f\,1}$	$L_{f\,2}$	L_{Tf1}	L_{Tf2}	W_{Tf1}	W_{Tf2}
1.53	5.12	1.69	2.34	1.15	1.2

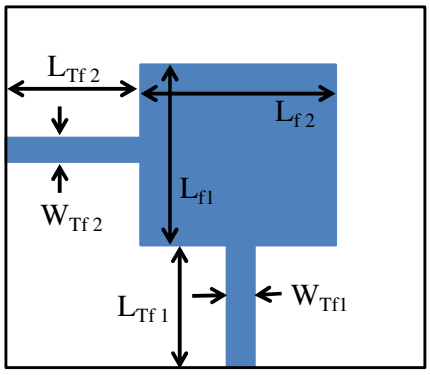

Fig. 5.10. Dual band MPA geometry

Figure 5.11(a) illustrates the fabricated antenna whereas Figs. 5.11(b) and (c) show the simulation and measured S_{11} and FRP in E and H planes at 59GHz and 63.5GHz, respectively. It should be noted that at a time only one port is connected to the VNA and the other one is kept open for one band measurements. As seen from Figs. 5.11(b)-(d), in all the cases the

measured and simulations results show good agreement at both of the resonant frequencies. Table 5.4 shows the measured performance parameters of the tested dual band antenna. It is clear from Table 5.4 that the measured -10dB S_{11} bandwidths at the two frequencies cover a reasonable portion of 60GHz-band. For duplexer applications, since high channel isolation is desirable, some sort of band pass filters may be embedded along with the transmission lines to enhance the inter-channel isolation [12-15].

Table 5.4. The dual band antenna performance

Frequency	Bandwidth	Frequency range	Gain	Beamwidth (E,H planes)
59GHz	2.61GHz	58.03-60.62GHz	9.3dBi	30^0, 46^0
63.5GHz	2.1GHz	62.35-64.45GHz	10.1dBi	19^0, 51^0

(a)

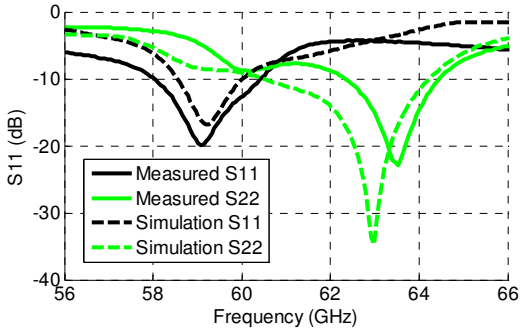

(b)

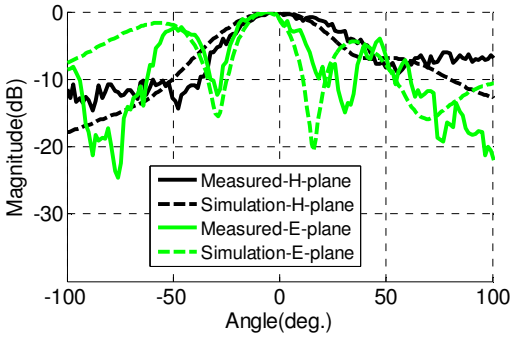

(c)

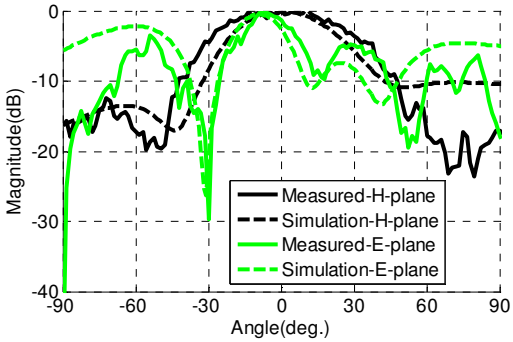

(d)

5.11. Simulation and measured results of 60GHz dual band MPA. (a) Fabricated prototype (b) S_{11}, and FRP in E and H planes at (c) 59GHz and (d) 63.5GHz

5.5. Conclusion

MPA arrays have been proposed for 60GHz WLAN/WPAN applications. A medium gain antenna has been presented for full wireless coverage in a $10\text{m} \times 10\text{m}$ room whereas a high gain antenna array has been designed for around 20m point to pint wireless communication. The performance of the proposed 60GHz antennas satisfied the requirements of IEEE 802.11ad and IEEE 802.15.3c standards for multi-gigabits/s 60GHz WLAN and WPAN applications. For the high gain MPA array, instead of using the conventional high impedance TL transitions in the feeding and matching network, low impedance TLs have been obtained by reverse matching technique to simplify the feeding structure for low power loss and high fabrication tolerance. Lastly, a dual band single patch microstrip antenna has been proposed for 60GHz-band duplexer applications. The antenna has been fabricated with simple etching process and the measured and simulations results showed good agreement. Since, high channel isolation is desirable for duplexer applications, some sort of band pass filters may be employed in the beginning of the feeding lines to reduce cross channel interference.

5.6. References

1. Bancroft, R., 2009. *Microstrip and printed antenna design*. The Institution of Engineering and Technology.
2. Balanis, C.A. ed., 2011. *Modern antenna handbook*. John Wiley & Sons.
3. Verma, L., Fakharzadeh, M. and Choi, S., 2013. Wifi on steroids: 802.11 ac and 802.11 ad. *IEEE Wireless Communications*, *20*(6), pp.30-35.
4. Rabbani, M.S. and Ghafouri-Shiraz, H., 2016. Improvement of microstrip patch antenna gain and bandwidth at 60 GHz and X bands for wireless applications. *IET Microwaves, Antennas & Propagation*, *10*(11), pp.1167-1173.

5. Karnfelt, C., Hallbjorner, P., Zirath, H. and Alping, A., 2006. High gain active microstrip antenna for 60-GHz WLAN/WPAN applications. *IEEE Transactions on Microwave Theory and Techniques*, *54*(6), pp.2593-2603.
6. Biglarbegian, B., Fakharzadeh, M., Busuioc, D., Nezhad-Ahmadi, M.R. and Safavi-Naeini, S., 2011. Optimized microstrip antenna arrays for emerging millimeter-wave wireless applications. *IEEE Transactions on antennas and propagation*, *59*(5), pp.1742-1747.
7. Qasim, A.M. and Rahman, T.A., 2010, November. A compact & high gain series array planar antenna for 60-GHz WPAN applications. In *Applied Electromagnetics (APACE), 2010 IEEE Asia-Pacific Conference on* (pp. 1-5). IEEE.
8. Vettikalladi, H., Lafond, O. and Himdi, M., 2009. High-efficient and high-gain superstrate antenna for 60-GHz indoor communication. *IEEE Antennas and Wireless Propagation Letters*, *8*, pp.1422-1425.
9. Artemenko, A., Maltsev, A., Mozharovskiy, A., Sevastyanov, A., Ssorin, V. and Maslennikov, R., 2013. Millimeter-wave electronically steerable integrated lens antennas for WLAN/WPAN applications. *IEEE Transactions on Antennas and Propagation*, *61*(4), pp.1665-1671.
10. Rabbani, M.S. and Ghafouri-Shiraz, H., 2017. High gain microstrip antenna array for 60 GHz band point to point WLAN/WPAN communications. *Microwave and Optical Technology Letters*, *59*(3), pp.511-514.
11. Online [accessed on 05th April 2016]: http://www.shf.de/wp-content/uploads/datasheets/datasheet_kpc_flange_launcher_185_302.pdf

12. Wang, D., Chin, K.S., Che, W., Chang, C.C. and Wu, Y., 2014. 60 GHz duplexer design using dual-mode SIW filters with single-sided transmission zeros. *Electronics Letters*, *50*(21), pp.1529-1531.
13. Bairavasubramanian, R., Pinel, S., Laskar, J. and Papapolymerou, J., 2006. Compact 60-GHz bandpass filters and duplexers on liquid crystal polymer technology. *IEEE microwave and wireless components letters*, *16*(5), pp.237-239.
14. Kuroki, F., Murata, Y. and Yoneyama, T., 2004. Filter-based NRD-guide duplexer with low loss and high isolation at 60 GHz. *Electronics Letters*, *40*(13), pp.808-810.
15. Lee, J.H., Kidera, N., DeJean, G., Pinel, S., Laskar, J. and Tentzeris, M.M., 2006. A V-band front-end with 3-D integrated cavity filters/duplexers and antenna in LTCC technologies. *IEEE transactions on microwave theory and techniques*, *54*(7), pp.2925-2936.
16. James, J.R., Hall, P.S. and Wood, C., 1981. *Microstrip antenna: Theory and design* (No. 12). Iet.

Chapter-6

Implementation of Frequency Selective Surface on the Proposed MPA

Abstract: In this chapter, implementation of planar double layer frequency selective surface (FSS), also known as partially reflective surface, on the improved size MPA has been presented at 60GHz-band frequencies. The FSS is excited through the microstrip antenna array of two ultra-wide patch elements. Both the FSS unit cell and the feeding patch elements are set to be the same in size and their dimensions are calculated based on the patch antenna size improvement method to convince the fabrication limitations of the PCB etching process. The performance of FSS antenna with different layer sizes (i.e. with different number of unit cells) has been studied by designing and testing them at 60GHz and it has been found that the proposed FSS structure with 12-elements in each of the FSS layers showed a good trade-off between the antenna gain, bandwidth and size. Finally, the concluded 12-elements FSS antenna is redesigned and tested at 10GHz to further verify the proposed designing concept and performance, because the fabrication tolerance and measurement accuracy at 10GHz are better than they are at 60GHz.

6.1 Introduction

As mentioned in Chapter-2, FSS antennas have been comparatively less explored for mm-wave and THz frequencies partly because in the traditional way a very large FSS area with fine PCB details is required for substantial improvement in antenna gain which may not be practical for compact wireless devices at the mentioned high frequencies [1-3]. Therefore, in order to eliminate the need of a large FSS array and incredibly small FSS unit cell for moderate to high antenna gain, it is proposed to apply double FSS layers in front of an improved gain feeding

element at a distance of 3rd multiple of the fundamental resonant cavity height [1]. Both the FSS unit cell and the feeding patch elements are set to be the same in dimensions and they are designed based on the patch antenna size improvement method to convince the fabrication limitations imposed by the conventional PCB etching method. Three double layers FSS antennas have been presented with 2, 12 and 24 elements in each of the FSS layers and the measured gains of 15.6dBi, 19.1dBi and 19.75dBi are obtained, respectively, at 63.72GHz. It has also been analysed that the overall antenna bandwidth is reduced when more layers and numbers of FSS elements are employed to improve the antenna gain. The tested antenna with 12 FSS unit cells in each layer showed a reasonable gain and bandwidth compromise for 60GHz-band point to point wireless applications [4, 5]. The measured and simulation results showed good agreement in all the cases.

Since, the antenna measurements at 60GHz incur several types of imperfections, the optimal 12-elements FSS antenna has been redesigned at 10GHz frequency and its performance has been further analysed through both simulation and practical measurements [1]. A good correlation has been observed between the FSS antennas designed at 10GHz and 60GHz frequencies.

6.2 Antenna Design Procedure

The FSS unit cell, FSS layout and the overall antenna structure are demonstrated in Figs. 6.1(a)-(c), respectively. The MPA array design with 2×1 elements presented in Section 4.2 (see Figs. 4.1(a) and 4.2(a)) is employed for feeding the FSS antenna with a slight optimisation in dimensions i.e. L=1.26mm, W=5.23mm, W_T=1mm, L_{T1}=2.29mm and L_{T2}=1.8mm (see Fig. 4.1(a)), to resonate at 63.72GHz. The FSS unit cell is a rectangular patch with the same substrate

and dimensions as those of the feeding patch element i.e. RT/Duroid5880 with substrate thickness 'h'=0.254mm and copper cladding '$t' = 17\mu m$.Three FSSs are designed with multiple number of unit cell elements i.e. 2-elements, 12-elements and 24-elements as depicted in Fig. 6.1(b). Then three FSS antennas are designed with two layers of each FSS (i.e. FSS1 and FSS2) in such a way that FSS1 is placed in front of the feeding patch antenna at a distance 'h_1' and the FSS2 is placed at the distance 'h_1' from FSS1 as shown in Fig. 6.1(c).

The proposed FSS antenna works based on the fundamental principles of Partially Reflective Surface, Leaky-Wave and Fabry-Perot Cavity antennas [2, 3, 6, 7]. The feeding antenna element radiates electromagnetic (EM) wave in the resonant cavity from where the wave is partially transmitted through the FSS and partially reflected back and forth within the cavity between the FSS and ground plane until it is either fully transmitted from the FSS or it has reached to the end of the cavity sides. This way, the FSS acts as a focussing lens to the EM wave of the resonance frequency. The relative directivity of the FSS is estimated by ray tracing analysis of the FSS unit cell [2]. According to the ray tracing theory, when a radiating source with radiation pattern F(α) is placed in between a conducting plane and FSS, as shown in Fig. 6.1, the electromagnetic (EM) wave encounters multiple reflections while propagating within the cavity. When the FSS acts as partially reflective surface (PRS), a part of the EM wave transmits through the FSS on each reflection until all of the EM energy is finished. If $\Gamma = Re^{j\varphi}$ is the reflection coefficient of the FSS, where R and φ are the magnitude and phase response, respectively, the total transmitted electric field intensity is given under lossless transmission as [8]:

$$E = \sum_{n=0}^{\infty} F(\alpha) E_0 \cdot \left(Re^{j\emptyset}\right)^n \cdot \sqrt{1 - R^2} \qquad (6.1)$$

Where E_0 is the maximum electric field intensity, $\emptyset$ is the phase variation due to the conducting screen, FSS and the path difference between them, and n is the number of reflections to EM wave. By using the basic trigonometry shown in Fig. 6.1, it can be shown that the phase difference between the n^{th} reflected ray and 0^{th} ray is given as:

$$n\emptyset = n\left[-\frac{4\pi}{\lambda}h_1 \cdot \cos(\alpha) - \pi - \varphi\right] \qquad (6.2)$$

Since $R < 1$, it can be shown by geometric series that for n=0

$$\sum_{n=0}^{\infty}\left(Re^{j\emptyset}\right)^n = \frac{1}{1 - Re^{j\emptyset}} \qquad (6.3)$$

By putting (6.2) and (6.3) into (6.1), it reads:

$$|E| = F(\alpha) \cdot |E_0| \cdot \sqrt{\frac{1 - R^2}{1 + R^2 - 2R \cdot \cos\left(\varphi - \pi - \frac{4\pi}{\lambda} \cdot h_1 \cdot \cos(\alpha)\right)}} \qquad (6.4)$$

Therefore, the power pattern can be given as:

$$P = \frac{1 - R^2}{1 + R^2 - 2R \cdot \cos(\varphi - \pi - \frac{4\pi}{\lambda} \cdot h_1 \cdot \cos(\alpha))} \qquad (6.5)$$

and the maximum power is obtained at $\alpha = 0$, and:

$$\varphi - \pi - \frac{4\pi}{\lambda} \cdot h_1 = 2N\pi, \qquad \text{where N is an integer} \qquad (6.6)$$

The Maximum power will be:

$$P = \frac{1 - R^2}{1 + R^2 - 2R} = \frac{1 + R}{1 - R} \qquad (6.7)$$

Consequently, the relative maximum antenna directivity 'D' in dB of the FSS is given as:

$$D(dBi) = 10\log\left[\frac{1+|\Gamma|}{1-|\Gamma|}\right] \qquad (6.8)$$

Where $|\Gamma|=R$ is the magnitude of reflection coefficient of the FSS unit cell.

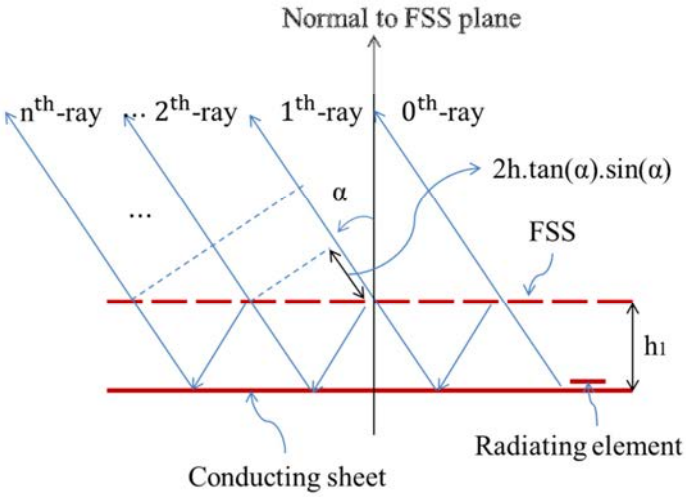

Fig. 6.1. The optic ray theory for FSS response estimation

From eq. (6.8) it is obvious that a high $|\Gamma|$ is required to attain high antenna directivity. As discussed in [7], the value of $|\Gamma|$ depends on the FSS geometry and it has been shown that a closely packed rectangular patch strip based FSS can produce the best directivity response. In our current case, we chose rectangular strips for the FSS but packed them widely (1.8mm separation (see Fig. 6.1(a))) to deal with the fabrication concerns with PCB etching process specially when designed for mm-wave and THz frequencies. The separation 'h_1' between the ground plane on a

dielectric material and FSS (see Fig. 6.2(c)) is approximated from (6.5) as follows and then it is optimized with CST Microwave Studio based simulation process explained in the next paragraph:

$$h_1 = \frac{N\lambda_0}{2} - \frac{\lambda_0}{4\pi}(\varphi - \theta) \qquad (6.9)$$

Where φ and θ are the phase angle of the reflection coefficients of FSS and dielectric based ground plane, respectively. The phase angle φ of the unit cell is obtained from the simulation results whereas θ is calculated by [3, 6]:

$$\theta = \pi - 2\tan^{-1}\left(\frac{\tan(2\pi h\sqrt{\varepsilon_r}/\lambda_0)}{\sqrt{\varepsilon_r}}\right) \qquad (6.10)$$

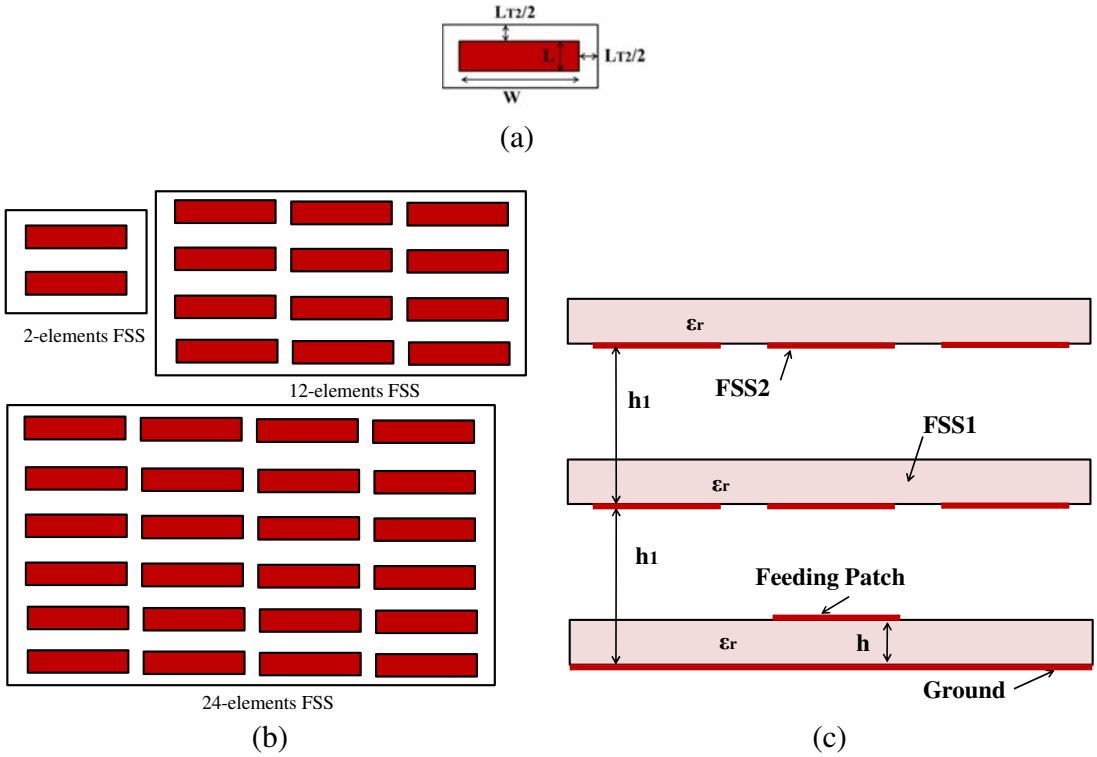

Fig. 6.2. Proposed FSS antenna layout. (a) FSS unit cell, (b) three examined FSS layers and (c) FSS antenna

The proposed FSS unit cell is simulated in CST Microwave Studio to get φ and |Γ| by defining the top and bottom boundaries as electric walls whereas the side boundaries as magnetic walls. The reflection coefficient response is recorded with both the single layer FSS unit cell and placing a second FSS unit cell at a distance of $3\times\lambda_0/2$ from the first FSS unit cell. Fig. 6.3 presents the simulated FSS unit cell layouts and their reflection coefficients results where (a) and (b) are the simulated single and double FSS unit cells, respectively, and (c) and (d) are the simulated magnitude and phase of the reflection coefficients. As seen from Fig. 6.3(c), |Γ| significantly improved from 0.56 to 0.75 when a second FSS unit cell is introduced at distance $3\times\lambda_0/2$ (see Fig. 6.2(b)). Therefore, a double layer FSS at the 3rd multiple of the fundamental resonant cavity height is proposed for the antennas' gain enhancement. It is found from Fig. 6.3(c) and (d) that |Γ|=0.756 and $\varphi=165.5^0$ at 63.72GHz frequency. Subsequently, from eq. (6.10) it is calculated that $\theta=139.47^0$. This way, we get the initial value of h_1=6.89mm for N=3 from eq. (6.9) and D=8.57dBi from eq. (6.8). Therefore, it is estimated that an antenna gain improvement of about 8dBi is accomplishable with the proposed double layered FSS structure. On the other hand, the maximum achievable half-power gain (-3dB down from maximum) fractional bandwidth 'BW_g' is approximated as [7]:

$$BW_g(\%) = \frac{\lambda_0}{2\pi\, h_1}\left[\frac{1-|\Gamma|}{\sqrt{|\Gamma|}}\right] \qquad (6.11)$$

Hence, from eq. (6.11), it is calculated that BW_g=1.94% may be obtained from the proposed structure of the FSS antenna.

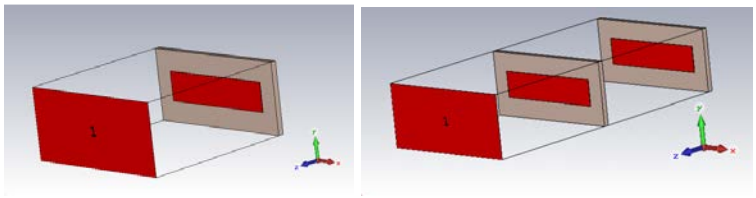

(a) (b)

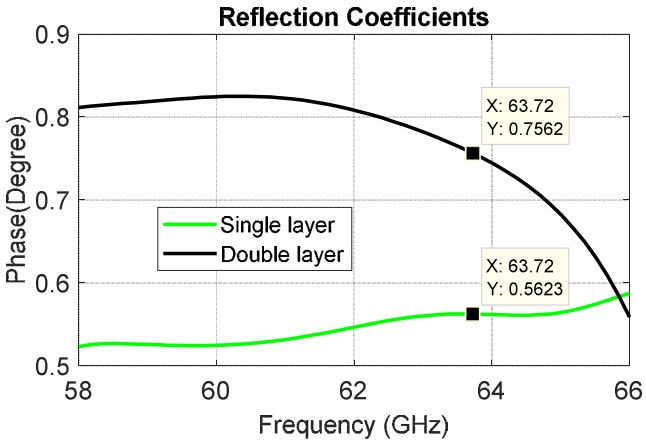

(c)

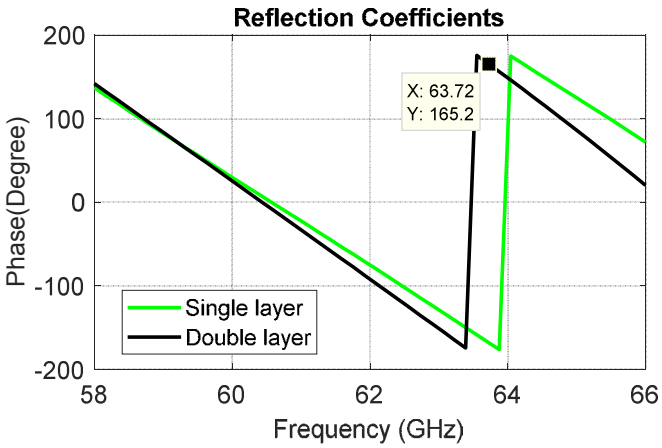

(d)

Fig. 6.3. FSS unit cell simulation results. (a) Simulated single FSS unit cell, (b) simulated double FSS unit cell, (c) magnitude of the reflection coefficients (|Γ|) and (d) phase angle (φ)

6.3 Results and Discussions

Three double layered FSS antennas i.e. 2-elements, 12-elements and 24-elements FSS antennas, have been fabricated and tested. For 2-elements FSS antenna the optimised h_1=7.38mm whereas for 12 and 24 elements FSS antennas the optimised h_1=7.15mm which are close to the estimated h_1=6.88mm. Figs. 6.4-6.6 illustrate the results of 2-elements, 12-elements and 24-elements FSS antennas, respectively, where (a)-(c) show fabricated antennas with experiment setup, S_{11}, and FRP in E and H planes at 63.72GHz, respectively. In all the cases the measured results agreed well with the simulations results. It can be seen from Fig. 6.6(b) that in contrast with the simulation S_{11} results, the measured S_{11} shows two resonance dips at around 63.72GHz which may be because of the tolerance in assembling the two large FSS layers for which the two resonant cavity heights slightly differ from each other. Table 6.1 shows the summary of the measured results for the feeding antenna (presented in Sections 4.2 and 4.3) and all of the three tested FSS antennas. It is clear from Table 6.1 that as compared to the feeding antenna, there is about 2.4dBi gain improvement in 2-elements FSS antenna but in case of 12-elements FSS the gain is improved by 5.9dBi whereas the gain is increased by a maximum value of 6.65dBi in case of 24-elements FSS antenna which is about 2dB less than the predicted gain improvement of 8.57dBi which is due to the limited FSS layers. However, comparing Figs. 6.3-6.5 with Fig. 4.4(a) reveals that the FSS antennas' S_{11} bandwidth has slightly reduced as compared to the feeding antenna but it is still wide enough to cover a vast portion of the 60GHz-band frequencies shown in Fig. 5.1. As described in chapter 5, since an antenna gain in the range of 13.7dBi-19.7dBi is required for an indoor short distance (10m-20m) WLAN/WPAN link with a

transmitted power of 0dBm, one of the designed FSS antennas can be deployed for indoor multi-gigabits/sec WLAN/WPAN link depending on the coverage distance [9].

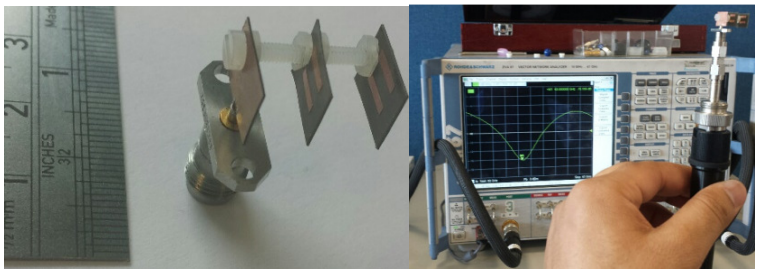

(a)

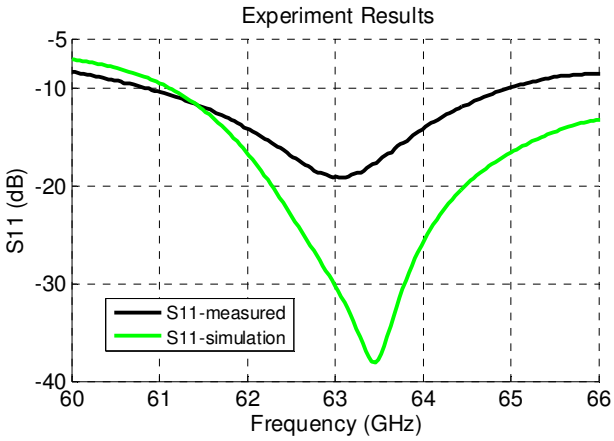

(b)

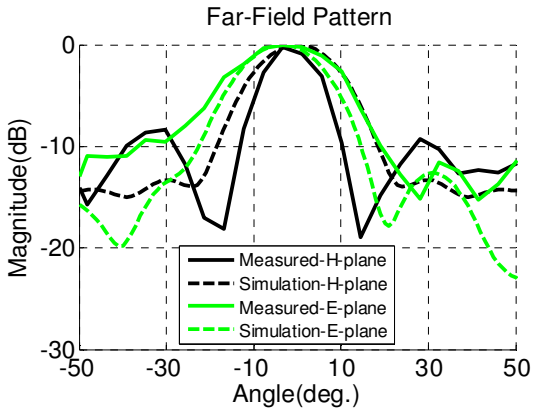

(c)

Fig. 6.4. Experiment results of 2-elements FSS antenna. (a) Fabricated antenna, (b) simulation and measured S_{11} and (c) simulation and measured FRP

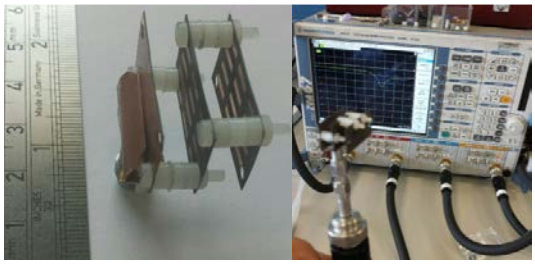

(a)

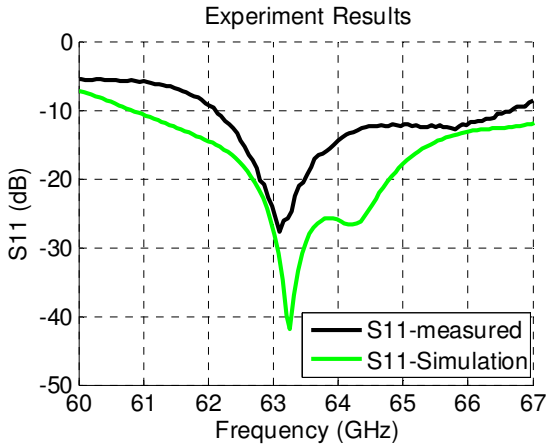

(b)

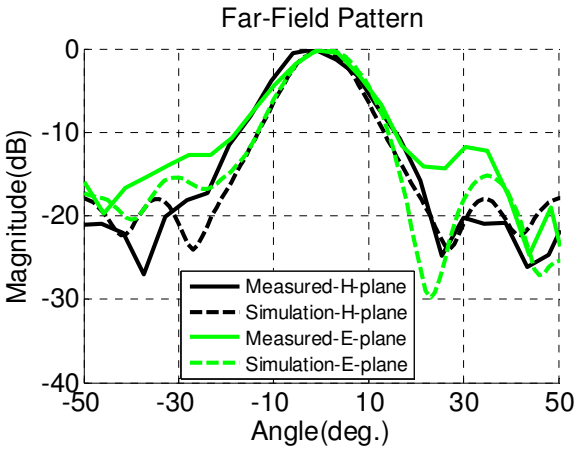

(c)

Fig. 6.5. Experiment results of 12-elements FSS antenna. (a) Fabricated antenna, (b) simulation and measured S_{11} and (c) simulation and measured FRP

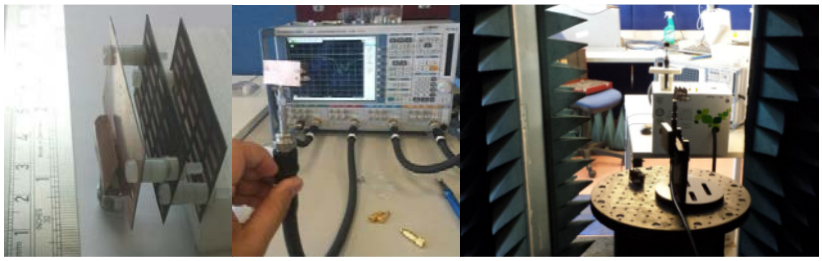

(a)

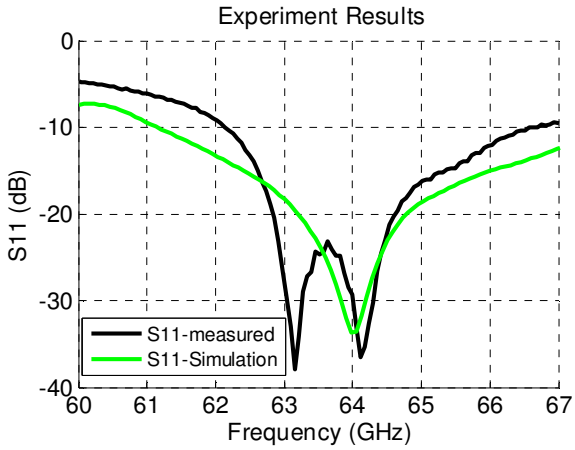

(b)

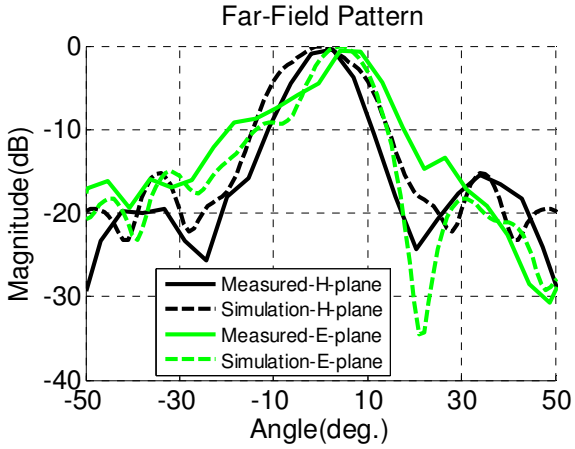

(c)

Fig. 6.6. Experiment results of 24-elements FSS antenna. (a) Fabricated antenna, (b) simulation and measured S_{11} and (c) simulation and measured FRP

Table 6.1. Summary of the 60GHz FSS antennas' performance

Antennas	S_{11} bandwidth	Gain
Feeding Antenna	5.55GHz	13.2dBi
2-elements FSS antenna	4.1GHz	15.6dBi
12-elements FSS antenna	4.57GHz	19.1dBi
24-elements FSS antenna	4.44GHz	19.75dBi

The process of gain improvement with the proposed FSS structures is further analysed based on the CST simulation results. For each of the FSS structures, a comparison is made between the gain frequency response of the (i) feeding antenna, (ii) single layer FSS antenna with the optimised fundamental resonant cavity height (N=1 in eq. (6.9)), (iii) single layer FSS antenna with the 3rd multiple of the resonant cavity height (N=3 in eq. (6.9)) and (iv) the proposed double layered FSS antenna with the 3rd multiple of the resonant cavity heights (N=3 in eq. (6.9)). Fig. 6.7 depicts the compared gain results where (a)-(c) show gain frequency responses of 2-elements, 12-elements and 24-elements FSS antennas, respectively. As seen from Figs. 6.7(a)-(c), in all of the three cases there is only a small gain improvement (1-2dBi) around the resonant frequency as compared to the feeding antenna when a single FSS is placed at the fundamental resonant cavity height but there is a significant gain enhancement when the resonant cavity height is increased to the 3rd order, whereas the gain improves to its maximum when a second FSS layer is placed at the 3rd order cavity height. However, it can also be noticed from Fig. 6.7 that antennas half power gain bandwidth shrinks both with increment in the FSS array size as well as with cavity height. In the case of 24-elements FSS antenna the gain bandwidth is 3.17GHz (4.93%) which is wider than the predicted 1.94% as calculated from eq. (6.11) which is due to 2dBi less gain improvement than predicted, as mentioned in the last paragraph. From Figs. 6.7(a)-(c), again it is obvious that

12-elements FSS antenna offers a good trade-off between the FSS array size and gain bandwidth (3.18GHz).

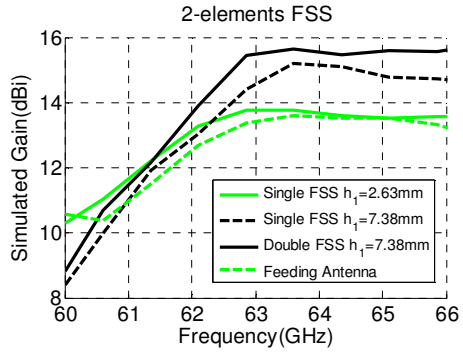

(a)

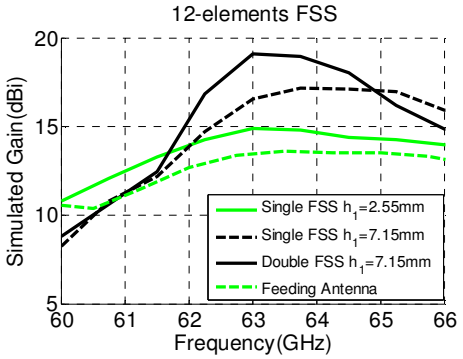

(b)

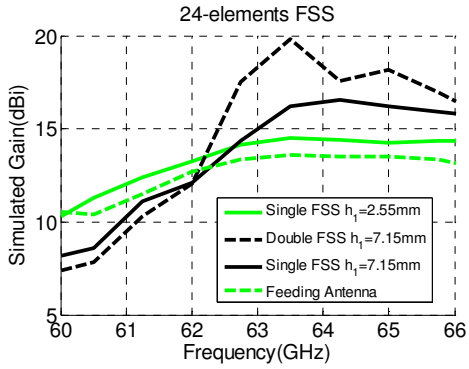

(c)

Fig. 6.7. Comparison of the gain improvement with the single and double layered FSS antennas at the fundamental and 3rd order resonant cavity heights. (a) 2-elements FSS antenna, (b) 12-elements FSS antenna and (c) 24-elements FSS antenna

6.4 FSS Antenna Re-designed at 10GHz

Based on the procedure explained in Section 6.2, the 12-elements FSS antenna is redesigned and tested at 10GHz frequency to examine the designing concept under a better testing environment. The FSSs' behaviour is studied under the ray tracing method to estimate the antenna gain enhancement at 10GHz. The improvement in the tested antenna performance is assessed across the state of the art FSS antennas at 10GHz reported in the literature.

6.4.1 Feeding Antenna and FSS Design

The microstrip antenna design given in Section 4.7, which is an array of two ultra-wide patch elements fed in series, is employed as feeding source for the 10GHz FSS antenna [4]. The antenna is designed on RT/Duroid5880 substrate with dielectric constant ε_r = 2.2, substrate thickness h= 1.57mm and copper cladding t=35μm. The feeding antenna geometry and the performance are demonstrated in Figs. 4.20-4.21. However, the ground and substrate area is extended to accommodate the 12-element FSS plane which slightly changed the measured gain to 13.2dBi. The FSS unit cell is a rectangular patch with the same substrate and dimensions as those of the feeding patch element i.e. L=9.03 and W=34.35 (see Fig. 6.2). The overall 10GHz FSS antenna structure is kept similar to the one presented at 60GHz 12-element FSS antenna in section 6.3.

Fig. 6.8(b) and (c) show the simulated reflection coefficient magnitude and phase of the double layer FSS unit cell with an optimised inter-separation of 46mm which corresponds to about 3rd

multiple of the operating half wavelength, respectively. From Fig. 6.8(b) and (c) it can be noticed that |Γ|=0.46 and ∠|Γ|=φ=129.6°. Substituting |Γ|=0.46 from Fig. 6.8(b) in eq. (6.8), it is predicted that an approximate improvement of 4.32dBi could be made in the feeding antenna's initial gain of 13.2dBi at 10GHz. with a semi-infinite size FSS. From (6.9), it can be computed that the resonant cavity height h_1=45.43mm.

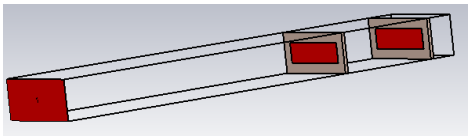

(a)

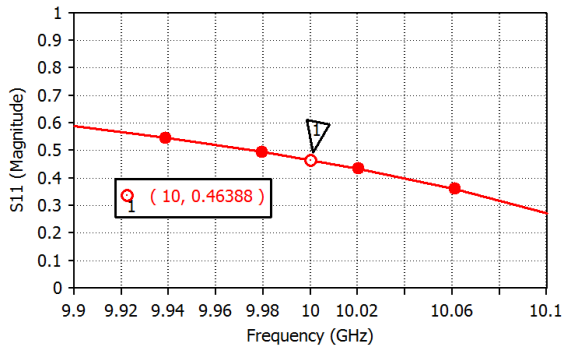

(b)

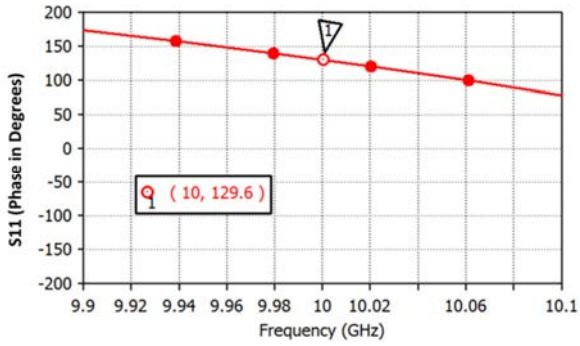

(c)

Fig. 6.8. FSS unit cell simulation results. (a) Simulated FSS unit cell, (b) magnitude of the reflection coefficients (|Γ|) and (c) phase angle (φ)

In order to visualise the process of antenna gain enhancement with the proposed distant double FSS layers, the antenna has been simulated with three ways; (i) with single FSS at h_1=16mm, (ii) with a single FSS layer at h_1=46mm and (iii) with the proposed double FSS layers each at h_1=46mm. Fig. 6.9 illustrates the simulated S_{11} and gain response in all the three cases. As seen from Fig. 6.9, for the single FSS layer placed at h_1=16mm the antenna gain is 14.72dBi at the peak resonant frequency of 9.9GHz. On the other hand, when h_1 in increased to 46mm the gain is improved to 17.1dBi. However, the gain reached to its maximum at 18.47dBi when a second FSS layer (FSS2) is placed at h_1=46mm from FSS1 which is fairly close to the mathematically predicted gain of 17.52dBi. Also, in this case, the antenna showed better S_{11} response compared to the single FSS antenna.

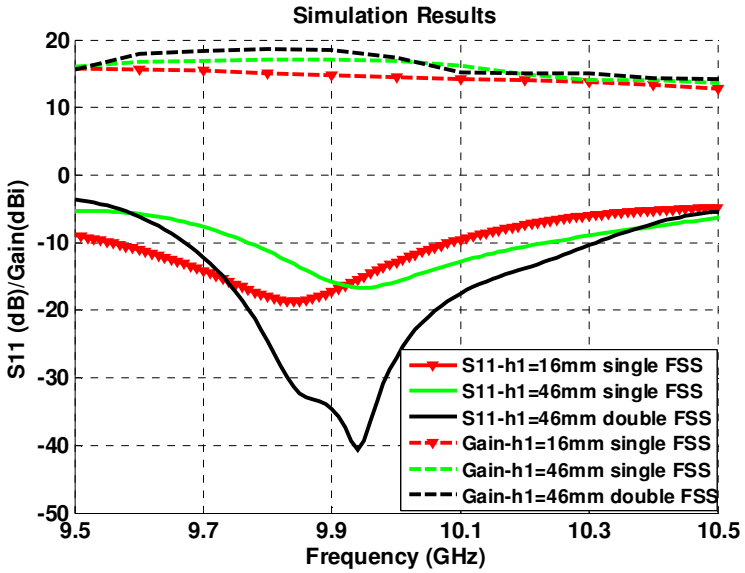

Fig. 6.9. Simulation S11 and gain results of the FSS antenna with single and double FSS layers at h_1 equal to 16mm and 46mm

6.4.2 10GHz FSS Antenna Results and Discussions

For practical verification of the predicted gain improvement with two FSS layers, the proposed 10GHz double layered 12-elements FSS antenna is fabricated and tested. Fig. 6.10 (a) shows the fabricated double FSS layers antenna and experiment setup. Fig. 6.10(b) presents the simulation and measured S_{11} and gain results of the proposed antenna whereas Fig. 6.10(c) depicts the simulation and measured FRP in E and H planes at peak resonance frequency of 9.9GHz. In all the cases the simulation and measured results show a close agreement. It is clear from Fig. 6.10(b) that the measured -10dB S_{11} bandwidth is 550MHz which is 5.55% of the central resonant frequency of 9.9GHz where the measured gain is 18.23dBi which is very close to the simulated gain of 18.47dBi.

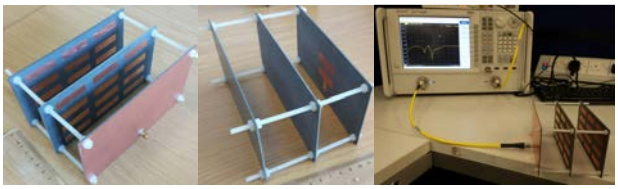

(a)

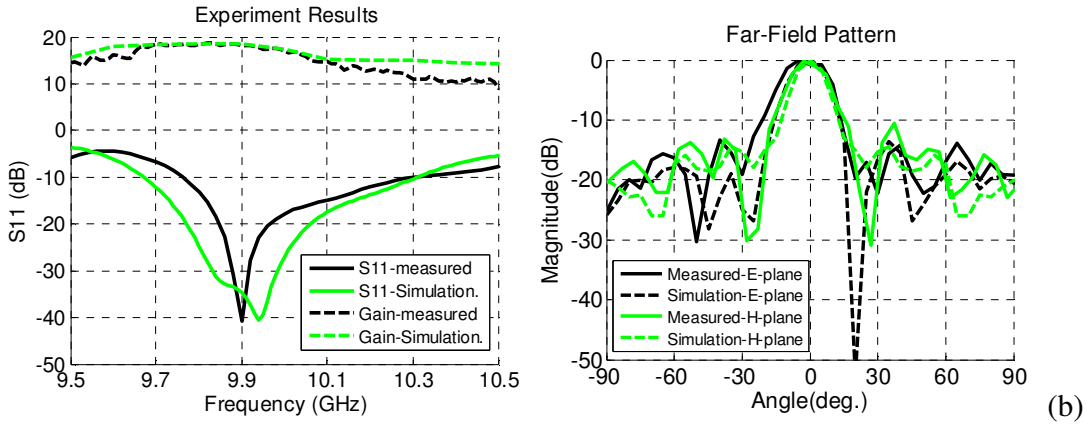

(b) (c)

Fig. 6.10 Experiment results of double layered FSS antenna (a) the fabricated antenna and experiment setup (b) S_{11} and (c) FRP at 9.9GHz

Finally, the measured gain (18.23dBi) of the double layered FSS antenna shown in Fig. 6.10(a) is further enhanced to 19.2dBi by placing two copper sheet reflectors across E-field vector of the antenna's E-field radiation. The metallic reflectors reduced the leakage of EM radiation and converged the radiation to the boresight angle which ultimately improved the antenna gain by 0.8dBi. The fabricated double FSS layers antenna with metallic reflectors is revealed in Fig. 6.11(a) and its simulation and measured S_{11} response and FRP at 9.8GHz are presented in Figs. 6.11(b) and (c), respectively. Again, the measured and simulation results show a close agreement. As seen from Fig. 6.11(b), both the measured S_{11} bandwidth and the maximum gain have improved to 660MHz and 19.13dBi, respectively. However, the gain frequency response of this antenna is narrower as compared to the gain frequency response of double layered FSS antenna without reflectors (see Fig. 6.10(b)). As compared to the FSS antennas operating at microwave frequencies reported in the literature [7, 10-12], the proposed 12-elements FSS antenna exhibits better trade-off between the antenna size and gain improvement. For instance, in [10] a single layer FSS based dual band antenna is designed at 6.9GHz and 13GHz frequencies and the gain values of 16.5dBi and 20.9dBi are achieved, respectively, with 121-elements FSS. Nonetheless, the 12-elements FSS antennas at both 60GHz and 10GHz show similarity in the performance and hence prove the designing concept.

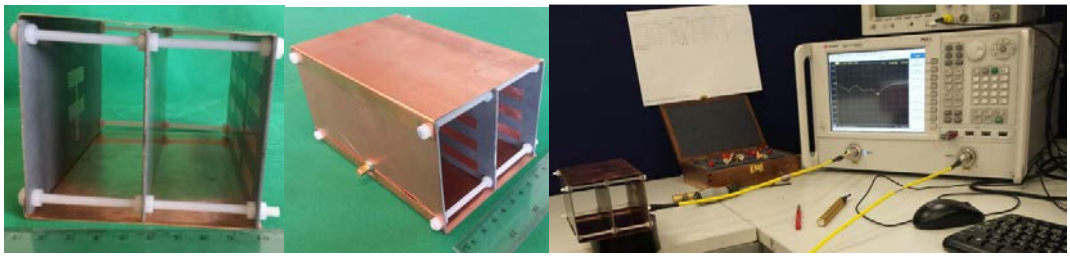

(a)

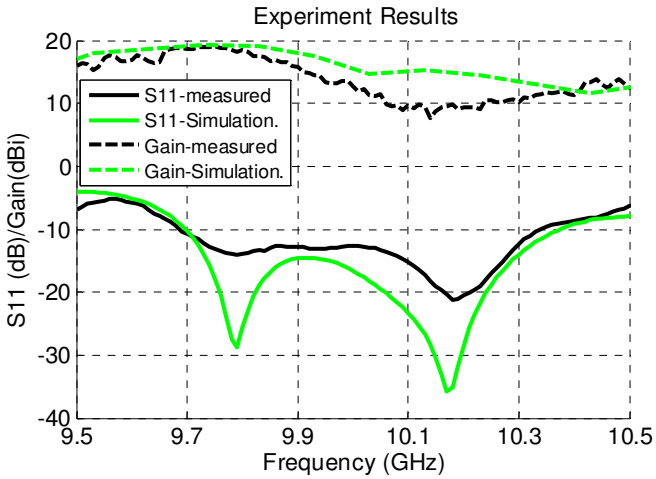

(b)

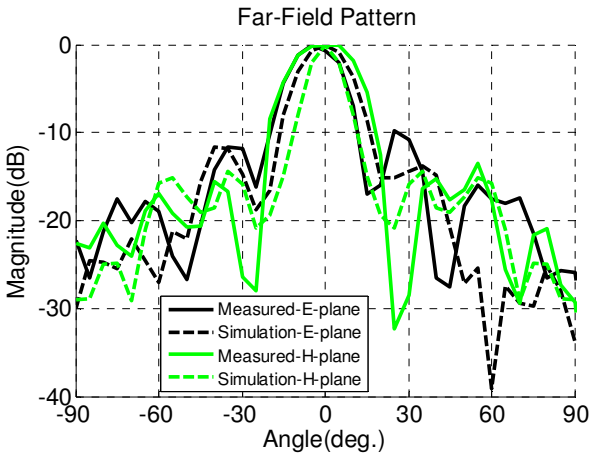

(c)

Fig. 6.11 Measured and simulation results of double layered FSS antenna with reflectors.

(a) Fabricated antenna and experiment setup (b) S11 and (c) far-field radiation patterns at 9.8GHz

6.5 Conclusion

In this paper, reduced array size of double layered FSS has been deployed to enhance the antenna gain for indoor 60GHz wireless applications. The FSS layers have been placed at 3rd multiple of the fundamental resonant cavity high to improve the feeding antenna gain (13.2dBi) by 6.65dBi. The dimensions of the feeding patch antenna and FSS unit cell are set to be the same and they have been calculated based on the size extension method to increase the antennas' fabrication tolerance with low cost PCB etching process. It has been found that with 2-elements FSS the antenna gain is improved to 15.6dBi but with 12-elements FSS the gain is boosted to 19.1dBi whereas it is further increased to 19.75dBi with 24-elements FSS. Therefore it is concluded that 12-elements FSS provides a good trade-off between the FSS array size and antenna gain improvement. The 12-element FSS is redesigned at 10GHz and a gain of 18.23dBi is measured where further boost in the gain is accomplished by adding copper walls across the E-field radiation and the final antenna gain has reached to 19.2dBi.

6.6. References

1. Rabbani, M.S. and Ghafouri-Shiraz, H., 2017. Frequency selective surface antenna for remote vital sign monitoring with ultra-wide band doppler radar. *Microwave and Optical Technology Letters*, *59*(4), pp.818-823.
2. Jha, K.R. and Singh, G., 2011. Design of highly directive cavity type terahertz antenna for wireless communication. *Optics Communications*, *284*(20), pp.4996-5002.
3. Jha, K.R. and Singh, G., 2013. Analysis of the Effect of Ground Plane Size on the Performance of a Probe-fed Cavity Resonator Microstrip Antenna. *Wireless personal communications*, *71*(2), pp.1511-1521.

4. Rabbani, M.S. and Ghafouri-Shiraz, H., 2016. Improvement of microstrip patch antenna gain and bandwidth at 60 GHz and X bands for wireless applications. *IET Microwaves, Antennas & Propagation*, *10*(11), pp.1167-1173.
5. Rabbani, M.S. and Ghafouri-Shiraz, H., 2017. High gain microstrip antenna array for 60 GHz band point to point WLAN/WPAN communications. *Microwave and Optical Technology Letters*, *59*(3), pp.511-514.
6. Chiu, C.H., Tatung Company, 2008. *Partially reflective surface antenna*. U.S. Patent 7,319,429.
7. Feresidis, A.P. and Vardaxoglou, J.C., 2001. High gain planar antenna using optimised partially reflective surfaces. *IEE Proceedings-Microwaves, Antennas and Propagation*, *148*(6), pp.345-350.
8. Trentini, G.V., 1956. Partially reflecting sheet arrays. IRE Transactions on Antennas and Propagation, 4(4), pp.666-671.
9. Verma, L., Fakharzadeh, M. and Choi, S., 2013. Wifi on steroids: 802.11 ac and 802.11 ad. *IEEE Wireless Communications*, *20*(6), pp.30-35.
10. Meng, F. and Sharma, S.K., 2015. A dual-band high-gain resonant cavity antenna with a single layer superstrate. *IEEE Transactions on Antennas and Propagation*, *63*(5), pp.2320-2325.
11. Liu, Z.G., Ge, Z.C. and Chen, X.Y., 2009. Research progress on Fabry-Perot resonator antenna. *Journal of Zhejiang University-SCIENCE A*, *10*(4), pp.583-588.
12. Liu, Z.G., 2010. Fabry-Perot resonator antenna. *Journal of Infrared, Millimeter, and Terahertz Waves*, *31*(4), pp.391-403.

Chapter-7

Implementation of Dielectric Lens and Defected Ground Structures on the Improved Size MPA

Abstract: In this chapter, firstly a resonant cavity based high gain dielectric lens antenna (DLA) has been presented for 60GHz-band (57.24-65.88GHz) wireless applications. The feeding element is a microstrip patch antenna (MPA) designed with size improvement method for laboratory based fabrication with printed circuit board (PCB) etching process. A semi-sphere dielectric lens is placed in front of the feeding antenna at a distance equal to about half-wavelength of the operating central frequency of 61GHz. Simulation analysis has been performed on the cavity height and lens radius to obtain an optimised antenna design for its best performance in term of gain (20.1dBi) and return loss (S_{11}) bandwidth (BW) (6.14GHz). Secondly, a diamond shape Defected Ground Structure (DGS) has been deployed on a rectangular MPA to improve the antenna's S_{11} BW and fabrication tolerance. The functionality of the DGS based antenna is first analysed and tested at 10GHz and then the concluded antenna structure is scaled up and tested at 60GHz-band frequencies.

7.1 Introduction

For 60GHz-band wireless applications, high gain and wideband antennas are desirable to compensate the link budget across the extensive path losses and to achieve high data rate [1-2]. Implementation of dielectric lens on various type of feeding elements is one of the popular options for high gain antenna designs [3]. In the recent decades, high gain antennas have been reported with dielectric lens for 60GHz-band wireless communications [3-5] and a maximum gain of 21.6dBi is reported in [3]. However, the reported antennas are fed through

conventional horn antennas which makes the overall antenna too heavy and bulky for compact 60GHz wireless devices [2].

On the other hand, various DGSs have been reported in the literature which exhibit very attractive resonant properties [6-9] and they have been widely used in the conventional microstrip antenna and filter designs to miniaturise their size [10, 11] as well as to improve their efficiency [11] and frequency response [12, 13] at microwave frequencies. However, the reported fine details and complex DGS based antennas may not be suitable for mm-wave frequency applications due to the antenna's low gain and fabrication apprehension by cost-effective PCB etching method.

In the present work, a high gain DLA is proposed for 60GHz-band frequencies. The DLA is fed with an improved size microstrip antenna array through an air filled resonant cavity. The optimised antenna yielded 20.1dBi maximum gain and 6.14GHz S_{11} bandwidth at the central frequency of 61GHz. Secondly, a diamond shape DGS based wide band MPA is proposed for 60GHz-band wireless applications. The DGS based antenna design is initially analysed and tested at 10GHz frequency and then the optimised prototype is re-designed and tested at 60GHz frequencies. The 60GHz DGS antenna's measured bandwidth is enlarged up to 3.5GHz with maximum measured gain of 8.50dBi. It is worth to mention that various DGS shapes (i.e. rectangular, circular and diamond) have been investigated with various sizes and positions to analyse their performances and found that the proposed DGS diamond shape exhibited the best performance in terms of S_{11} bandwidth, efficiency and gain.

7.2 Dielectric Lens Antenna

7.2.1 Lens Antenna Design

Fig.7.1 illustrates the geometry and dimensional parameters of the proposed DLA. As shown in Fig. 7.1, a dielectric lens of Polytetrafluoroethylene (PTFE) material with radius 'R' is

placed on top of the feeding element at a distance ‘a’. The height ‘a’ of the air gap is set to be equal to half of the operating free space wavelength to make it resonant at 61GHz [5, 14, 15]. Both of the dimensions ‘a’ and ‘R’ are analysed and optimised in CST Microwave Studio to attain a maximum antenna gain.

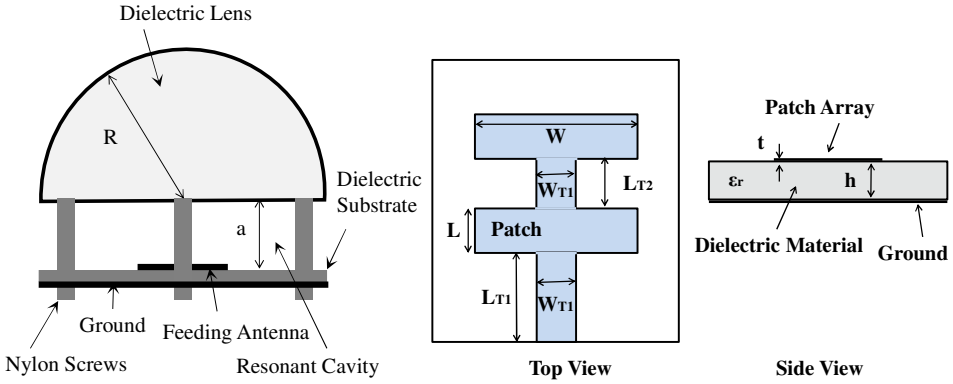

Fig. 7.1. Geometry of the proposed DLA. (a) Overall DLA structure and (b) feeding antenna

The feeding element is a microstrip antenna array of two ultra-wide patches fed in series and fabricated on RT/Duroid5880 substrate with dielectric constant ε_r=2.2, thickness h=0.254mm and copper cladding t=17.5μm (see Fig. 7.1(b)). The designing principle and measured and simulation results of the feeding antenna have been demonstrated in Section 4.2. The measured S_{11} BW and gain of the feeding antenna are around 5GHz and 13.5dBi, respectively. However, in the present implementation the ground plane and substrate areas of the feeding antenna have been extended to accommodate the dielectric lens, as shown in Fig. 7.1(a).

7.2.2 Lens Antenna Results and Discussions

Based on the procedure explained in the last sections, a DLA is designed at 61GHz. The optimised antenna dimensions are shown in Table 7.1. The lens is manufactured through milling process and the feeding antenna element is fabricated with PCB etching process. Fig.

7.2(a) demonstrates the proposed DLA prototype and experiment setup. The lens and feeding element are assembled with Nylon screws to minimise their effect on the antenna performance. A 1.85mm flange launcher is employed to connect the DLA to Vector Network Analyser. The flange launcher is connected to the feeding antenna through probe feeding via a Glass Bead.

Table 7.1. Dimensions in mm of the proposed DLA

L	W	L_{T1}	L_{T2}	W_{T1}	R	a
1.34	5.1	2.42	1.88	0.86	11	2.5

Fig. 7.2(b) shows the simulation and measured S_{11} results and Fig. 7.2(c) represents the far-field radiation patterns (FRP) results in E and H planes at 61GHz. It is clear from Figs. 7.2(b) and (c) that the measured and simulation results show fairly close agreement. There is about 1% shift in the measured central resonance frequency as compared to the simulation one which is within the fabrication tolerance limit usually achieved at mm-wave frequencies [1,14]. As seen from Fig. 7.2(c) that there is comparatively larger difference between the simulation and measured FRP at the side angles which could be attributed to the side effect of the connector and the fixture set up including the dielectric pillars in the resonant cavity which have not been included in the simulated model. The other sources of the dissimilarities between the measured and simulation FRP can be explained as a combined effect of the side reflections and miss alignment between the transmitter and receiver antennas [1]. The measured -10dB S_{11} BW and peak gain at 61GHz are 6.14GHz (about 10% of the central frequency) and 20.1dBi, respectively. The measured antenna bandwidth covers a significant portion of 60GHz-band.

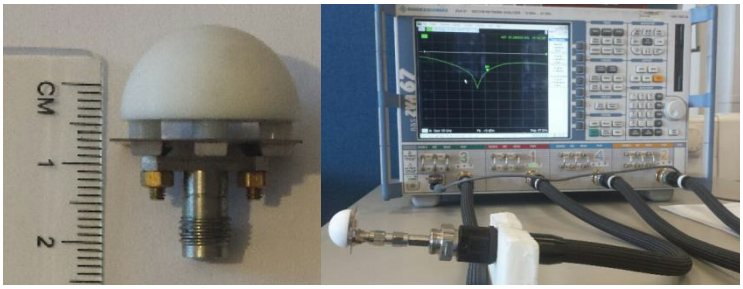

(a)

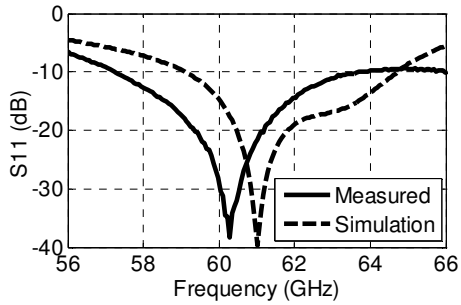

(b)

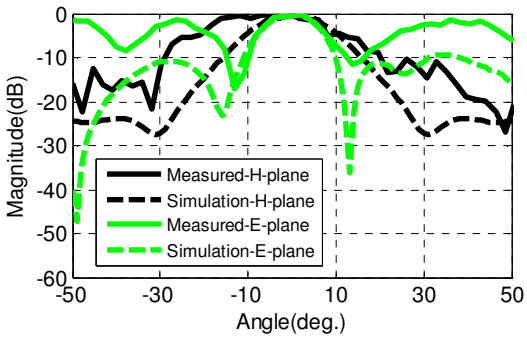

(c)

Fig. 7.2. DLA experiment and results. (a) Fabricated prototype and experiment setup, (b) S_{11} results and (c) FRP in E and H planes at 61GHz

Figs. 7.3 and 7.4 illustrate the effect of change in DLA's dimensions 'a' and 'R', respectively, on the antenna performance. Figs. 7.3(a) and 7.4(a) depict the impact of 'a' and 'R', respectively, on the antenna gain whereas Figs. 7.3(b) and 7.4(b) show the effect of 'a' and 'R', respectively, on the S_{11} response. It can be noticed from Figs. 7.3 and 7.4 that the mentioned antenna dimensions have significant impact on the antenna's peak gain whereas the antenna's S_{11} response is not so much sensitive to these dimensions. It is also clear that the

chosen optimised values of these dimensions, i.e. a=2.5mm and R=11mm, give the maximum simulation gain of 20dBi.

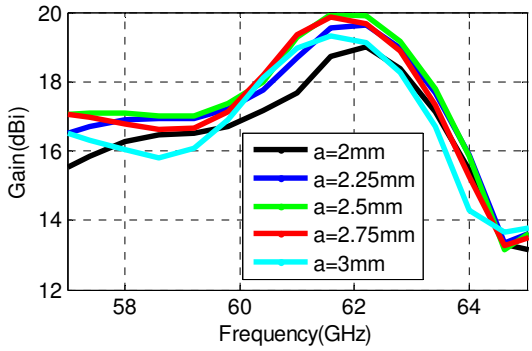

(a)

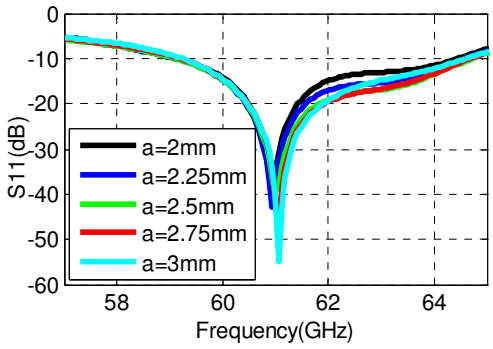

(b)

Fig. 7.3. Effect of the antenna dimension 'a' on its performance. (a) Effect of 'a' on the antenna gain and (b) effect of 'a' on the antenna's S_{11} response

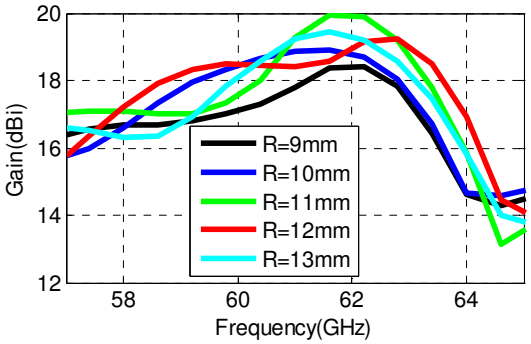

(a)

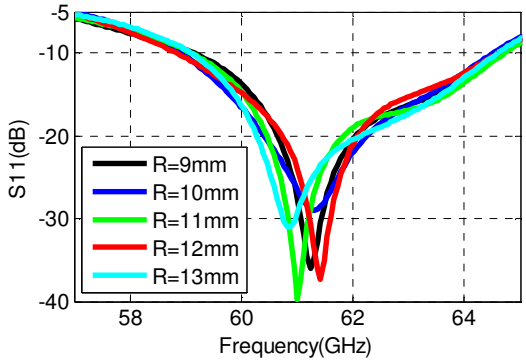

(b)

Fig. 7.4. Effect of the antenna dimension 'R' on its performance. (a) Effect of 'R' on the antenna gain and (b) effect of 'R' on the antenna's S_{11} response

7.3 Defected Ground Structure based MPA

7.3.1 Antenna Design Procedure

The DGS based MPA is designed on a low loss RT/Duroid5880 substrate material. Figs. 7.5(a)-(c) show the geometry and the dimensional parameters of the proposed antenna structure. The antenna is comprised of an improved size patch element at the front layer and a diamond shape DGS of width 'W_d' and length 'L' on the ground layer. Fig. 7.5(d) illustrates the equivalent LCR circuit of the proposed antenna where the top and bottom LCR resonators correspond to the equivalent circuits of the patch element and DGS, respectively [16]. The patch antenna and TL dimensions are calculated with the size improvement method as

presented in Chapter-3 where M=N=P=1 are chosen in eqs. 3.1, 3.2 and 3.6. The DGS length is set to be equal to the patch length 'L' however its width W_d is optimized to be about W/2.5 for the best S_{11} response. The ground width and length are set as Wg =W+6h and Lg =L+6h, respectively. The final antenna dimensions are optimised with the help of CST Microwave Studio to achieve the best antenna performance.

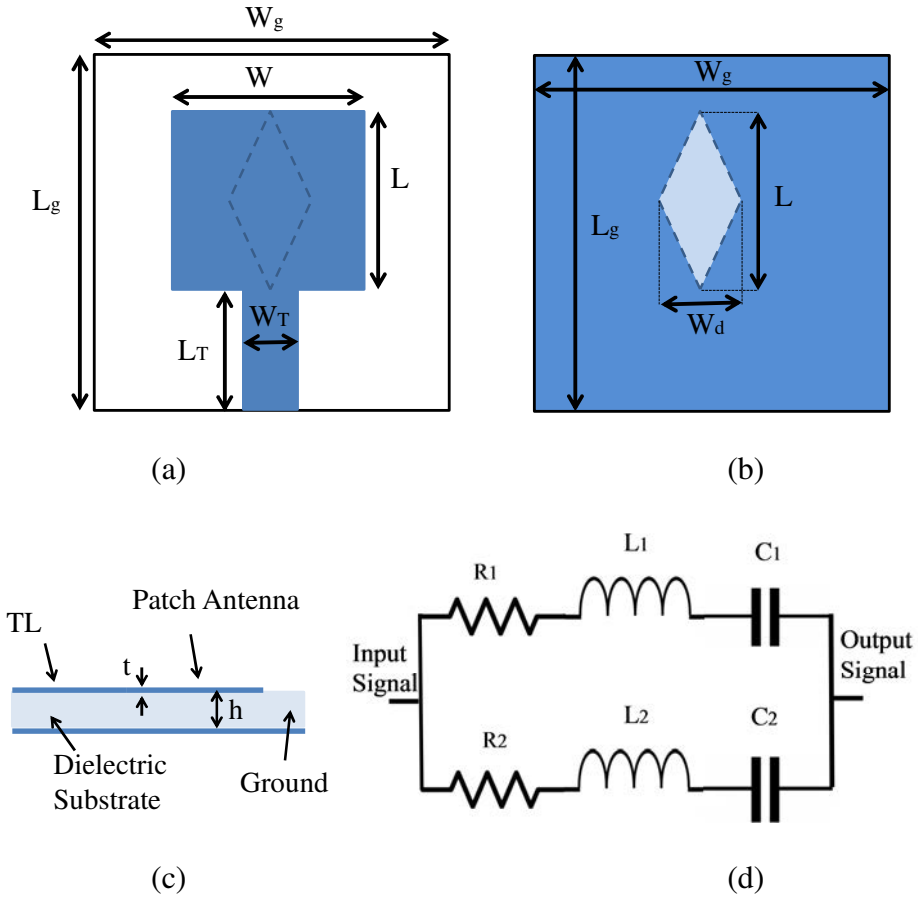

Fig. 7.5. Geometry of the proposed DGS antenna

7.3.2 DGS Antenna Analysis at 10GHz

Two rectangular MPA are initially designed and fabricated at 10GHz without DGS; one with PCB thickness h=0.787mm and other with h=1.57mm as shown in Figs. 7.6(a) and (b). Then these two antennas are re-designed and fabricated with the diamond shaped DGS on their ground layers as shown in Figs. 7.6(c) and (d), respectively. The optimised dimensions of

these four antennas are provided in Table 7.2 where it can be noticed that all of the antennas dimensions are producible with the conventional low cost PCB etching technique.

Table 7.2 Dimensions in mm of 10GHz antennas.

Antennas	L	W	L_T	W_T	W_d	h
7.6(a)	28.93	34.35	25.94	2.54	0	0.787
7.6(b)	28.55	34.45	25.64	3.6	0	1.57
7.6(c)	28.93	34.35	25.94	1.6	12.7	0.787
7.6(d)	28.55	34.45	25.64	3	14	1.57

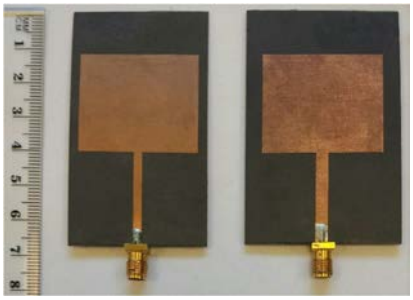

(a) (b)

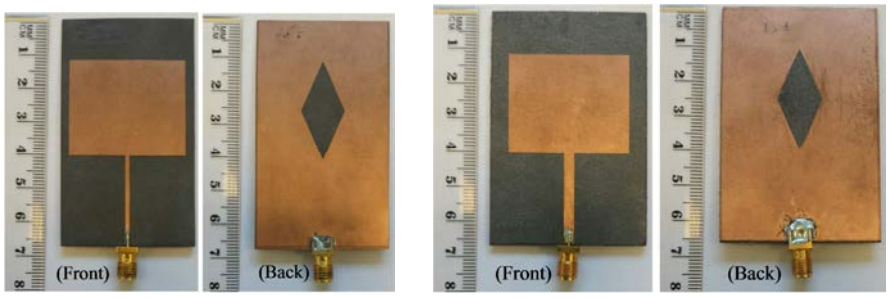

(c) (d)

Fig. 7.6. Fabricated DGS antennas prototypes

Figs. 7.7 and 7.8 show the simulation and measured S_{11} and FRP of antennas without DGS shown in Figs. 7.6(a) and (b), respectively, where (a) represents S_{11} response and (b) and (c) show FRP in E and H planes, respectively. As seen from Figs. 7.7 and 7.8 that in all cases both the measured and simulation results are in close agreement. It is clear from Fig. 7(a), the

measured -10dB S_{11} BW and maximum gain of antenna shown in 7.6(a) at 10.1GHz are 210MHz and 8.36dBi, respectively. The far-field pattern of this antenna in H-plane has only a single radiation beam whereas in E-plane it has three beams as expected. Similarly, for the antenna shown in Fig. 7.6(b) the measured BW and gain at 10GHz are 230MHz and 8.69dBi, respectively (see Fig. 7.8). The BW of this antenna has improved by 20MHz as compared with the antenna shown in Fig. 7.6(a) which is due to the deployment of the thicker substrate. However, the FRP of both antennas are almost similar (see Figs. 7.7(b)-(c) and 7.8(b)-(c)).

Figs. 7.9 and 7.10 show the simulation and measured S_{11} and FRP at 10GHz for both DGS based antennas shown in Figs. 7.6(c) and (d), respectively. The measured -10dB S_{11} BW of the antenna 7.6(c) (i.e. on h=0.787mm) is 350MHz which is about 67% more than that without DGS (i.e. Fig. 7.6(a)). Fig. 7.9(a) clearly shows that the implementation of the DGS has added a second resonance in the S_{11} response near the original resonance which enhances the overall S_{11} bandwidth. The measured antenna gain at 10GHz is 8.2dBi. Comparison of the results shown in Figs. 7.7(b) and 7.9(b) clearly indicates that, presence of DGS has not caused any significant changes in the radiation patterns of the two antennas.

As seen from Fig. 7.10, the measured -10dB S_{11} BW of the DGS antenna on h=1.57mm shown in Fig. 7.6(d) is 580MHz. This BW is about 1.65 times the BW of DGS antenna with h=0.787mm (see Fig. 7.9) and also about 2.5 times the BW of antenna with h=1.57mm but without DGS (Fig. 7.6(b)). The gain at 10GHz of the antenna shown in Fig 7.6(d) is about 8.91dB. However, the S_{11} response of this antenna within the pass band is higher than that of the antenna shown in Fig. 7.6(c) which is due to the use of a thicker substrate. The antenna's FRP results are shown in Figs. 7.10(b) and (c) which are similar to those of the antenna shown in Fig. 7.6(c).

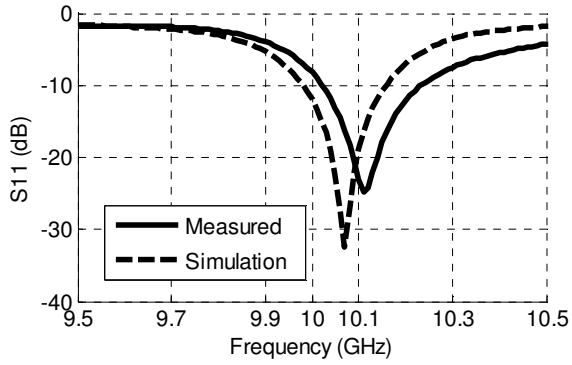

(a)

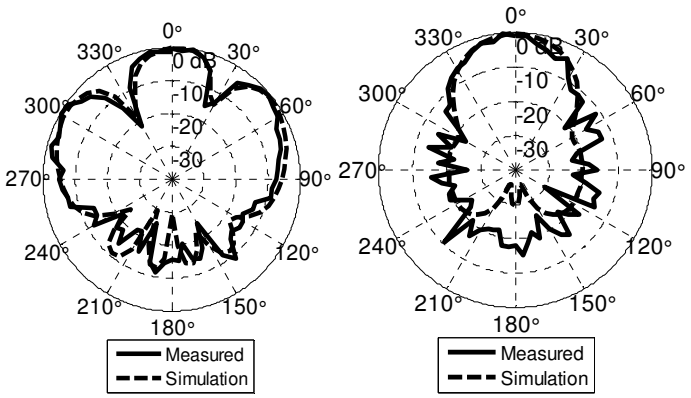

(b) (c)

Fig. 7.7. Simulated and measured results of the antenna shown in Fig. 7.6(a) (h=0.787mm)

(a) S_{11}, FRP at 10.1GHz in (b) E-plane and (c) H-plane.

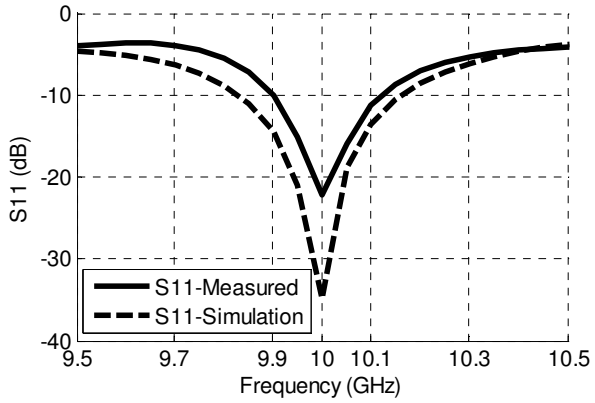

(a)

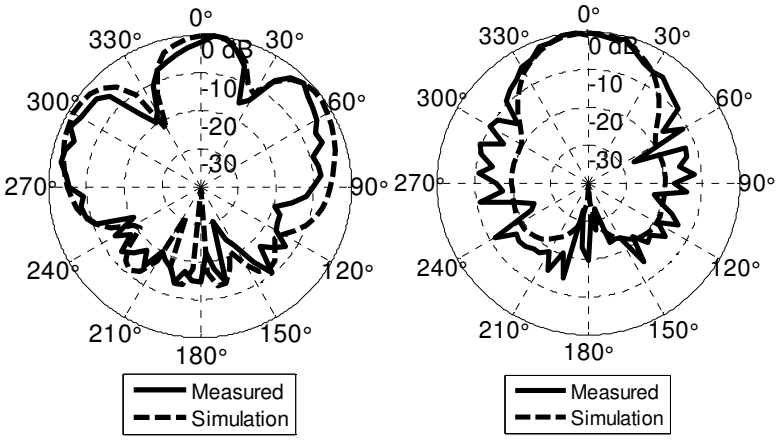

(b) (c)

Fig. 7.8. Simulated and measured results of the antenna shown in Fig. 7.6(b) (h=1.57mm)

(a) S_{11}, FRP at 10GHz in (b) E-plane and (c) H-plane.

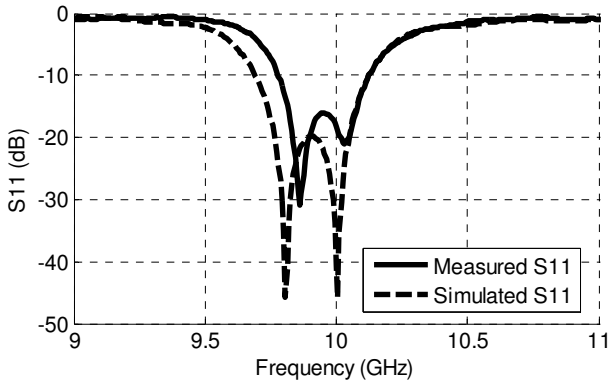

(a)

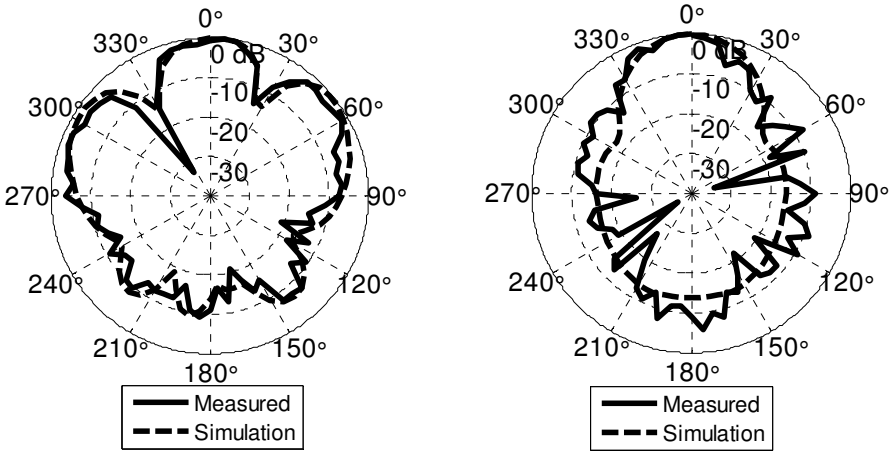

(b) (c)

Fig. 7.9. Simulated and measured results of the antenna shown in Fig. 7.6(c) (h=0.787mm with DGS). (a) S_{11}, FRP at 10GHz in (b) E-plane and (c) H-plane.

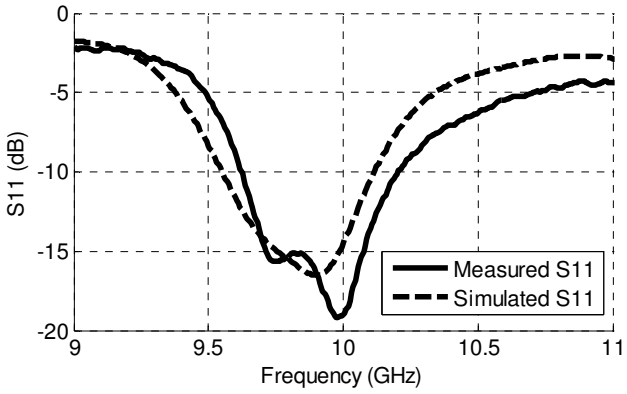

(a)

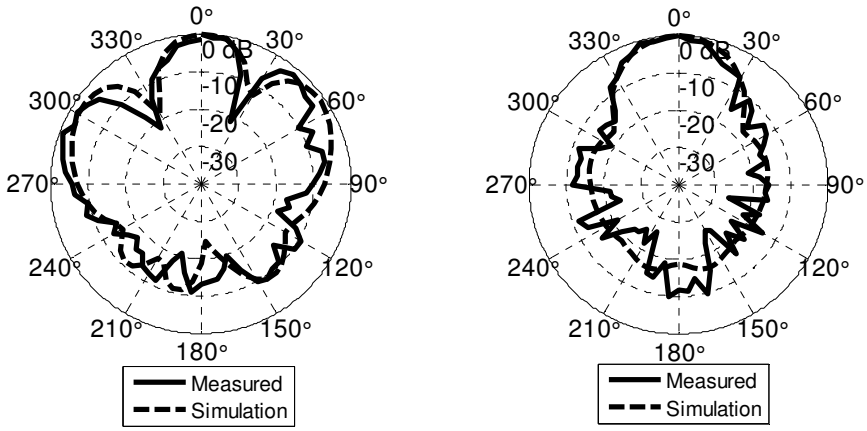

(b) (c)

Fig. 7.10. Simulated and measured results of the antenna shown in Fig. 7.6(d) (h=1.57mm with DGS). (a) S_{11}, FRP at 10GHz in (b) E-plane and (c) H-plane.

Figs. 7.11(a) and (b) demonstrate the surface current distribution on the patch in the DGS based antennas 7.6(c) and 7.6(d), respectively, where it is clear that the current is in-phase at the top and bottom sections of the patch whereas it is out of phase in the patch centre which is due to the TM30 operating mode and explains the reason of 3 beams in the FRP in E-plane.

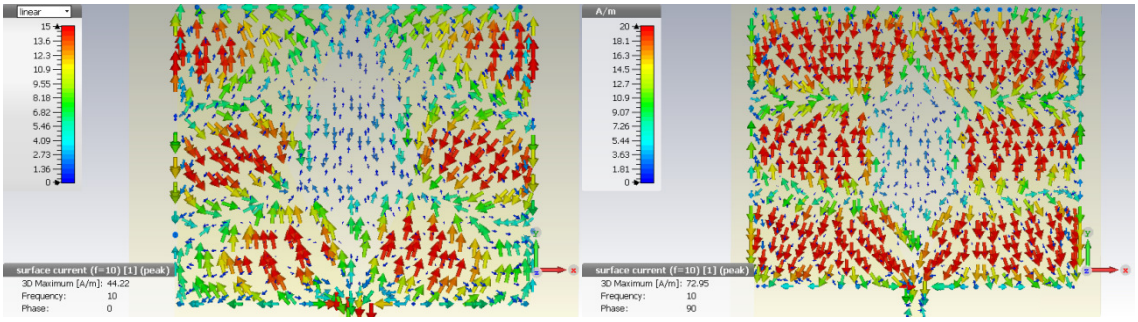

(a) (b)

Fig. 7.11 Surface current distribution at 10GHz on (a) antenna 7.6(c) and (b) antenna 7.6(d).

The effect of the change in DGS width (W_d) has been studied by re-producing and testing the antenna shown in Fig. 7.6(d) with three different DGS widths of 12.7mm, 13mm and 14mm. Fig. 7.12 illustrates the measured S_{11} response of these three antennas where it can be seen that the maximum ripple level in the pass band (S_{11max}) can be minimised by increasing the DGS width, however, this reduces the BW response. In fact, in Fig. 7.12 the first and second resonances are due to the DGS and patch resonators, respectively (see Fig. 7.5(d). By increasing W_d, the overall DGS slot area is increased which reduces the capacitance in the equivalent circuit. This reduction in the capacitance rises the frequency of the first resonance ($f = 1/(2\pi\sqrt{L_2C_2})$) as shown in Fig. 7.12 which consequently brings the two resonances closer. As a result, the overall bandwidth is shrunk and the ripple level in the middle is dropped.

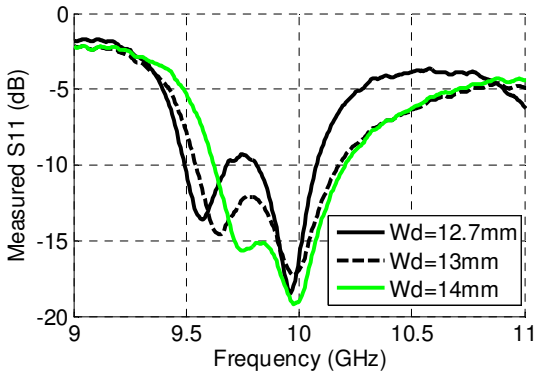

Fig. 7.12. Measured S_{11} of DGS antennas 7.6(d) as a function of the DGS width.

The measured bandwidth, S_{11max} and gain of all antennas shown in Fig. 7.6 are summarised in Table 7.3. From Table 7.3 it is obvious that the bandwidth of the microstrip antenna can be roughly doubled by implementing the proposed DGS giving an extra benefit of improved gain in the pass band, without disturbing the far-field radiation characteristics of the antenna.

Table 7.3. 10GHz DGS antennas' performance.

Antennas	BW (MHz)	Gain (dBi)
7.6(a)	210	8.36
7.6(b)	230	8.69
7.6(c)	350	8.2
7.6(d)	580	8.91

7.3.3 DGS Antenna at 60GHz-band

Finally, the proposed diamond shape DGS is implemented on a MPA designed at 60GHz frequency on the same 'RT/Duroid5880' material but with substrate thickness h=0.254mm by using the same concept as explained in Section 7.2. Figs. 7.13(a) and (b) show the front and back views of the fabricated antenna prototype, respectively. The antenna's optimised dimensions are listed in Table 7.4. It may worth to mention that all of the antenna dimensions are well above 152µm limit imposed by the cost effective PCB etching process.

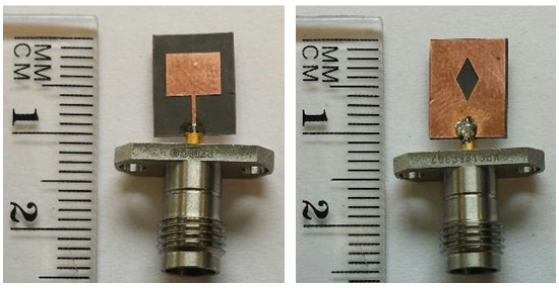

(a) (b)

Fig. 7.13. 60GHz fabricated DGS antenna. (a) Front view and (b) back view.

Table 7.4. Dimensions in mm of 60GHz DGS antenna

L	W	LT	WT	Wd	h
4.64	5.6	4.17	0.49	2.28	0.254

The antenna's simulation and measured S_{11} results are shown in Fig. 7.14(a) where it can be seen that the measured and simulation responses are closely related. The antenna's measured S_{11} BW is 3.5GHz centred at about 60GHz and the measured gain is 8.50dBi. The simulated and measured FRP at 60GHz in E and H planes are illustrated in Figs. 7.14(b) and (c), respectively. Some distortions have been observed in the E-plane FRP as seen in Fig. 7.14(b) which are attributed to the multi-path reflections and obstructions from the surroundings including the effect of V-connector's body, as mentioned in [3, 17]. It is expected that the radiation performance of 60GHz antenna can be improved when the antenna is used without V-connector i.e. it is integrated with on-board devices [3, 18].

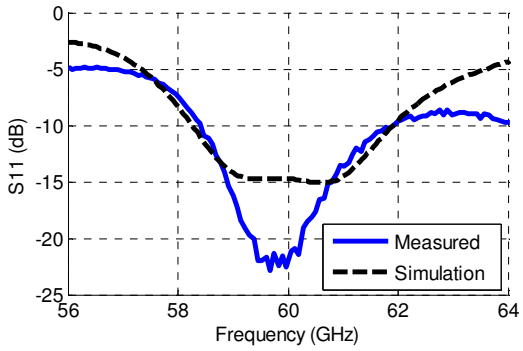

(a)

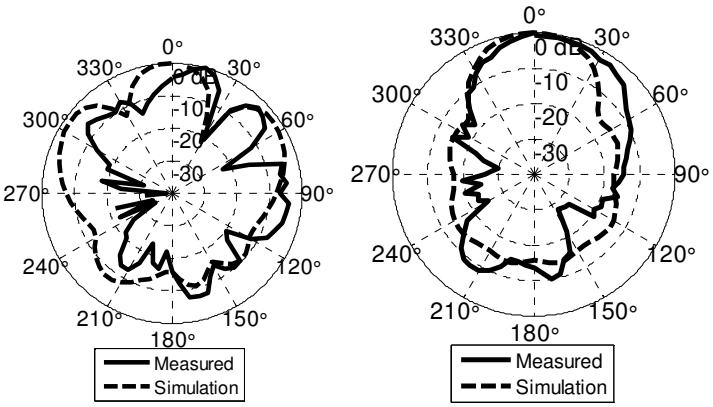

(b) (c)

Fig. 7.14 Simulated and measured results of 60GHz DGS antenna. (a) S_{11}, and FRP at 60GHz in (b) E-plane and (c) H-plane.

7.4 Conclusion

A resonant cavity based DLA has been presented for 60GHz-band wireless applications. The implementation of dielectric lens improved the BW and gain of the feeding antenna element by about 1GHz and 6.5dBi, respectively, giving the maximum measured DLA BW of 6.14GHz and gain of 20.1dBi. Secondly, a diamond shape DGS based MPA is proposed to increase the antenna BW and fabrication tolerance at 60GHz-band frequencies. It has been found that the DGS antenna's BW and S_{11} response in the pass band can be controlled by the DGS width. Moreover, both the DLA and DGS antenna designing concept could be particularly useful to design and fabricate cost-effective antennas at even higher mm-wave frequencies.

7.5 References

1. Rabbani, M.S. and Ghafouri-Shiraz, H., 2016. Improvement of microstrip patch antenna gain and bandwidth at 60 GHz and X bands for wireless applications. *IET Microwaves, Antennas & Propagation*, *10*(11), pp.1167-1173.
2. Rabbani, M.S. and Ghafouri-Shiraz, H., 2017. High gain microstrip antenna array for 60 GHz band point to point WLAN/WPAN communications. *Microwave and Optical Technology Letters*, *59*(3), pp.511-514.
3. Artemenko, A., Maltsev, A., Mozharovskiy, A., Sevastyanov, A., Ssorin, V. and Maslennikov, R., 2013. Millimeter-wave electronically steerable integrated lens antennas for WLAN/WPAN applications. *IEEE Transactions on Antennas and Propagation*, *61*(4), pp.1665-1671.

4. Costa, J.R., Lima, E.B. and Fernandes, C.A., 2009. Compact beam-steerable lens antenna for 60-GHz wireless communications. *IEEE Transactions on Antennas and Propagation*, *57*(10), pp.2926-2933.
5. Costa, J.R., Lima, E.B. and Fernandes, C.A., 2009. Compact beam-steerable lens antenna for 60-GHz wireless communications. *IEEE Transactions on Antennas and Propagation*, *57*(10), pp.2926-2933.
6. Saqib Rabbani, M. and Ghafouri-Shiraz, H., 2016. Microstrip antennas for X-band and MM-wave frequencies based on diamond shape defected ground structure and size extension method. *Microwave and Optical Technology Letters*, *58*(12), pp.2836-2841.
7. Weng, L.H., Guo, Y.C., Shi, X.W. and Chen, X.Q., 2008. An overview on defected ground structure. *Progress In Electromagnetics Research B*, *7*, pp.173-189.
8. Breed, G., 2008. An introduction to defected ground structures in microstrip circuits. *High Frequency Electronics*, *7*, pp.50-54.
9. Wang, C.J. and Lin, C.S., 2008. Compact DGS resonator with improvement of Q-factor. *Electronics Letters*, *44*(15), pp.908-910.
10. Raval, F., Kosta, Y.P., Makwana, J. and Patel, A.V., 2013, April. Design & implementation of reduced size microstrip patch antenna with metamaterial defected ground plane. In *Communications and Signal Processing (ICCSP), 2013 International Conference on* (pp. 186-190). IEEE.
11. Arya, A.K., Kartikeyan, M.V. and Patnaik, A., 2010, September. On the size reduction of microstrip antenna with DGS. In *Infrared Millimeter and Terahertz Waves (IRMMW-THz), 2010 35th International Conference on* (pp. 1-3). IEEE.
12. Chung, Y., Jeon, S.S., Kim, S., Ahn, D., Choi, J.I. and Itoh, T., 2004. Multifunctional microstrip transmission lines integrated with defected ground structure for RF front-end

application. *IEEE Transactions on Microwave Theory and Techniques*, *52*(5), pp.1425-1432.

13. Zhu, F., Gao, S., Ho, A.T., Abd-Alhameed, R.A., See, C.H., Brown, T.W., Li, J., Wei, G. and Xu, J., 2013. Multiple band-notched UWB antenna with band-rejected elements integrated in the feed line. *IEEE Transactions on Antennas and Propagation*, *61*(8), pp.3952-3960.
14. Rabbani, M.S. and Ghafouri-Shiraz, H., 2017. Frequency selective surface antenna for remote vital sign monitoring with ultra-wide band doppler radar. *Microwave and Optical Technology Letters*, *59*(4), pp.818-823.
15. Rabbani, M.S. and Ghafouri-Shiraz, H., Ultra-Wide Patch Antenna Array Design at 60 GHz Band for Remote Vital Sign Monitoring with Doppler Radar Principle. *Journal of Infrared, Millimeter, and Terahertz Waves*, pp.1-19.
16. Bansal, P., Sidhu, E. and Goyal, S., 2015. Equivalent circuit modeling of slotted microstrip patch antenna. *IJRET: International Journal of Research in Engineering and Technology, eISSN*, pp.2319-1163.
17. Säily, J., Lamminen, A. and Francey, J., 2011, May. Low cost high gain antenna arrays for 60 GHz millimetre wave identification (MMID). In *Sixth ESA Workshop on Millimetre-Wave Technology and Applications-Fourth Global Symposium Millimetre Waves, Espoo, Finland*.
18. Seok, E., Cao, C., Shim, D., Arenas, D.J., Tanner, D.B., Hung, C.M. and Kenneth, K.O., 2008, February. A 410GHz CMOS push-push oscillator with an on-chip patch antenna. In *Solid-State Circuits Conference, 2008. ISSCC 2008. Digest of Technical Papers. IEEE International* (pp. 472-629). IEEE.

Chapter-8

Evaluation of Gain Enhancement in Improved Size Large MPA Arrays

Abstract: A number of microstrip antenna arrays have been designed based on the improved size patch elements with different substrate heights to evaluate the gain enhancement in practical measurements. Initially, microstrip patch antenna arrays (MPAAs) have been designed, analysed and tested at 10GHz frequency and then the optimised high gain (~21dBi) array is fabricated and tested at 60GHz-band frequencies. It has been found that the loss emergence due to the long feeding transmission line (TL) network severely degrades the antenna gain in large MPAAs on the thicker substrates. However, the gain can be significantly enhanced in large MPAAs by employing (a) relatively thinner substrate but it shrinks the return loss (S_{11}) bandwidth (BW) and increases the side lob level (SLL).

8.1 Introduction

In the modern point to point wireless communications, it has become very common to enhance the gain of microstrip antennas by constituting arrays of multiple patch elements due to the simplicity and cost effectiveness of this approach [1-13]. However, at microwave frequencies (<30GHz) this technique is limited by the exceptionally large antenna size acquired for high gain (>20dBi) arrays [6]. On the other hand, at mm-wave and THz frequencies even though a large MPAA can fit in a small area due to small form factor, this approach is restricted by the declined antenna efficiency and gain due to the substantial power losses commenced by the extended feeding network which is vital to deliver matched electrical signal to each of the radiating elements [1, 2, 12, 13]. Theoretically, the number of patch elements should be doubled in a symmetrical MPAA to enhance the antenna gain by

about 3dB [3]. But at mm-wave and THz frequencies this relationship does not proceed even for the first doubling of the patch elements due to the mentioned substantive loss contribution.

Several MPAAs have been reported in the literature, as discussed in Chapter 2, but most of them are individually designed for a specific application. In [6], the performance of two microstrip antenna arrays at 10GHz frequency has been studied in (a) computer simulation environment. The first array presented in [6] consisted of four patches which yielded 12.56dBi gain, 75% efficiency and -14.84dB SLL. In the second array reported in [6], the numbers of patch elements were doubled to 8 which slightly improved the gain to 13.9dBi but dropped the antenna efficiency down to 63.2% and increased the SLL to -11.58dB. However, there is a gap in the literature regarding the gain evaluation and performance analysis of large MPAA prototypes and their applicability at mm-wave frequencies.

Therefore, in the present work a study has been carried out to evaluate the MPAAs gain enhancement with (a) multiple number of patch elements to figure out a reasonable trade-off between the arrays' gain and size. Also, the effect of the substrate thickness, which is a major source of the losses in the associated microstrip TL network, is investigated on the MPAAs gain performance. Moreover, low impedance TLs have been proposed for the feeding and matching network to keep the lines sufficiently wide to fabricate with the cost-effective PCB etching method especially at mm-wave frequencies.

8.2 Microstrip Patch Antenna Array Designs at 10GHz

8.2.1 Antenna Arrays on Substrate Thickness of 1.57mm

Based on the method explained in section 3.2, initially 3 MPAAs, i.e. with 2×1 (2-elements), 4×2 (8-elements) and 4×4 (16-elements) patches, are designed at 10GHz frequency on

RT/Duroid5880 material with substrate thickness 'h' =1.57mm. Figs. 8.1(a), (b) and (c) show the geometries of 2-elements, 8-elements and 16-elements arrays, respectively. The patch dimensions are calculated based on the procedure explained in Section 4.2. In the 2-elements MPAA, W_{T2} is set to be $W_{T1}/2$ to minimise the SLL [3]. The antenna input impedance is matched to the standard 50Ω impedance through the impedance transformers of length 'L_{T1}' as shown in Fig. 8.1. The rest of the feeding TL network in 8-elements and 16-elements arrays consists of the horizontal 50Ω lines with width W_{T3} and the vertical 35Ω lines with width W_{T1} (see Fig. 8.1). The vertical 35Ω lines work as impedance transformer to match the 25Ω resultant impedance, i.e. 50Ω||50Ω at the T-junction on the 50Ω horizontal lines, with the lower stage 50Ω line (i.e. $\sqrt{50\Omega \times 25\Omega} = 35.35\Omega$).

Table 8.1 shows the dimensions of the 3 MPAAs designed on the PCB thickness of 1.57mm. The separation 'S' between the parallel patch elements is optimised to be 10mm. Figs. 8.2, 8.3 and 8.4 depict the experiment results of 2-elements, 8-elements and 16-elements MPAAs, respectively, where (a), (b), (c) and (d) illustrate the fabricated prototype, S_{11} response, 2-dimentional (2-D) normalized (with the maximum gain) far-field radiation patterns (FRP) and 3-dimentinal (3-D) simulation FRP, respectively. As seen from Figs. 8.2-8.4(c)'s that when more elements are added in series the main radiation lobes squint down in E-plane due to the additional losses incurred along the extended TL path. Table 8.2 summarises the performance parameters of these three MPAAs where it can be noticed that increasing the number of patch elements from 2 to 8 improved the antenna gain by about 1.8dB. However, further doubling the patch elements to 16 enhanced the gain by 2dB yielding a maximum gain to 17.7dBi. It can also be seen that increasing the patch elements reduced the S_{11} BW and increased the SLL.

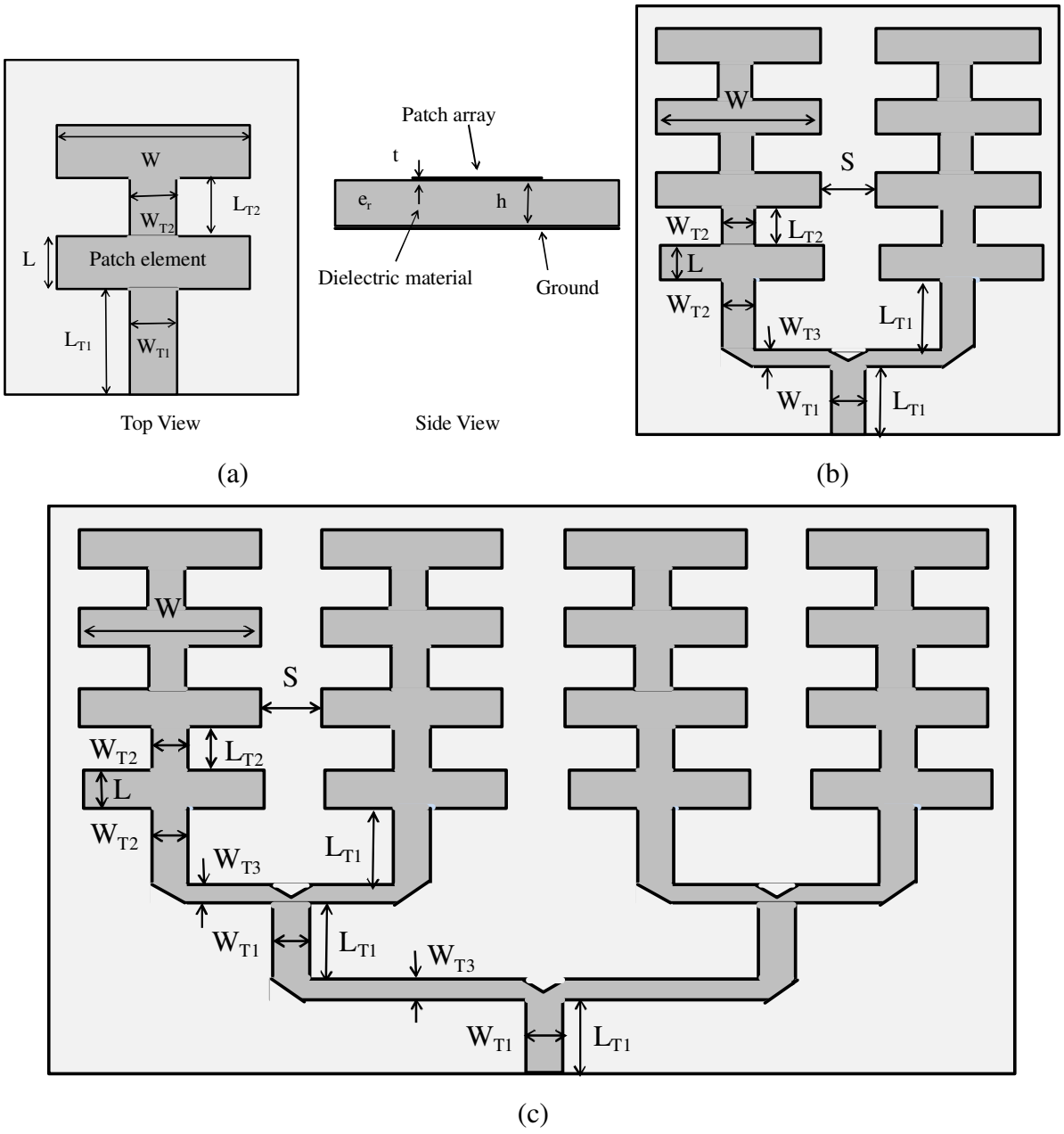

Fig. 8.1. Geometry of (a) 2-elements, (b) 8-elements and (c) 16-elements MPAAs

Table 8.1. Dimensions in mm of MPAAs with h=1.57mm

MPAA	L	W	L_{T1}	W_{T1}	L_{T2}	W_{T2}	W_{T3}
2-elements	8.66	34.45	14.89	7.79	8.66	3.9	-
8-elements	8.66	32	15.63	5.11	9	3.33	3.63
16-elements	8.66	33	15.63	6	9	3	3.63

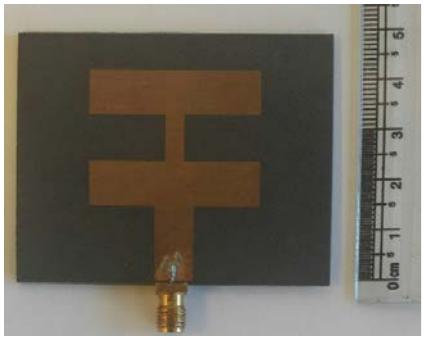

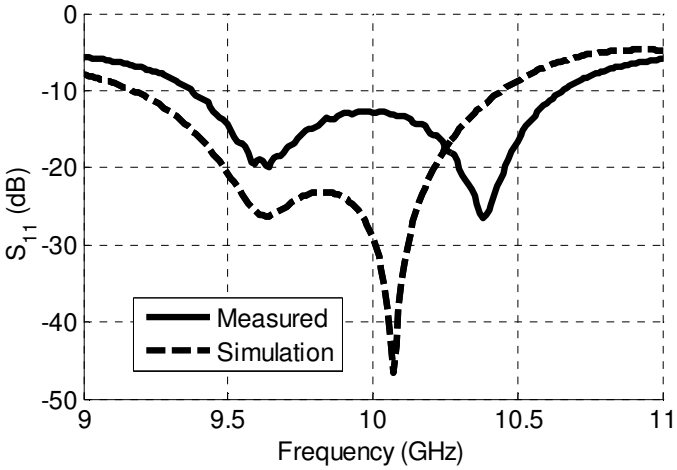

(a) (b)

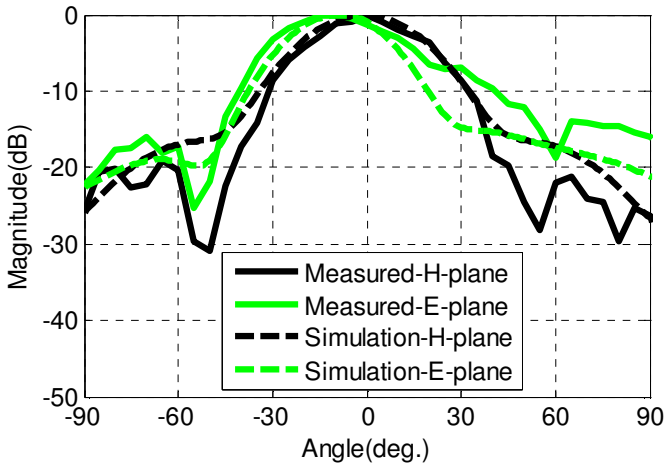

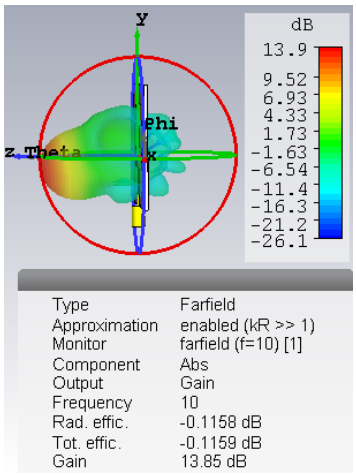

(c) (d)

Fig. 8.2. Experiment results of 2-elements MPAA designed at 1.57mm thick PCB.

(a) Fabricated prototype, (b) S_{11}, (c) 2-D FRP and (d) 3-D simulation FRP

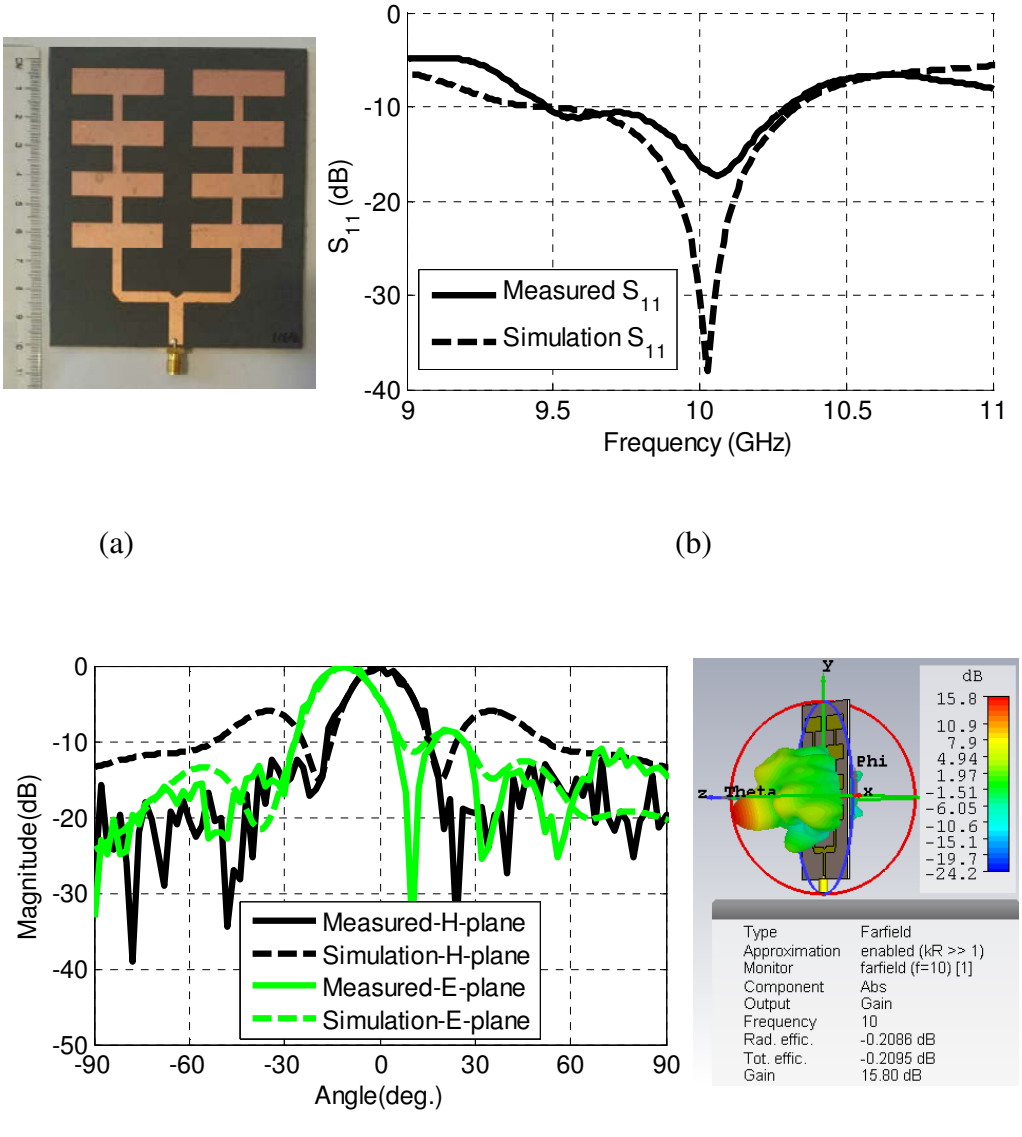

Fig. 8.3. Experiment results of 8-elements MPAA designed at 1.57mm thick PCB.

(a) Fabricated prototype, (b) S_{11}, (c) 2-D FRP and (d) 3-D simulation FRP

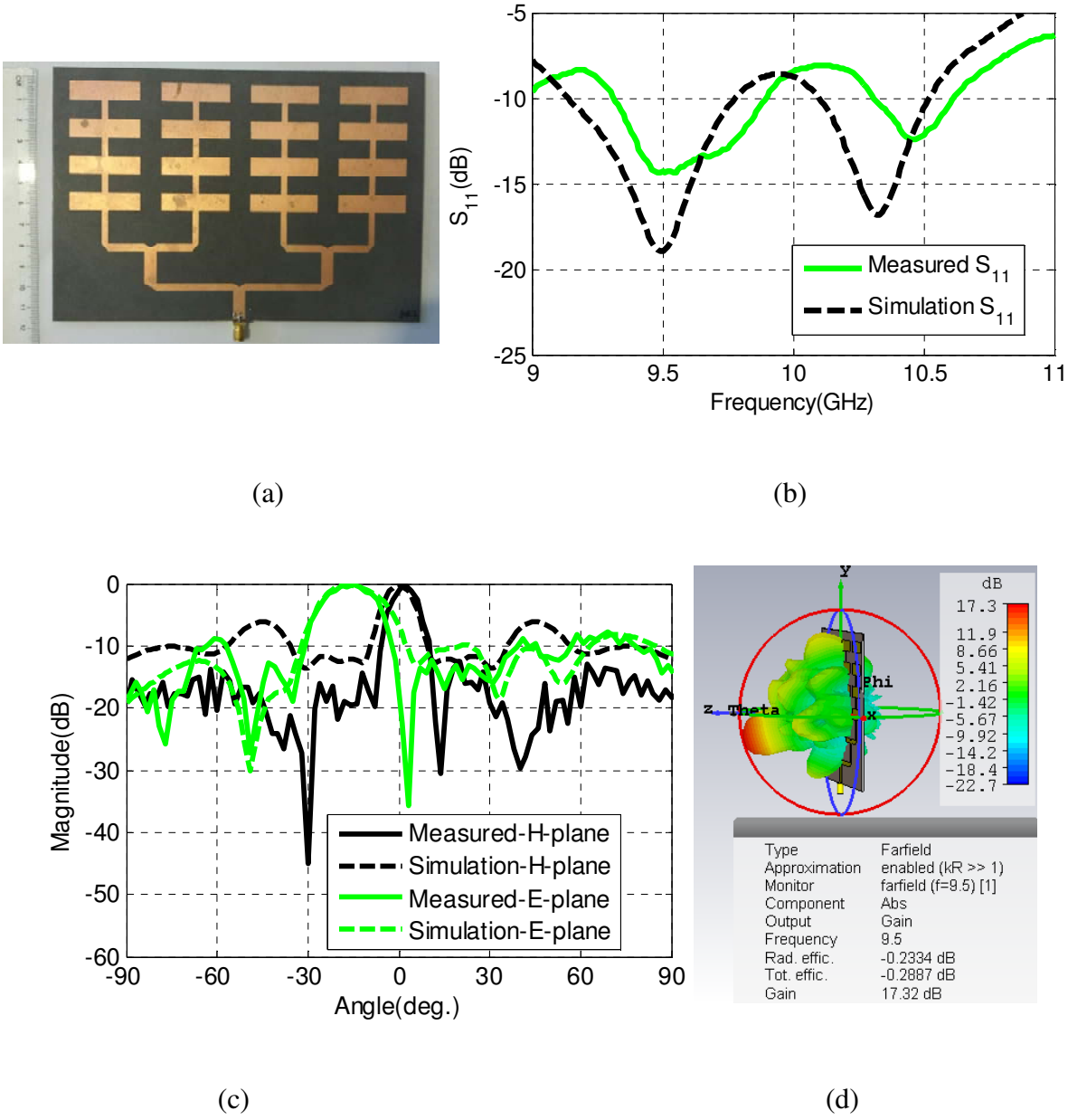

Fig. 8.4. Experiment results of 16-elements MPAA designed at 1.57mm thick PCB.

(a) Fabricated prototype, (b) S_{11}, (c) 2-D FRP and (d) 3-D simulation FRP

Table 8.2. Performance of MPAAs with h=1.57mm

MPAA	BW (MHz)		Gain (dBi)		SLL(dB)	
	Simu.	Meas.	Simu.	Meas.	Simu.	Meas.
2-elements	1250	1228	13.85	13.93	-19	-14.02
8-elements	400	823	15.8	15.68	-6	-8.29
16-elements	640	586	17.32	17.7	-7.91	-7.3

8.2.2 Antenna Arrays on Substrate Thickness of 0.508mm

Three similar MPAAs as presented in the last section are designed on the PCB thickness of 0.508mm. Table 8.3 shows the dimensions of these three MPAAs. The separation between the parallel patch elements S=9.73mm. Figs. 8.5, 8.6 and 8.7 demonstrate the experiment results of these 2-elements, 8-elements and 16-elements MPAAs, respectively, where (a), (b), (c) and (d) present the fabricated prototype, S_{11} response, 2-D FRP and 3-D simulation FRP, respectively. Table 4 shows the performance parameters of these three MPAAs where it is clear that increasing the number of patch elements from 2 to 8 improved the gain by about 4.66dB and further doubling the patch elements to 16 boosted the antenna gain by 3.1dB yielding the maximum gain of 21.1dBi. Comparing Table 4 with Table 2, it can be concluded that the thinner substrate is more suitable to obtain high gain in larger MPAAs. However, S_{11} and BW of the larger MPAAs with thinner substrate become even narrower.

Table 8.3. Dimensions in mm of MPAAs with h=0.508mm

MPAA	L	W	L_{T1}	W_{T1}	L_{T2}	W_{T2}	W_{T3}
2-elements	9.46	36	14.46	3	9.46	1.5	-
8-elements	9.19	32.25	14.59	1.73	9.19	2.18	1.27
16-elements	9.19	31.5	14.6	1.75	9	2.18	1.28

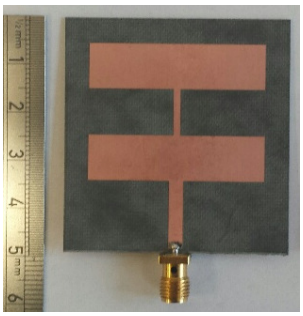

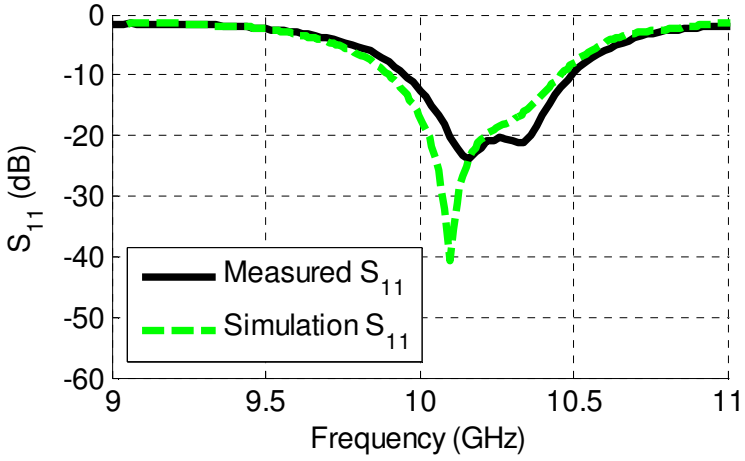

(a) (b)

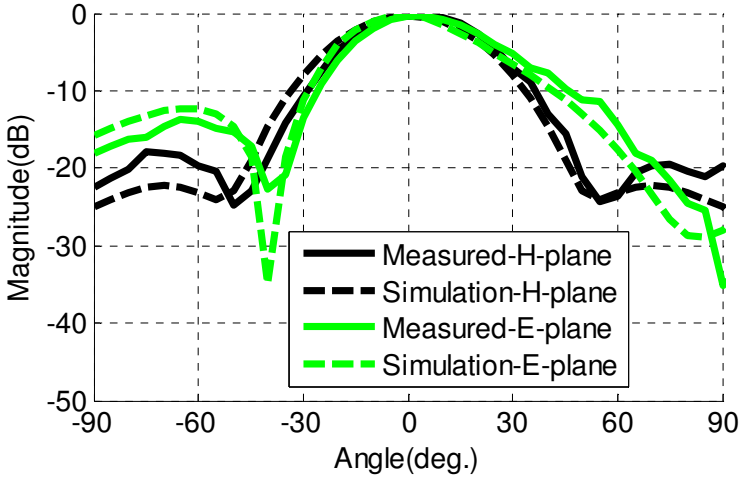

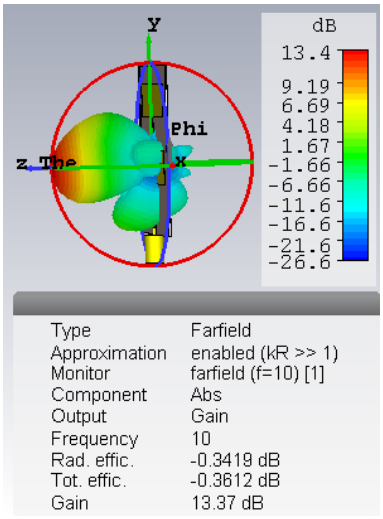

(c) (d)

Fig. 8.5. Experiment results of 2-elements MPAA designed at 0.508mm thick PCB.

(a) Fabricated prototype, (b) S_{11}, (c) 2-D FRP and (d) 3-D simulation FRP

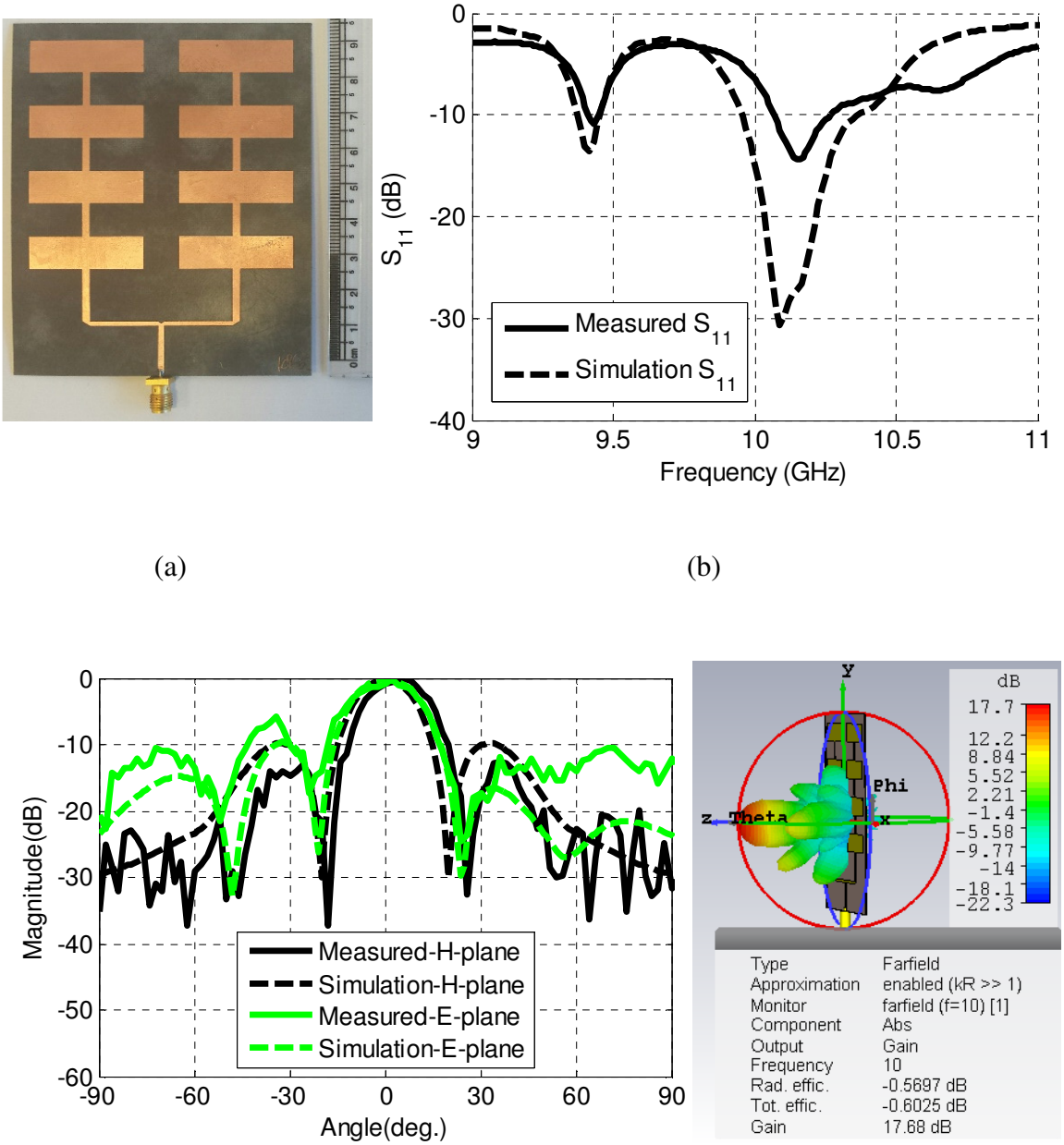

Fig. 8.6. Experiment results of 8-elements MPAA designed at 0.508mm thick PCB.

(a) Fabricated prototype, (b) S11, (c) 2-D FRP and (d) 3-D simulation FRP

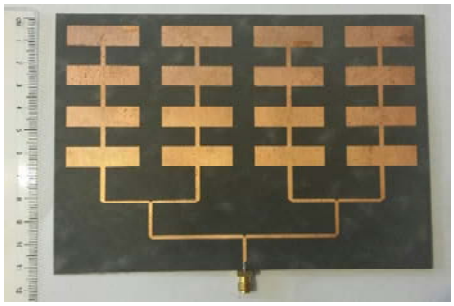

(a)

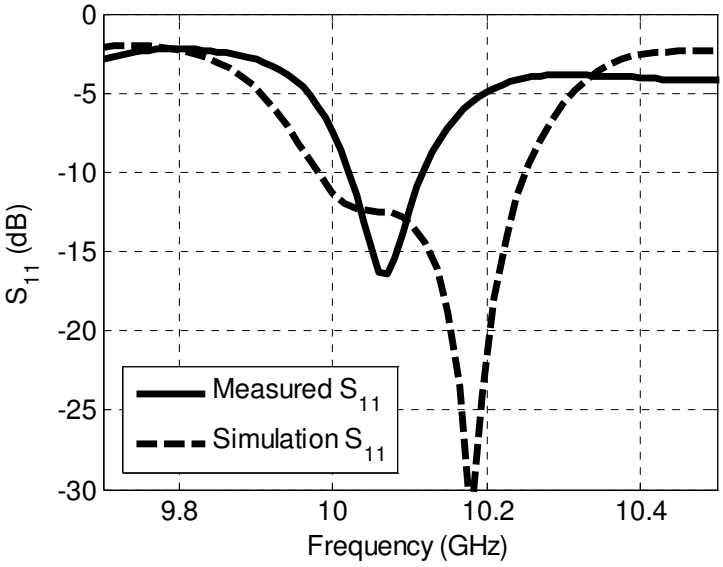

(b)

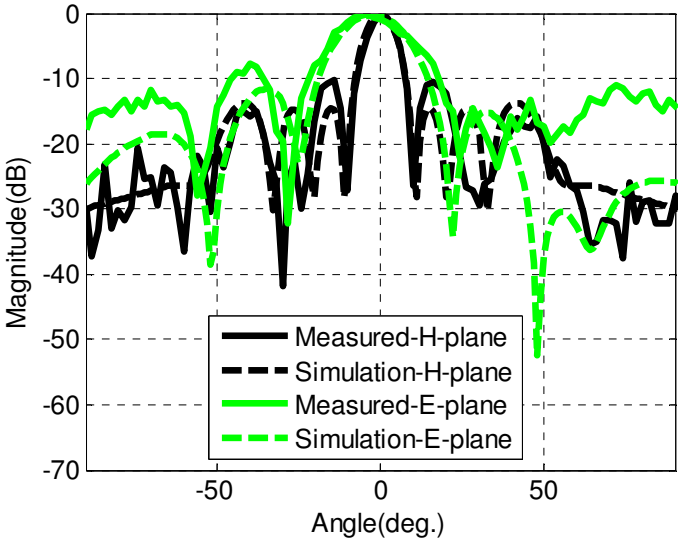

(c)

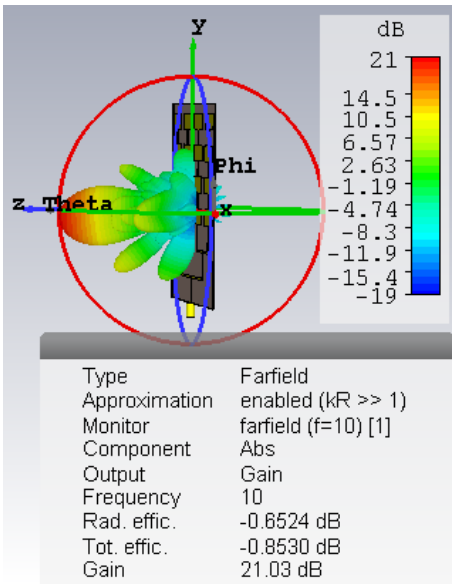

(d)

Fig. 8.7. Experiment results of 16-elements MPAA designed at 0.508mm thick PCB.

(a) Fabricated prototype, (b) S_{11}, (c) 2-D FRP and (d) 3-D simulation FRP

Table 8.4. Performance of MPAAs with h=0.508mm

MPAA	BW (MHz)		Gain (dBi)		SLL (dB)	
	Simu.	Meas.	Simu.	Meas.	Simu.	Meas.
2-elements	560	537	13.37	13.33	-12.26	-13.83
8-elements	450	200	17.68	17.99	-9.8	-5.8
16-elements	310	230	21.03	21.1	-10.29	-7.75

In the next stage, based on the conclusion drawn in the last paragraph, a large MPAA is designed at 10GHz with 32-elements on the PCB thickness of 0.508mm. Fig. 8.8 shows the geometry of 32-elements MPAA and Table 8.5 presents its optimised dimensions. Fig. 8.9 demonstrate the experiment results of 32-elements 10GHz MPAA where (a), (b), (c) and (d) show the fabricated prototype, S_{11} response, 2-D FRP and 3-D simulation FRP, respectively. Table 8.6 shows the performance parameters of this array. Comparing these results with 16-elements MPAA results presented in Table 8.4 it is apparent that further doubling the patch elements to 32 improved the measured gain by 1.17dB to 22.27dBi but the S_{11} BW is shrunk down to 80MHz and the SLL is increased to -4.88dB.

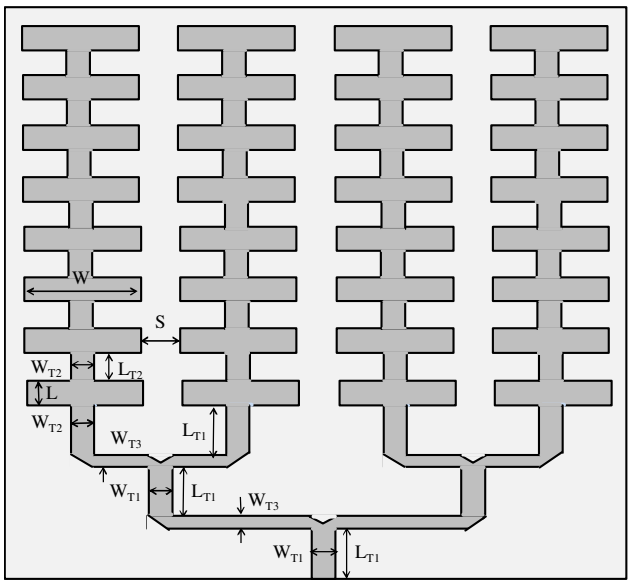

Fig. 8.8 Geometry of 32-elements MPAAs

Table 8.5. Dimensions in mm of 32-elements 10GHz MPAA with h=0.508mm

L	W	L_{T1}	W_{T1}	L_{T2}	W_{T2}	W_{T3}	S
9.19	33	14	1.75	8.67	2.56	1.28	9.73

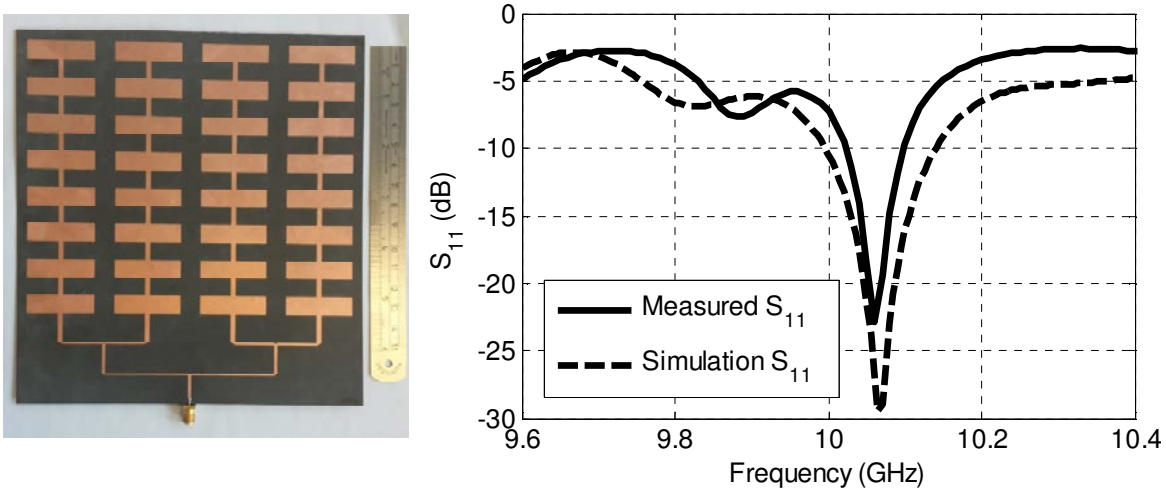

(a) (b)

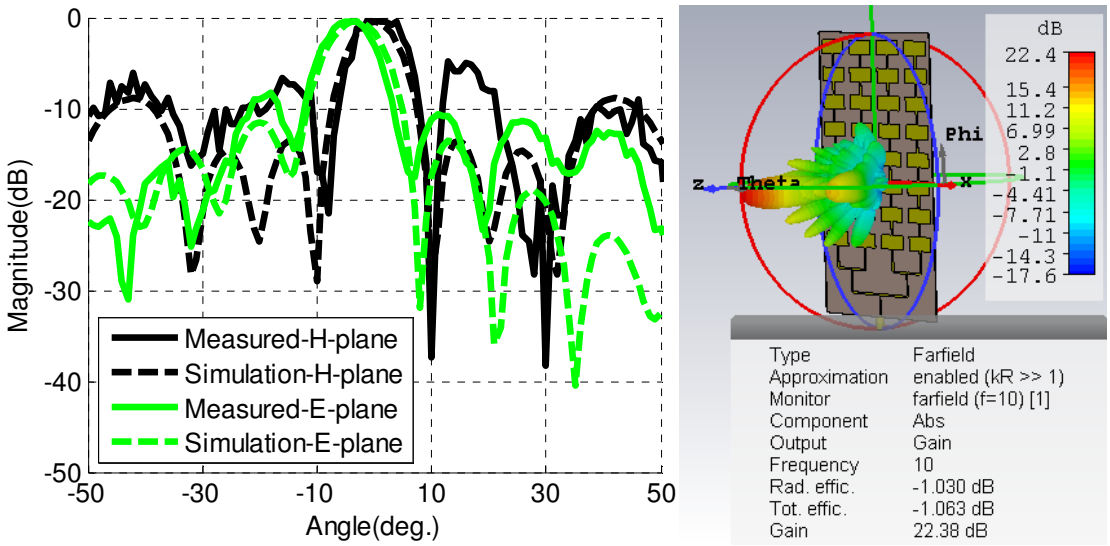

(c) (d)

Fig. 8.9. Experiment results of 32-elements 10GHz MPAA designed at 0.508mm thick PCB.

(a) Fabricated prototype, (b) S_{11}, (c) 2-D FRP and (d) 3-D simulation FRP

Table 8.6. Performance of 32-elements 10GHz MPAAs with h=0.508mm

BW (MHz)		Gain (dBi)		SLL (dB)	
Simu.	Meas.	Simu.	Meas.	Simu.	Meas.
150	80	22.38	22.27	-8.83	-4.88

8.3 MPA Array Design at 60GHz

The 32-elements MPAA design presented in the last section is redesigned at 60GHz frequency on the same material but with substrate thickness h=0.127mm. Table 8.7 shows the dimensions of the 60GHz MPAA where it is clear that the antenna dimensions are well above the PCB etching limit of 152μm track width/gap [3]. Fig. 8.10 demonstrates the experiment results of this MPAA where (a), (b), (c) and (d) represent the fabricated prototype, S_{11} response, 2-D FRP and 3-D simulation FRP at the central resonant frequency of 60.5GHz, respectively. As seen from Fig. 8.10, the measured and simulation results show a close agreement. Table 8.8 summarises the antenna's overall performance parameters. The measured -10dB S_{11} BW and maximum gain at 60.5GHz of this array are 2.39GHz and 20.5dBi, respectively. The measured gain is relatively lower than that of the 32-element array at 10GHz due to the fact that the substrate's thickness of 0.127mm at 60GHz is relatively thicker (i.e. h/λ_0=0.0254, where λ_0 is the free space wavelength of the operating frequency) than 0.508mm at 10GHz (i.e. h/λ_0=0.0169).

Table 8.7. Dimensions in mm of 60GHz MPAA with h=0.127mm

L	W	L_{T1}	W_{T1}	L_{T2}	W_{T2}	W_{T3}	S
1.45	5	2.8	0.42	1.45	0.62	0.3	1.58

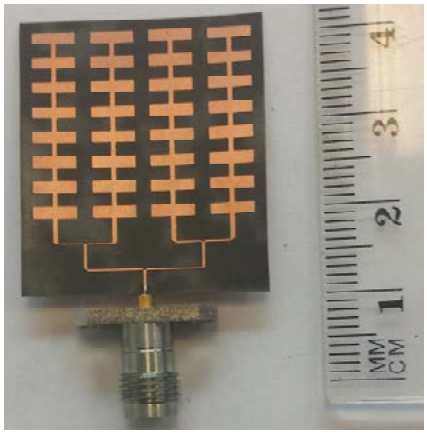

(a)

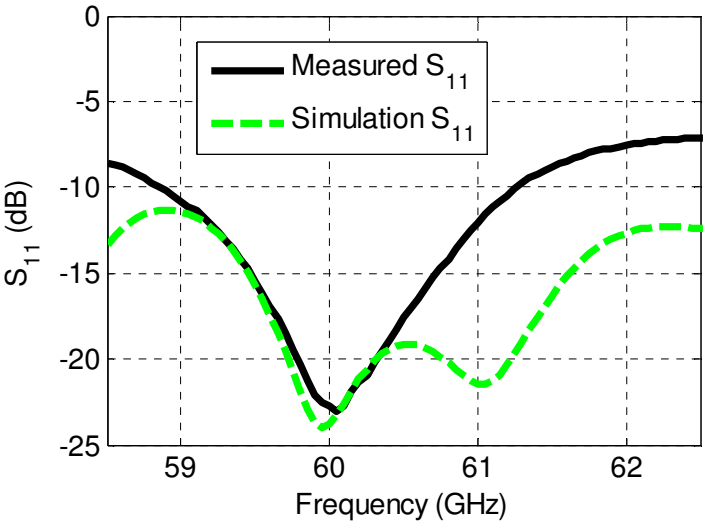

(b)

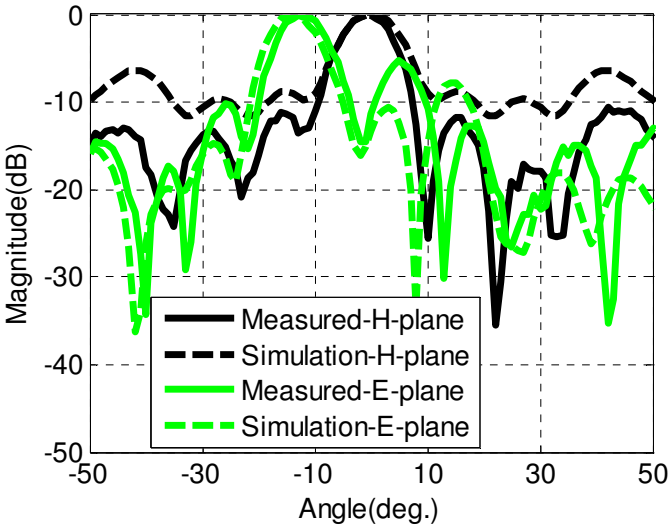

(c)

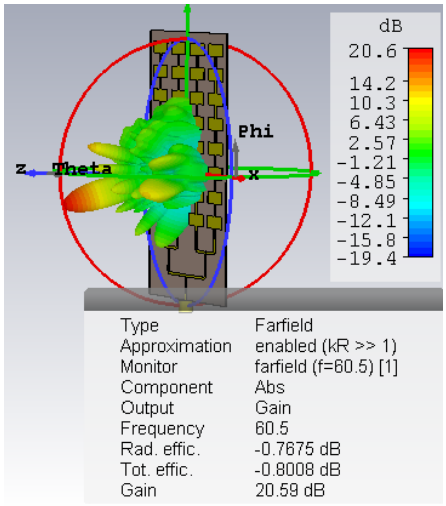

(d)

Fig. 8.10. Experiment results of 32-elements 60GHz MPAA designed at 0.127mm thick PCB.

(a) Fabricated prototype, (b) S_{11}, (c) 2-D FRP and (d) 3-D simulation FRP

Table 8.8. Performance of 60GHz MPAAs with h=0.127mm

BW (GHz)		Gain (dBi)		SLL (dB)	
Simu.	Meas.	Simu.	Meas.	Simu.	Meas.
3.31 (S_{11}<-12dB)	2.39	20.59	20.50	-6.41	-5.32

8.4 Conclusion

The performance of improved size microstrip antenna arrays has been studied at 10GHz frequencies by designing and testing several prototypes with various number of patch elements on two different substrate thickness. It has been found that a thin PCB substrate is desirable for high gain large MPAA designs. Subsequently, high gain antenna arrays have been designed with 32 patch elements on relatively thin substrates and tested at 10GHz and 60GHz frequencies and maximum measured gain of 22.27dB and 20.1dBi have been achieved at 10GHz and 60GHz, respectively. Also, about a 12^0 angle beam squint in the main radiation lobe has been observed in case of the presented 60GHz array due to the long series feed of the patch elements. Furthermore, the SLL is increased in the large MPAAs which may be minimised by applying lobe grating methods as discussed in [3]. The designing approach may be particularly useful to make cost effective microstrip antenna arrays at even higher frequencies of mm-wave and THz bands by employing even thinner substrates.

8.5 References

1. Rabbani, M. and Ghafouri-Shiraz, H., 2017. Liquid Crystalline Polymer Substrate Based THz Microstrip Antenna Arrays for Medical Applications. *IEEE Antennas and Wireless Propagation Letters*. DOI: 10.1109/LAWP.2017.2647825

2. Rabbani, M.S. and Ghafouri-Shiraz, H., 2016. Improvement of microstrip patch antenna gain and bandwidth at 60 GHz and X bands for wireless applications. *IET Microwaves, Antennas & Propagation*, *10*(11), pp.1167-1173. DOI: 10.1049/iet-map.2015.0672

3. Bancroft, R., 2009. *Microstrip and printed antenna design*. The Institution of Engineering and Technology.

4. Carrasco, E., Barba, M. and Encinar, J.A., 2012. X-band reflectarray antenna with switching-beam using PIN diodes and gathered elements. *IEEE Transactions on Antennas and Propagation*, *60*(12), pp.5700-5708.

5. Vallecchi, A. and Gentili, G.B., 2007, November. A shaped-beam hybrid coupling microstrip planar array antenna for X-band dual polarization airport surveillance radars. In *Antennas and Propagation, 2007. EuCAP 2007. The Second European Conference on* (pp. 1-7). IET.

6. Murugan, D., Madhan, M.G. and Piramasubramanian, S., 2012, July. Design and performance prediction of 10GHz micro strip array antenna structures. In *Computing Communication & Networking Technologies (ICCCNT), 2012 Third International Conference on* (pp. 1-5). IEEE.

7. Karnfelt, C., Hallbjorner, P., Zirath, H. and Alping, A., 2006. High gain active microstrip antenna for 60-GHz WLAN/WPAN applications. *IEEE Transactions on Microwave Theory and Techniques*, *54*(6), pp.2593-2603.

8. Biglarbegian, B., Fakharzadeh, M., Busuioc, D., Nezhad-Ahmadi, M.R. and Safavi-Naeini, S., 2011. Optimized microstrip antenna arrays for emerging millimeter-wave wireless applications. *IEEE Transactions on antennas and propagation*, *59*(5), pp.1742-1747.

9. Qasim, A.M. and Rahman, T.A., 2010, November. A compact & high gain series array planar antenna for 60-GHz WPAN applications. In *Applied Electromagnetics (APACE), 2010 IEEE Asia-Pacific Conference on* (pp. 1-5). IEEE.

10. Pan, H.K., Horine, B.D., Ruberto, M. and Ravid, S., 2011, July. Mm-wave phased array antenna and system integration on semi-flex packaging. In *Antennas and Propagation (APSURSI), 2011 IEEE International Symposium on* (pp. 2059-2062). IEEE.

11. Lu, B., Luo, J., Zhang, L., Zhang, L., Yue, R. and Wang, Y., 2014, June. A patch antenna array for 60-GHz WPAN based on polypropylene composite substrate. In *Electron Devices and Solid-State Circuits (EDSSC), 2014 IEEE International Conference on* (pp. 1-2). IEEE.

12. Rabbani, M.S. and Ghafouri-Shiraz, H., 2017. High gain microstrip antenna array for 60 GHz band point to point WLAN/WPAN communications. *Microwave and Optical Technology Letters*, *59*(3), pp.511-514.

13. Rabbani, M.S. and Ghafouri-Shiraz, H., Ultra-Wide Patch Antenna Array Design at 60 GHz Band for Remote Vital Sign Monitoring with Doppler Radar Principle. *Journal of Infrared, Millimeter, and Terahertz Waves*, pp.1-19.

Chapter-9

Conclusion and Future Prospectives

Abstract:

In this chapter, a conclusion has been drawn on the overall outcome of the presented research work on microstrip antenna design and measurement for mm-wave and THz applications. Moreover, the future prospectives have been discussed with regards to the proposed antenna design, fabrication, applications and testing at the mentioned frequencies. Finally, the necessity of new equipment and techniques has been described for prototyping and measurements of the cost-effective microstrip antenna structures for emerging mm-wave and THz wireless applications.

9.1 Size Improvement of Microstrip Patch Antennas for THz Frequencies

A method has been proposed to improve the dimensions of microstrip patch antenna (MPA) and the associated feeding and impedance matching line to convince the PCB fabrication limit of 152μm line width/gap for low cost, high tolerance and better performance at mm-wave and lower THz frequency bands. For this purpose, the following three fundamental modifications have been proposed on the conventional MPA design theory [1]:

(i) the patch antenna is operated at one of its higher order modes whose resonance and radiations characteristics are found to be closely matched to its fundamental mode.

(ii) the antenna input impedance is exceptionally reduced by extending the patch width to obtain low impedance wide feeding transmission lines (TLs)

(iii) the impedance transformation is carried out by setting the matching TL lengths equal to higher odd multiples of the operating quarter wavelength

The working theory of the exploited modifications has been fully analysed and a set of generalised equations has been established to calculate the dimensions of MPA [2]. Several MPAs have been designed on various dielectric substrate heights and materials at 10GHz, 60GHz, 100GHz, 635GHz and 835GHz frequencies to examine the proposed method [1-3]. The fabricated antenna prototypes have been tested at 10GHz, 60GHz and 100GHz frequencies to practically validate the proposed designing concept [1-3]. A good match has been achieved between the measured and expected results in all the cases which proved that the tolerance level has been elevated in fabrication and measurements especially at mm-wave frequencies. Subsequently, the MPA size improvement method has made it easier to implement and study numerous existing techniques like constituting arrays, applying frequency selective surface, lens and defected ground structure to enhance the antenna capabilities at mm-wave and THz frequencies. In the future, the MPAs may be designed with the proposed method and tested at even higher frequencies like 300GHz, 540GHz, 635GHz and 835GHz for various applications in communications and medical sectors [4].

9.2 Performance Improvement of the Proposed MPA Design

A number of existing techniques with some sort of necessary modifications have been employed on the proposed antenna structure to study and improve the antenna performance at mm-wave frequencies [5-7]. These techniques include:

i. Designing of large microstrip antenna arrays to achieve high antenna gain

ii. Employment of partially reflective surfaces (PRSs) for high gain and wide bandwidth performance

iii. Implementation of dielectric lens for high gain performance

iv. Deployment of Defective Ground Structure (DGS) for wide return loss bandwidth

The following alterations have been made to the above techniques to mitigate the mechanical fabrication concerns and to enrich the electrical performance:

- Reverse impedance matching technique has been introduced to feed the array elements with low impedance wide TLs to ease the fabrication complexities and to meliorate the loss performance in the feeding network.
- Double PRS layers with wider separating distances have been deployed on the proposed MPA to efficiently improved the antenna gain and to release the fabrication and assembling complications.
- A wide resonant cavity based dielectric lens has been employed in front of the proposed MPA to enhance the antenna gain and bandwidth as well as to simplify the fabrication and assembling process.
- A novel diamond shape DGS has been implemented underneath the proposed patch element to attain a wider return loss response. The suggested DGS dimensions are easy to etch with the low cost high tolerant PCB fabrication process.

The above techniques have been tested at mm-wave frequencies so far and have shown high potency to be implemented and tested at THz frequencies. Therefore, further investigation may be carried out on this topic in future, in order to figure out the feasibility and limitations of these antenna designing approaches at THz frequencies [8].

9.3 The Proposed Antennas Applications

MPAs have been designed and tested for the following three emerging applications in highly demanded areas of mm-wave and THz communications and detections:

- 60GHz-band multi-gigabits/sec Wireless Local Area Network (WLAN) and Wireless Personal Area Network (WPAN) [9]
- Remote non-contact vital signs monitoring with Doppler radar technique [6,10,11]
- Cancer detection with THz spectroscopy [4]

The performance of the tested prototype antennas satisfied the specifications required for each of the mentioned applications. The implementation procedure of the designed antennas for WLAN/WPAN applications has been described in detail. The antennas designed for remote vital signs monitoring at 60GHz-band frequencies have been employed to detect respiration and heart beat rates of a person from various distances within lab environments and very accurate results have been achieved. In future, the performance of the proposed antenna may be studied in real life scenarios of the mentioned applications as follows:

- To measure the maximum achievable data rate and signal quality for WLAN/WPAN in dynamic environment within an ordinary room/office.
- To study the accuracy of the vital signs detection in outdoor open areas for even longer distance, and within an Automobile/ambulance environments.
- To investigate the results accuracy and practical limitations of cancer detection at 0.635THz and 0.835THz frequencies.

Moreover, it can be anticipated from the presented work that the proposed method can be used to design and investigate MPAs for numerous other wireless applications like 5G mobile communications [12,13], traffic and transport control [14], on-body biosensors network [15], and research and development work [16-17].

9.4 Antenna Prototyping and Measurements

An extensive work on antenna prototyping and measurements has been presented at mm-wave frequencies [1-5,7-11]. In all the cases, the measured return loss and radiation performance of the tested antennas showed close agreement (<3% deviations) with the expected results. However, more research is required on MPA fabrication and measurements at THz frequencies especially within the transmission windows below 1THz [1] to figure out the tolerance levels in fabrication with the PCB etching processes and pragmatical antenna performance.

Most of the testing equipment operating at THz frequencies are connected with antennas via hallow metallic waveguide ports due to low loss performance of the waveguide components. Therefore, transition adaptors are essentially required for mechanical compatibility of the antenna feeding microstrip line with the waveguide components. This may raise the cost, inaccuracy and complexity of MPA testing at THz frequencies due to the additional parts and abnormalities in the transition path. Consequently, it is desirable to analyse the existing microstrip to other waveguide transitions methods as well as to develop new techniques to excite the microstrip antenna structures directly through the waveguide lines at THz frequencies [18, 19]. For this purpose, Micromachining tools and techniques could be particularly useful along with PCB etching methods for antenna prototyping and measurements [20].

On the other hand, remarkable research work is vital to design a robust automated mechanism for antenna's far-field radiation patterns measurements in both E and H planes at THz frequencies. This may include designing of the anechoic chambers with new absorbing materials, dynamic fixture, low loss flexible cables and controlling software applications.

Finally, it is remarked that mm-wave and THz wireless technologies are progressing efficiently to acquire maturity for various real life applications. Thus, it can be anticipated that the wireless technologies at mm-wave and THz frequency bands will be playing an important role to improve the life quality of a common person in coming years through versatile, emerging and novel applications.

9.5 References

1. Rabbani, M.S. and Ghafouri-Shiraz, H., 2015. Size improvement of rectangular microstrip patch antenna at MM-wave and terahertz frequencies. Microwave and Optical Technology Letters, 57(11), pp.2585-2589.
2. Rabbani, M.S. and Ghafouri-Shiraz, H., 2016. Fabrication tolerance and gain improvements of microstrip patch antenna at terahertz frequencies. Microwave and Optical Technology Letters, 58(8), pp.1819-1824.
3. Rabbani, M.S. and Ghafouri-Shiraz, H., 2015, December. Improvement of microstrip antenna's gain, bandwidth and fabrication tolerance at terahertz frequency bands. In Wideband and Multi-Band Antennas and Arrays for Civil, Security & Military Applications (pp. 1-3). IET.
4. Rabbani, M.S. and Ghafouri-Shiraz, H., 2017. Liquid Crystalline Polymer Substrate Based THz Microstrip Antenna Arrays for Medical Applications. IEEE Antennas and Wireless Propagation Letters.

5. Rabbani, M.S. and Ghafouri-Shiraz, H., 2017. High gain microstrip antenna array for 60 GHz band point to point WLAN/WPAN communications. Microwave and Optical Technology Letters, 59(3), pp.511-514.
6. Rabbani, M.S. and Ghafouri-Shiraz, H., 2017. Frequency selective surface antenna for remote vital sign monitoring with ultra-wide band doppler radar. Microwave and Optical Technology Letters, 59(4), pp.818-823.
7. Saqib Rabbani, M. and Ghafouri-Shiraz, H., 2016. Microstrip antennas for X-band and MM-wave frequencies based on diamond shape defected ground structure and size extension method. Microwave and Optical Technology Letters, 58(12), pp.2836-2841.
8. Rabbani, M.S. and Ghafouri-Shiraz, H., 2017, March. Evaluation of Gain Enhancement in Large Microstrip Antenna Arrays for Mm-wave Applications. IET Colloquium on Millimetre-wave and Terahertz Engineering & Technology 2017. IET Proceedings. Glasgow. (Accepted in March 2017)
9. Rabbani, M.S. and Ghafouri-Shiraz, H., 2016. Improvement of microstrip patch antenna gain and bandwidth at 60 GHz and X bands for wireless applications. IET Microwaves, Antennas & Propagation, 10(11), pp.1167-1173.
10. Rabbani, M.S. and Ghafouri-Shiraz, H., 2016. Ultra-Wide Patch Antenna Array Design at 60 GHz Band for Remote Vital Sign Monitoring with Doppler Radar Principle. Journal of Infrared, Millimeter, and Terahertz Waves, pp.1-19.
11. Rabbani, M.S. and Ghafouri-Shiraz, H., 2017, February. 60 GHz Microstrip Antenna for Remote Vital Sign Monitoring in Automobile Applications. Antennas, Propagation & RF Technology for Transport and Autonomous Platforms. IET proceedings, 2017. Birmingham. (Accepted in February 2017)

12. Dehos, C., González, J.L., De Domenico, A., Kténas, D. and Dussopt, L., 2014. Millimeter-wave access and backhauling: the solution to the exponential data traffic increase in 5G mobile communications systems?. IEEE Communications Magazine, 52(9), pp.88-95.
13. Bangerter, B., Talwar, S., Arefi, R. and Stewart, K., 2014. Networks and devices for the 5G era. IEEE Communications Magazine, 52(2), pp.90-96.
14. Hasch, J., Topak, E., Schnabel, R., Zwick, T., Weigel, R. and Waldschmidt, C., 2012. Millimeter-wave technology for automotive radar sensors in the 77 GHz frequency band. IEEE Transactions on Microwave Theory and Techniques, 60(3), pp.845-860.
15. Yang, K., Pellegrini, A., Munoz, M.O., Brizzi, A., Alomainy, A. and Hao, Y., 2015. Numerical analysis and characterization of THz propagation channel for body-centric nano-communications. IEEE Transactions on Terahertz Science and technology, 5(3), pp.419-426.
16. Kleine-Ostmann, T. and Nagatsuma, T., 2011. A review on terahertz communications research. Journal of Infrared, Millimeter, and Terahertz Waves, 32(2), pp.143-171.
17. Rappaport, T.S., Sun, S., Mayzus, R., Zhao, H., Azar, Y., Wang, K., Wong, G.N., Schulz, J.K., Samimi, M. and Gutierrez, F., 2013. Millimeter wave mobile communications for 5G cellular: It will work!. IEEE access, 1, pp.335-349.
18. Ponchak, G.E. and Simons, R.N., 1990. A new rectangular waveguide to coplanar waveguide transition. NASA-TM-102477, E-5264, NAS 1.15:102477
19. Deslandes, D. and Wu, K., 2005. Analysis and design of current probe transition from grounded coplanar to substrate integrated rectangular waveguides. IEEE Transactions on Microwave Theory and Techniques, 53(8), pp.2487-2494.

20. Lubecke, V.M., Mizuno, K. and Rebeiz, G.M., 1998. Micromachining for terahertz applications. *IEEE transactions on microwave theory and techniques*, *46*(11), pp.1821-1831.

Appendix A

A1. Matlab Programme for RVSM:

The RVSM data is process in Matlab by using the following main signal processing steps:

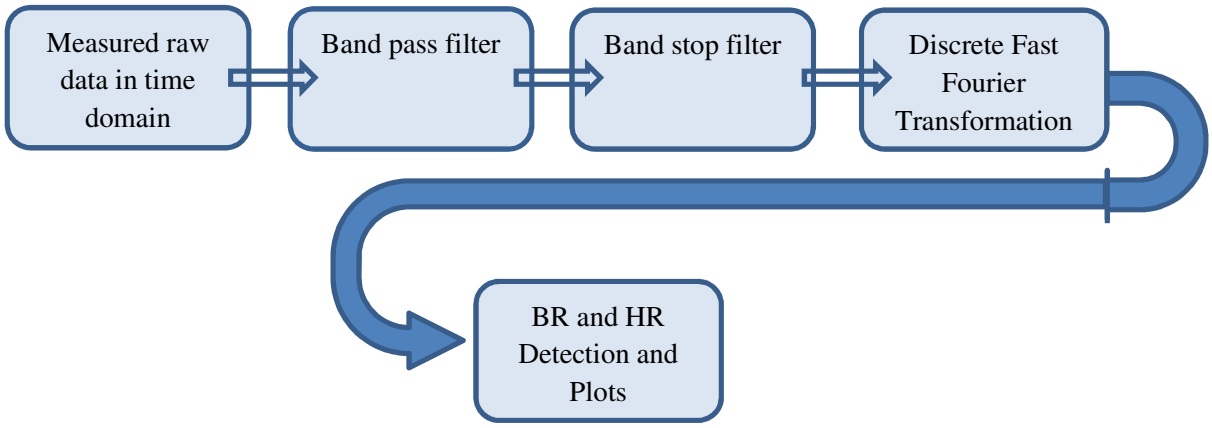

a. Matlab Code:

```
close all;
clear all;
clc;

f0=63.4*10^9; % used tone frequency
c=3*10^8;
l0=c/f0;        % wavelength
pi=3.1416;

file1=xlsread('VSM165.xls');  % measured RVSM data

                % Define the filters's cutoff frequencies based on
                % the expected BR and values (1/min)

fB1=10;                  % Expected min respiration rate/min
fB2=41;                  % Expected max respiration rate/min
fH1=61;                  % Expected min heart rate/min
fH2=98;                 % Expected max heart rate/min
f1=10;
f2=98;          % (f1 and f2 define the range of total expected frequencies

%%%%%%%%%%%%%%%       Time domain Plot           %%%%%%%%%%%%

ST=60.18;            %in sec   60GHz experiment
ST=ST/60;        %  in Min
L=length(file1(1:1:end,2))-1;     % Total No. of samples (-1 when L is odd)
```

```
Fs=L/ST;            % sampling frequency
y1=0:ST/L:ST;
y2=file1(1:1:end,2);

figure(1)
subplot(311)
plot(y1.*60,y2,'-k','LineWidth',3)
title('Measured Raw Data', 'FontSize', 14);
xlabel('Time (sec)','FontSize', 12);
ylabel('S21 phase (degree)','FontSize', 12);
set(gca,'FontSize',12);
grid on


                %%      Band Pass Filter %%


NF=Fs/2;          % Nequest Frequency in min

[b1,a1]=butter(10,[f1/NF,f2/NF],'bandpass');
y2=filter(b1,a1,y2);

H1=freqz(b1,a1,floor(NF));
Wn=0:1/(NF-1):1;

figure(2)
subplot(211)
plot(Wn.*NF,abs(H1),'-k','LineWidth',3);
title('BPF Response','FontSize', 14)
xlabel('Frequency (1/min)','FontSize', 12);
ylabel('Magnitude','FontSize', 12);
set(gca,'FontSize',12);
grid on


                %%      Band Stop Filter   %%

[b2,a2]=butter(10,[30/NF,65/NF],'stop');
y2=filter(b2,a2,y2);

H2=freqz(b2,a2,floor(NF));
Wn=0:1/(NF-1):1;

subplot(212)
plot(Wn.*NF,abs(H2),'-k','LineWidth',3);
title('BSF Response','FontSize', 14)
xlabel('Frequency (1/min)','FontSize', 12);
ylabel('Magnitude','FontSize', 12);
set(gca,'FontSize',12);
grid on

figure(1)
subplot(312)
plot(y1.*60,y2,'-k','LineWidth',3)
```

```
title('Filtered Data','FontSize', 14);
xlabel('Time (sec)','FontSize', 12);
ylabel('S21 phase (deg.)','FontSize', 12);
set(gca,'FontSize',12);
grid on



                %% DFFT calculations  %%

f = Fs*(0:(L/2))/L;
Y = fft(y2);

P2 = abs(Y/L);
P1 = P2(1:round(L/2+0));  %% instead of 1 add 0 for for 20 sec datawhen
                          %every third sample is chosen

if length(P1)~=length(f) %% just to match the length of vetors "f" and "P1"
P1 = P2(1:round(L/2+1));
end

P1(2:end-1) = 2*P1(2:end-1);
P1=2*P1; % P1 is the magnitude to top half cycle of the wave( phase change)
         % total phase change due to the respiration is twice

fmax=max(f);
Lf=length(f);
gf=fmax/(Lf-1);              %   Freq interval(freq. bin)

B1=round(fB1/gf);            %% Breathing window start freq.
B2=round(fB2/gf);            %% Breathing window end freq.
H1=round(fH1/gf);            %% Heart window start at freq.
H2=round(fH2/gf);            %% Heart window end freq.
W1=round(f1/gf);             %% overall window start freq.
W2=round(f2/gf);             %% overall window end freq.

             %%%         Breathing Rate calculation      %%

[maxB, indxB]=max(P1(B1:B2,1));

BR=(indxB+B1-2)*gf;
fprintf('\nBreathing Rate =%f /min\n',round(BR));

meanB=mean(P1);
DPhB=maxB;                 %%  Delta Phase in Breathing
fprintf('\nPhase variation with Breathing =%f Deg.\n',DPhB);

%DxB=DPhB*l0/4/pi;           %% Chest movement (delta x)without
                            %intermodulation
%fprintf('\nChest movement with Breathing =%f mm\n\n\n',DxB*10^3);

             %%%         Heat Rate       %%

[maxH, indxH]=max(P1(H1:H2,1));
```

```
HR=(indxH+H1-2)*gf;
fprintf('\nHeart Rate =%f /min\n',round(HR));

meanH=mean(P1);
DPhH=maxH;                %%  Delta Phase in Breathing
fprintf('\nPhase variation with Heart =%f Deg.\n',DPhH);

%DxH=DPhH*l0/4/pi;           %% Chest movement (delta x)without
                             %intermodulation
%fprintf('\nChest movement with Heart =%f mm\n\n\n',DxH*10^3);

figure(1)
subplot(313);
plot(f(1,W1:W2),P1(W1:W2,1),'-k','LineWidth',3)
title('Breath/Heart Rate Peaks','FontSize', 14);
xlabel('Frequency (1/Min)','FontSize', 12);
ylabel('S21 phase (deg)','FontSize', 12);
set(gca,'FontSize',12);
grid on

%%      End
```

A2. Results:

a. Extracted data:

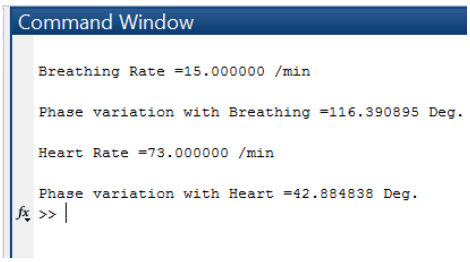

Fig. A1. Extracted data

b: Results plots:

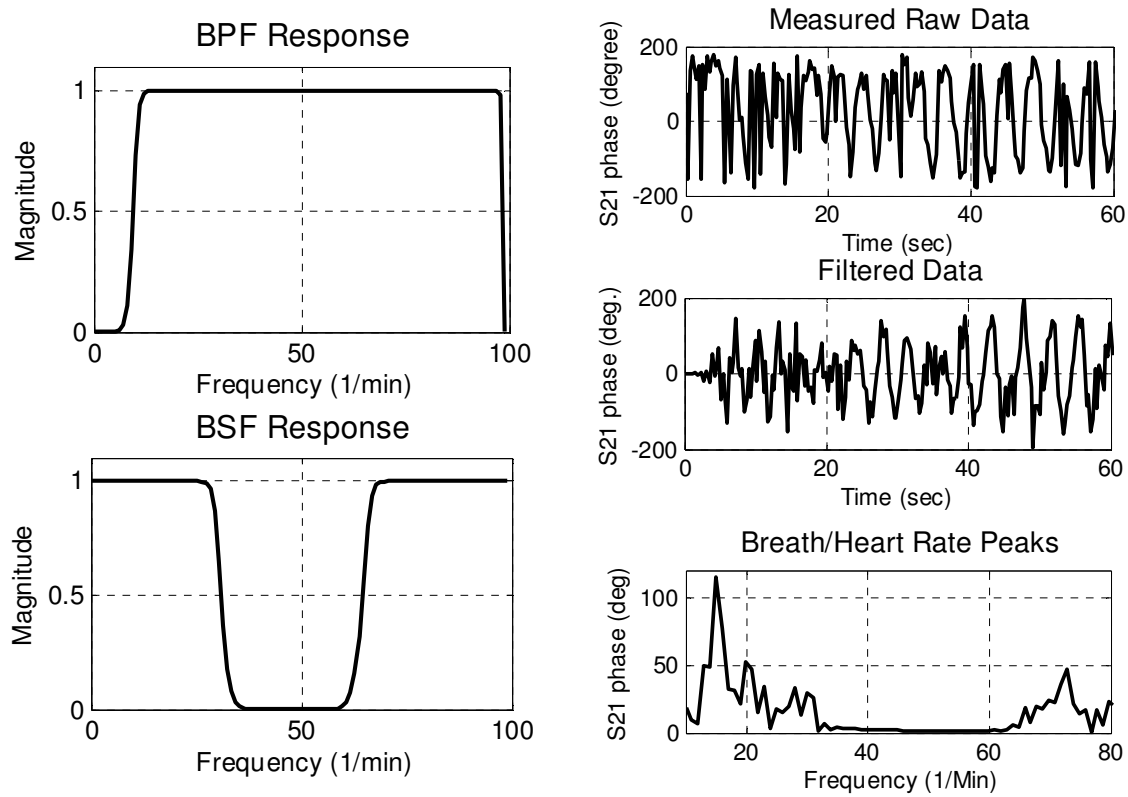

(a) (b)

Fig. A2. Results Plots. (a) Band pass filter (top) and band stop filter (bottom) responses, and (b) RVSM results